ELSEVIER

Synthetic Metals 108 (2000) 173–222

SYNTHETIC METALS

www.elsevier.com/locate/synmet

Review

2-mm Waveband electron paramagnetic resonance spectroscopy of conducting polymers

V.I. Krinichnyi *

Institute of Problems of Chemical Physics, Russian Academy of Sciences, 14 Institutski Prospect, Chernogolovka, MR 142432, Russia

Received 29 January 1999; received in revised form 28 September 1999; accepted 1 October 1999

Abstract

The review summarizes the aspects of utilization of a high-resolution 2-mm waveband electron paramagnetic resonance (EPR) spectroscopy combined with the modified methods of spin label and probe, steady-state saturation of spin-packets and saturation transfer in the study of conducting polymers. The theoretical background of the magnetic parameters, saturation, relaxation and dynamics study of nonlinear charge carriers in conducting polymers is briefly described in the first part. The second part deals with the peculiarities of EPR experiments at 2-mm waveband. The final part is devoted to an original data obtained in 2-mm waveband EPR study of the nature, relaxation, and dynamics of paramagnetic centers delocalized on nonlinear charge carriers as well as the mechanisms of charge transfer in polyacetylene, polythiophene, poly(*p*-phenylene), polypyrrole, poly(*bis*-alkylthioacetylene), polyaniline, and poly(tetrathiofulvalene) with different doping levels.

Keywords: Conducting polymers; Electron paramagnetic resonance; Electron relaxation; Spin/charge dynamics

1. Introduction

Various compounds can be attributed to organic conductors, such as molecular crystals based on charge transfer complexes and ion-radial salts, fullerenes, platinum complexes with cyanide ligands, phtalocyanines, dyes, metal-containing polymers [1–4], etc. These compounds are interesting from the scientific standpoint, concerning the study of fundamental problems of charge transfer. Of a special interest are organic conducting polymers as a new class of electronic materials [5–13]. They have attracted considerable attention, since the investigation of these systems has generated entirely new scientific conceptions and a potential for its perspective application in molecular electronics [14–21].

These materials have a highly anisotropic quasi-one-dimensional (Q1D) π-conducting structure with a delocalized charge carrier which makes such systems fundamentally different from traditional inorganic semiconductors (for example, silicon and selenium) and from common insulating polymers (for example, polyethylene). Their chain structure leads to a strong coupling of electron states to conformational excitations, solitons and polarons, peculiar to Q1D system. Electric conductivity of conducting polymers as films or powders can be varied under control by more then 12 orders of magnitude with chemical or electrochemical introduction of various counterions (oxidation or reduction of polymer chains); therefore, their properties range from insulator ($\sigma_{DC} \sim 10^{-10}$–$10^{-8}$ S/m) to semiconductor and then to metal ($\sigma_{DC} \sim 10^{4}$–10^{6} S/m) [12,13]. The metallic properties of conducting polymers strongly depend on their structure, morphology, and quality [22,23]. The introduction of anions BF_4^-, ClO_4^-, AsF_5^-, J_3^-, $FeCl_4^-$, MnO_4^-, etc., into a polymer induces a positive charge on a polymer chain and thus leads to p-type conductivity of the polymer. N-type conductivity is realized under polymer doping Li^+, K^+, Na^+, and other ions of alkali metals. Thus, the type of conductivity of such compounds is defined by the nature of the introduced counterion.

In traditional 3D inorganic semiconductors, fourfold (or sixfold, etc.) coordination of each atom to its neighbor through covalent bonds leads to a rigid structure. Therefore, electron excitations may be usually considered in the context of this rigid structure, leading to the conventional conception of electrons and holes as dominant excitations.

* Tel.: +7-95-5245087; fax: +7-96-5153588; e-mail: kivi@cat.icp.ac.ru

0379-6779/00/$ - see front matter
PII: S0379-6779(99)00262-3

The situation with conducting polymer semiconductors is quite different: 1D structure makes these systems generally more susceptible to structural distortion. Therefore, electronic-physical properties of conducting polymers may be conventionally considered in the frames of bands theory [24] as well as of soliton and polaron theory [25,26], based on Peierls instability [27], characteristic of Q1D systems.

As the original properties of conducting polymers are related to the existence of paramagnetic centers (PC) localized or/and delocalized along the polymer chains, a great number of electron paramagnetic resonance (EPR) studies have been performed during the last decades [28,29]. Organic conducting polymers are characterized by a carbon π-electron system and have a partially filled energy band structure, which is responsible for important electron properties of these systems. Therefore, EPR spectroscopy is one of the most widely used and productive physical methods in structural and dynamic studies of polymer systems, which contain free radicals, ion-radicals, molecules in triplet states, transition metal complexes and other PCs. Let the perspectives of EPR method in the investigation of conducting polymers be considered.

At solving these problems at traditional, 3-cm waveband, the restrictions of EPR method emerged clearly, being associated in particular with that the signals of organic free radicals were registered in a narrow magnetic field range and it resulted in the overlapping of the lines of complex spectra or spectra of different radicals with close *g*-factor values. Thus, new experimental techniques which improve the efficiency of EPR spectroscopy in the study of solid-state systems were recently developed. They are: electron spin echo spectroscopy [30,31], method based on the effect of spin polarization, in which EPR signal is registered optically [32], methods of double electron-nuclear resonance [33,34], microwave frequency saturation transfer EPR (ST-EPR) method [35], EPR in nonuniform fields [36] and some others.

However, most of these methods may be applied only to solve specific problems and investigate special objects. The transition to higher magnetic fields and registration frequencies should be the most common method to increase the precision and informativity of the method. Earlier it was shown [37,38], that 2-mm waveband EPR spectroscopy enables the profound investigation of the structure, dynamics, other specific characteristics of radical centers and their local environment, and elementary charge transfer processes in different solid-state systems.

This review reports the possibilities of 2-mm waveband EPR spectroscopy of high spectral resolution over *g*-factor and summarizes the original principle results, obtained in the investigation of various conducting polymers at this waveband during the last years in the Institute of Problems of Chemical Physics in Chernogolovka, Russia.

Section 1 of the review presents a concise summary of theoretical fundamentals of EPR spectroscopy and spin transfer mechanisms in the systems of lower dimensionality necessary for the interpretation of experimental results. The peculiarities of 2-mm EPR technique and experimental methods are briefly considered in Section 2. Finally, the advantages of 2-mm waveband EPR spectroscopy are described in the study of some known conducting polymers using the steady-state saturation of spin-packets, spin label and probe, and saturation transfer methods, applied to this registration band.

2. Theoretical backgrounds of spin resonance and transfer in conducting polymers

2.1. The magnetic parameters of organic radicals obtained by EPR spectroscopy

All paramagnetic compounds possess an unpaired electron, which interaction with external magnetic field and with electron and nuclear spins are generally described by the following Hamiltonian

$$H = \gamma_e \hbar m \boldsymbol{B}_0 - \gamma_e \hbar S \sum_{i=1} a I_i - \gamma_e \gamma_p \hbar^2 S I_i \times \int \psi^*(x) \frac{1 - 3\cos^2\theta}{\boldsymbol{r}^3} \psi(x) \mathrm{d}\tau \quad (1)$$

where γ_e and γ_p are the hydromagnetic ratio for electron and proton, respectively, $\hbar = h/2\pi$ is the Planck constant, S is the electron spin operator, I_z is z-components of nuclear spin operator, $\langle a \rangle = 1/3(A_{xx} + A_{yy} + A_{zz})$ is an isotropic hyperfine interaction (HFI) constant, A_{ij} is an anisotropic hyperfine constant, θ is the angle between the magnetic field $\boldsymbol{B}_0$ vector and $\boldsymbol{r}$ vector, which is the vector between dipole moments of electron spin and the i-th nucleus, x is the electron spin coordinate, $\psi(0)$ is a wave function proportional to a probability of the localization or the density of an unpaired electron near the interacting nucleus. The isotropic HFI constant a is not equal to zero only for the electrons, possessing a nonzero spin density $\rho(0) = [\psi(0)]^2$, that is, for *s*-electrons.

The first term of the Hamiltonian characterizes the electron Zeeman interaction. If at the registration frequency $\omega_e = 2\pi\nu_e$ the resonance condition

$$h\omega_e = \gamma_e \hbar \boldsymbol{B}_0 \quad (2)$$

is fulfilled, an unpaired electron absorbs an energy quantum and is transferred to a higher excited site. The second term of Eq. (1) defines the nuclear interaction and the third one is the contribution of nuclear Zeeman interaction.

One of the most significant characteristics of a paramagnetic compound is its *g*-factor, which is the ratio of electron mechanic momentum to a magnetic moment. It is stipulated by the distribution of spin density in a radical fragment, the energy of excited configurations and spin-orbit interaction. For a free *s*-electron ($S = J = 1/2$, $L = 0$)

possesses g-factor equal to 2. Relativity correction yields $g = 2.00232$. However, the splitting factor of p- and d-electrons which possesses an orbital moment not equal to zero differs commonly from g_e and varies in a wide range.

If an atomic nucleus is located in the origin, the intensity of magnetic field, induced by electron orbital motion is equal to zero on for s-electrons and the intensity differs from zero in the case of p- and d-electrons (for whom $L \neq 0$). Thus, the nuclei of atoms, having p- or d-electrons are affected by a strong magnetic field, induced by an electron orbital magnetic moment.

As g-factor depends on a paramagnetic molecule orientation in an external magnetic field, it is defined by **g** tensor of the second order [39]

$$\begin{vmatrix} g_{xx} & & \\ & g_{yy} & \\ & & g_{zz} \end{vmatrix} = \begin{vmatrix} 2\left(1+\frac{\lambda}{\Delta E_{n\pi^*}}\right) & & \\ & 2\left(1+\frac{\lambda}{\Delta E_{\sigma\pi^*}}\right) & \\ & & 2 \end{vmatrix} \quad (3)$$

This was a more simple case of the complete spin localization on a single nucleus, that is, $\rho(0) = 1$. In most cases, $\rho(0) < 1$; therefore, the correction must be done, that is, the numerator of both parts of Eq. (3) should be multiplied in addition by a coefficient $\rho(0)$. It is reasonable that the sign of $\Delta g = 2\lambda/\Delta E_{ij}$ is generally defined by that of ΔE_{ij}. If the depinning of orbital moment is stipulated by the excitation of the filled electron shells ($n \rightarrow \pi^*$ and $\sigma \rightarrow \pi^*$ transitions), then $\Delta E_{ij} < 0$ and $\Delta g > 0$. The orbital motion being due to the initiation of interenergetic transitions of unfilled electron shells ($\pi \rightarrow \sigma^*$ transitions), the values are $\Delta E_{ij} > 0$ and $\Delta g < 0$. In the latter case, $\Delta E\pi\sigma^*$ is large; therefore, g_{zz} of most radicals is close to g_e. The radicals, including heteroatoms (O, N, F, S, Cl, etc.) have a small energy of $n \rightarrow \pi^*$ transition. Besides, the constants of electron orbital interaction with these nuclei are greater than that with carbon nucleus. This results in a substantial deviation in g_{xx} and g_{yy} from g_e. The inequality $g_{xx} > g_{yy} > g_{zz} \approx g_e$ always holds for radicals of this type.

In some cases, an unpaired electron cloud is partially or completely localized near a nucleus, which has the nonzero spin value. Then the interactions of magnetic moments of electron spins with that of radical nucleus result in the observation of a multiple hyperfine structure (HFS) rather than a single signal in a spectrum. The type of splitting, spectrum multiplexity and the relative intensity of its components give the evidence for an electron cloud configuration in a radical. A constant of superfine interaction is another important parameter of PC.

Magnetic moments μ_I of a paramagnetic molecule nuclear spins induce an additional magnetic field in an unpaired electron location region, that can enhance or attenuate the external magnetic field $\boldsymbol{B}_0$ depending on the distribution of nuclear spins. Such additional intramolecular fields cause a splitting of energy levels α and β into sublevels; therefore, the resonance condition (2) is realized with different $\boldsymbol{B}_0$ values. According to selection principles $\Delta m_s = 1$ for electron and $\Delta m_I = 0$ for nuclear spin transitions, the additional intramolecular fields result in the increase of a number of possible resonance transitions with a number of interacting nuclear spins.

It should be emphasized that these speculations are correct in the case of a complete unpaired electron localization on a nucleus, that is, when $\rho(0) = 1$. If the electron is delocalized over several nuclei, its constant of isotropic HFI with each of them is defined by spin density on the i-th nucleus, which is described by the McConnell relationship

$$a_i = Q\rho_i(0) \quad (4)$$

where Q is the proportionality factor equal to 2.2–3.5 mT for different radicals, and $\sum_i \rho_i(0) = 1$.

Thus, the magnetic parameters of PCs depend on the configuration of an unpaired electron molecular orbital, which is defined by the strong Coulombic and exchange interactions, and on the molecular structure. In most cases, such an interaction is more complicated and therefore, additional molecular quantum-chemical calculations must be used. In general, the static electron susceptibility χ_0 of N spins is the sum of a temperature-dependent paramagnetic response of localized Curie PC χ_C and the Pauli susceptibility of the Fermi gas χ_P [40],

$$\chi_0 = \chi_C + \chi_P = \frac{Ng^2\mu_B^2}{4k_BT} + 2\mu_B^2 n(\varepsilon_F) \quad (5)$$

where μ_B is the Bohr magneton, k_B is the Boltzmann constant, and $n(\varepsilon_F)$ is the density of states at the Fermi level ε_F. The contributions of χ_C and χ_P terms to the total magnetic susceptibility can vary at the system modification and depend on various factors, for example, on the nature and mobility of charge carriers.

2.2. Spin relaxation and dynamics of nonlinear charge carriers in conducting polymers

Electron spins being in the thermal equilibrium are distributed to energy levels according to the Boltzmann's law. If this equilibrium is somehow disturbed, it relaxes with the longitudinal (spin-lattice) T_1 and the transverse (spin–spin) T_2 relaxation times. An electron spin is always affected in a real system by local magnetic fields, induced by another nuclear and electron n spins [41]:

$$B_{loc}^2 = \left(\frac{\mu_0}{4\pi}\right)^2 \frac{1}{4n}\gamma_e^2\hbar^2 S(S+1) \times \sum_{i,j} \frac{\left(1-3\cos^2\theta_{ij}\right)}{r_{ij}^6} = \frac{M_2}{3\gamma_e^2} \quad (6)$$

where θ is the angle between $\boldsymbol{r}_{ij}$ and $\boldsymbol{B}_0$ vectors and M_2 is the second moment of a spectral line. The probability of Raman relaxation of PC localized on the chains in π-conducting Q1D polymers is determined as following [42]

$$P = P_{\mathrm{D}} + P_{\mathrm{R}} = k_1 n \boldsymbol{B}_0^{-2} T + k_2 n \boldsymbol{B}_0^{-2} T^2 \tag{7}$$

The spin interaction with the environment leads to that a line of a finite width and a shape, depending on an interaction rate, is registered rather than δ-function, characteristic of an isolated spin. The line with Lorentzian shape and maximum intensity between extrema $I_{\max}^{\mathrm{L}}$ is registered when a line broadening is stipulated by fast fluctuating local magnetic fields as compared with the time of spin-lattice transitions [43]

$$I_{\mathrm{L}} = \frac{16}{9} I_{\mathrm{L}}^{\max} \frac{(B - \boldsymbol{B}_0)}{\Delta B_{\mathrm{pp}}^{\mathrm{L}}} \left[1 + \frac{4}{3} \frac{(B - \boldsymbol{B}_0)^2}{\left(\Delta B_{\mathrm{pp}}^{\mathrm{L}}\right)^2} \right]^{-2} \tag{8}$$

where $\Delta B_{\mathrm{pp}}^{\mathrm{L}}$ is the line width between the extrema. In the opposite case, the line is defined by Gaussian distribution function [43]

$$I_{\mathrm{G}} = \sqrt{e}\, I_{\mathrm{G}}^{\max} \frac{(B - \boldsymbol{B}_0)}{\Delta B_{\mathrm{pp}}^{G}} \exp\left[- \frac{2(B - \boldsymbol{B}_0)^2}{\left(\Delta B_{\mathrm{pp}}^{G}\right)^2} \right] \tag{9}$$

Spin–spin exchange interactions, realized in a paramagnetic system, may result in some cases in the appearance of more complicated line shapes, described by a convolution of Lorentzian with Gaussian. The line shape analysis of spin-modified systems enables the definition of radical distribution peculiarities and their local concentrations. For example, when the equivalent PCs with concentration n are arranged chaotically, the line shape is attributed to Lorentzian distribution function with the width [44] $\Delta B_{\mathrm{pp}}^{\mathrm{L}} = 4\lambda_{\mathrm{e}} \hbar n$ and with PC, arranged regularly, it is the case of Gaussian with the width $\Delta B_{\mathrm{pp}}^{\mathrm{L}} = 2\gamma_{\mathrm{e}} \hbar n$. In the mixed cases, the line shape transforms to Lorentzian one at a distance from the center $\delta B \le 4\gamma_{\mathrm{e}} \hbar / r^3$ (here r is a distance between magnetic dipoles) and with the width $\Delta B_{\mathrm{pp}}^{\mathrm{L}} = 4\gamma_{\mathrm{e}} \hbar n$ in the center and it becomes of Gaussian type on the tails at $\delta B_{\mathrm{pp}}^{\mathrm{G}} \ge \gamma_{\mathrm{e}} \hbar / r^3$ and with the width of $\Delta B_{\mathrm{pp}}^{\mathrm{G}} = \gamma_{\mathrm{e}} \hbar \sqrt{n / r^3}$. Finally, in a real spin system, an exchange with ν_{ex} frequency, which can provide an additional acceleration to relaxation processes is always realized between spin-packets separated by $\Delta \omega_{ij}$ distance. In this case, the spin–spin relaxation rate is derived from the formula [45]

$$T_2^{-1} = T_{2_0}^{-1} + \frac{\Delta \omega_{ij}^2}{8 \nu_{\mathrm{ex}}} \tag{10}$$

where $T_{2_0}^{-1}$ is the line width at the absence of an interaction between PC.

Spin relaxation is essentially accelerated when different channels of energy exchange between spin reservoir and a lattice appear, for example, owing to the defrosting of spin mobility and/or other molecular processes. For an example, the relaxation in solids is affected by lattice oscillations, slow rotation, and torsion (libration) molecule motions.

Another channel for an electron relaxation is the fast electron spin diffusion. The approach of random walk treatment [46] provides, that the depinning of 1D and 3D spin diffusion with $\nu_{\parallel,\perp}$ frequency changes the time of spin–spin relaxation of a spin-packet in solids in the motionally narrowed regime according to [47]

$$T_2^3 = T_{2_0}^4 \nu_{\parallel} \tag{11}$$

$$T_2 = T_{2_0}^2 \nu_{\perp} \tag{12}$$

where T_{2_0} is spin–spin relaxation time without spin mobility.

An asymmetry of EPR spectrum (so-called Dyson-like line [48]) is often observed on investigating the compounds exhibiting a sufficient conductivity. This effect is attributed to a skin-layer formation on a sample surface, which is caused by the interaction of charge carriers with an electromagnetic polarizing field. The thickness of skin-layer δ is

$$\delta = \frac{1}{\sqrt{\pi \mu_0 \nu_{\mathrm{e}} \sigma_{\mathrm{AC}}}} \tag{13}$$

where μ_0 is the permeability of the vacuum and σ_{AC} is a specific conductivity of a sample. The depth of an electromagnetic field penetration into a sample is limited by δ value and depends on a sample paramagnetic susceptibility, which varies in a resonance region. This phenomenon affects the absorption of electromagnetic energy, incident on a sample. When the skin-layer thickness is less than a characteristic size of a sample, the time of charge carrier diffusion through the skin-layer becomes essentially less than a spin relaxation time. Therefore, when the size of a sample is comparable with the skin-layer thickness, a line shape distortion characterized by an asymmetry factor A/B (the ratio of intensities of the spectral positive peak to negative one), arises together with its shift into lower fields and the drop of technique sensitivity.

Spin motion induces a local magnetic field $B_{\mathrm{loc}}(t)$, fluctuating rapidly with time in the point of another (electron or nuclear) spin arrangement due to dipole and hyperfine spin–spin interactions. Diffusion dynamics of particles is the most appropriately characterized with a motion propagator $P(r, r_0, t)$ in EPR theory. $P_{\mathrm{tr}}(r, r_0, t)\mathrm{d}r$ value for translating propagator of motion characterizes the probability of that, if the j-th particle is located in r_0 point with respect to the i-th particle at the initial moment, then it is located in $(r + \mathrm{d}r)$ range with respect to a new location of the i-th particle at $t = \tau$ moment.

An analytical form of motion propagator depends on the diffusion dynamics model, applied to condensed systems [49]. This propagator is a solution of a well-known Brownian diffusion equation

$$\frac{\mathrm{d}P(r, r_0 \tau)}{\mathrm{d}t} = \mathbf{D} \Delta P(r, r_0, \tau) \tag{14}$$

with the initial condition $P(r,r_0,t)=\delta(r-r_0)$, where $\mathbf{D}=[D_i]$, $D_i=\nu_i c_i$ is the diffusion coefficient, ν_i is a diffusion rate and c_{1i} is a proportionality constant, considering the discreteness of a real system, i is unit vector of molecular coordinate system. The solution of Eq. (14) is the following for the case of 1D spin diffusion

$$P(r,r_0,\tau)=\frac{1}{\sqrt{4\pi\nu_\parallel\tau}}\exp\left[-\frac{(r-r_0)^2}{4\nu_\parallel c_\parallel^2\tau}\right]\exp(-\nu_\perp\tau) \tag{15}$$

where $\nu_\parallel$ and $\nu_\perp$ are intrachain and interchain spin diffusion rates, respectively. The latter exponent multiplier of Eq. (15) is introduced because of spin interaction hopping probability.

The diffusion motion has an ordered character in solids and is realized over crystal lattice centers. For this case, the motion propagator is estimated with lattice sums and depends on the symmetry and parameters of a lattice. Some lattice sums have been calculated earlier [49,50].

The experimental electron relaxation time values enable the establishment of molecular dynamics in condensed media in terms of the models described above. The relationship between electron relaxation times and parameters of molecular mobility is defined by the Hamiltonian of interaction and the accepted model of molecular mobility. This relationship can be generally written as $T_{1,2}=f[J(\omega)]$, where $J(\omega)$ is a function of spectral density, which is of significance in EPR relaxation theory. Fourier transformation of auto-correlation function $G(\tau)=B_{\mathrm{loc}}(t)\,B_{\mathrm{loc}}(t+\tau)$ of a fluctuating field performs as $J(\omega)$ spectral components (harmonics) summation within ω variation range of $0<\omega<\infty$

$$J(\omega)=\int_{\infty}^{+\infty}\overline{G(\tau)}\exp(-i\omega\tau)\mathrm{d}\tau \tag{16}$$

A vinculum in Eq. (16) indicates $G(\tau)$ value averaging over spin ensemble. Therefore, if $G(\tau)$ function varies for each molecule and every t moment, the average function value is, however, equal for all molecules and does not depend on t. Oscillations, coming into a resonance at a frequency multiple of $\nu_0=\omega_0/2\pi$, induce the transitions between ground and excited spin states and result in the acceleration of spin-lattice relaxation. The spin system having given an energy quantum to a lattice reservoir comes back to equilibrium with a lattice after T_1 period of time. Therefore, the measured T_1 value is to be proportional to a power $J(\omega)$ or spectral density of $G(t)$ time correlation function of a fluctuating local field. Thus, a frequency dependence of $J(\omega)$ spectral density can be obtained on measuring spin-lattice relaxation time as a function of frequency.

Time correlation function may be conventionally expressed with a motion propagator [49]

$$G(\tau)=\int\int A(r_0,t)\,P(r,r_0,\tau)\,F(r_0)\,F^*(r)\mathrm{d}r\mathrm{d}r_0 \tag{17}$$

for a homogeneous system and with

$$G(\tau)=c_i\sum_{r}^{n}\sum_{r_0}^{n}A(r_0,t)\,P(r,r_0,\tau)\,F(r_0)\,F^*(r)\mathrm{d}r\mathrm{d}r_0 \tag{18}$$

for a discrete system. Here $F(t)$ is a random time function; $F(r)$ is a function of probability of two spins location at r distance at t moment; $A(r,t)$ is a probability of spin location at r distance at t moment, which is equal to spin concentration n. The proportional coefficient c_i in Eq. (18) is equal to the lattice constant of the discrete system. $F(r_0)F^*(r)$ product depends on a dipole and a scalar spin interaction. The motion propagator $P(r,r_0,t)$ is mainly defined by spin dynamics dimension; therefore, the spin motion dimension is also reflected in $J(\omega)$ spectral density, which appears as Fourier-image of $G(r,r_0,t)$ (see Eq. (16)).

The function of spectral density is more complex for 1D translation diffusion. Fourier-image of $G(r,r_0,t)$ is [51]

$$J_{1\mathrm{D}}(r,r_0,\omega)=J_{1\mathrm{D}}(\omega)\,f_{1\mathrm{D}}(r-r_0,\omega) \tag{19}$$

where

$$J_{1\mathrm{D}}(\omega)=\frac{1}{\sqrt{4\pi\nu_\parallel\nu_\perp}}\sqrt{\frac{1+\sqrt{1+(\omega/2\nu_\perp)^2}}{1+(\omega/2\nu_\perp)^2}}$$

$$=\begin{cases}(4\pi\nu_\parallel\omega)^{-1/2}, & \text{at } \nu_\parallel\gg\omega\gg\nu_\perp\\ (4\pi\nu_\parallel\nu_\perp)^{-1/2}, & \text{at } \omega\ll\nu_\perp\end{cases}, \tag{20}$$

$$f_{1\mathrm{D}}(r-r_0,\omega)=\exp(-xu)\left(\cos xu-\frac{\upsilon}{u}\sin xu\right),$$

$$x=c_\parallel|r-r_0|\sqrt{2\nu_\perp/\nu_\parallel},$$

$$u=\sqrt{1+\frac{\sqrt{1+(\omega/2\nu_\parallel)^2}}{2}},$$

$$\upsilon=\sqrt{\frac{1-\sqrt{1+(\omega/2\nu_\parallel)^2}}{2}}.$$

Eq. (19) is used for analyzing the short-range scalar coupling at the low-frequency range $\omega\ll\nu_\parallel c^2/(r_0-r)^2$. $f_{1\mathrm{D}}(r-r_0,\omega)\approx 1$ at this frequency range; therefore, Eq. (19) can be also used for dipole coupling analysis. At $\omega\ll\nu_\parallel c^2/(r_0-r)^2$ frequencies, the spectral density of auto-correlation function appears as follows:

$$J(\omega)=nJ_{1\mathrm{D}}(\omega)\sum_{r}^{n}\sum_{r_0}^{n}F(r_0)F^*(r)\,f_{1\mathrm{D}}(|r-r_0|)$$

$$=nJ_{1\mathrm{D}}(\omega)\sum_{r}^{n}\sum_{r_0}^{n}\frac{(1-3\cos^2\vartheta)^2}{r_1^3r_2^3} \tag{21}$$

where n is in the present case the probability of spin location at r_1 at initial time moment and ϑ is the angle between $\boldsymbol{r}_1$ and $\boldsymbol{r}_2$ vectors.

Let the general relationships for relaxation times be written. An assumption must be done, that dipole and scalar HFIs are realized between electron and nuclear spins. A dipole interaction is more strong and anisotropic, while a scalar HFI is isotropic and significantly weaker. Other interactions do not depend on spin dynamics and yield a small contribution to T_1 and T_2; therefore, they may be neglected.

For the case of dipole–dipole interaction between unpaired electrons, the expressions for electron relaxation rates are [49]

$$T_1^{-1} = \frac{2}{3}\alpha^2 S(S+1)n\left[J(\omega_e) + J(2\omega_e)\right] \tag{22a}$$

$$T_2^{-1} = \frac{3}{8}\alpha^2 S(S+1)n\left[J(0) + 10J(\omega_e) + J(2\omega_e)\right] \tag{22b}$$

where $\alpha = \mu_0\gamma_e\gamma_p h/2$, or in case of polycrystalline samples after the averaging over spin ensemble

$$T_1^{-1} = \langle\Delta\omega^2\rangle\left[J(\omega_e) + 4J(2\omega_e)\right] \tag{23a}$$

$$T_2^{-1} = \frac{1}{2}\langle\Delta\omega^2\rangle\left[3J(0) + 5J(\omega_e) + 2J(2\omega_e)\right] \tag{23b}$$

where $\langle\Delta\omega^2\rangle = 1/5(\mu_0/4\pi)^2\gamma_e^4\hbar^2 S(S+1)\Sigma\Sigma(1-3\cos^2\theta)^2 r_1^{-3}r_2^{-3}$. Note, that in the case of preferable dipole–dipole interaction of PC, the equations for relaxation rates of PC in partially oriented system with polymer chains orientation degree A consist of two terms

$$T_1^{-1} = A\langle\Delta\omega^2\rangle\left[P_1 J(\omega_e) + 4P_2 J(2\omega_e)\right] + (1-A)\langle\Delta\omega^2\rangle\left[P_1^{\perp} J(\omega_e) + 4P_2^{\perp} J(2\omega_e)\right] \tag{24a}$$

$$T_2^{-1} = \frac{A}{2}\langle\Delta\omega^2\rangle\left[3P_0 J(0) + 5P_1 J(\omega_e) + 2P_2 J(2\omega_e)\right] + \frac{1-A}{2}\langle\Delta\omega^2\rangle\left[3P_0^{\perp} J(0) + 5P_1^{\perp} J(\omega_e) + 2P_2 J(2\omega_e)\right] \tag{24b}$$

where P_i and $P_i^{\perp}$ are attributed to oriented and chaotically situated chains, respectively.

The equations, presented above reveal that spin transitions are induced by dipole–dipole interaction on the first and the second harmonics of the polarizing field. The equations for contributions into relaxation rates under a common $\omega_e \gg \omega_I$ condition are

$$T_1^{-1} = \frac{1}{3}\alpha^2 I(I+1)n\Sigma\Sigma J(\omega_e) \times\left[2 + \frac{S(S+1)(\langle I_z\rangle - I_0)}{I(I+1)(\langle S_z\rangle - S_0)}\right] \tag{25a}$$

$$T_2^{-1} = \frac{1}{30}\alpha^2 I(I+1)n\Sigma\Sigma\left[4J(0) + 3J(\omega_I) + 13J(\omega_e)\right] \tag{25b}$$

The isotropic HFI contribution to electron relaxation rates yields

$$T_1^{-1} = \frac{1}{3}\alpha^2 I(I+1)n_p J(\omega_e - \omega_I)_e) \times\left[1 - \frac{S(S+1)(\langle I_z\rangle - I_0)}{I(I+1)(\langle S_z\rangle - S_0)}\right] \tag{26a}$$

$$T_2^{-1} = \frac{1}{6}\alpha^2 I(I+1)n_p\left[J(0) + J(\omega_e - \omega_I)\right] \tag{26b}$$

where n_p is nuclear spin concentration. The averaged lattice sum Σ_{ij} is estimated for each interaction type. The relationships, presented above, are correct either for rotation or translation diffusion at corresponding functions $J(\omega)$ of spectral density.

The contribution of spin-lattice relaxation, including $(\langle I_z\rangle\text{-}I_0)/(\langle S_z\rangle\text{-}S_0)$ multiplier, corrects for cross-relaxation between electron and nuclear spins, stipulated by Overhauser effect [49]. This contribution may be ignored in strong magnetic fields, because the probability P_{cr} of cross-relaxation processes decreases with the growth of an external magnetic field intensity $\boldsymbol{B}_0$ according to [52]

$$P_{cr} = k_1\exp\left(-\frac{\hbar^2\gamma_e^2\boldsymbol{B}_0^2}{k_B T}\right) \tag{27}$$

where k_1 is constant. It derives from the equations, that $T_1 > T_2$ at $\omega_e \to \infty$ and $T_1 \approx T_2$ at $\omega_e \to 0$. If T_1 is always a function of the first and the second harmonics of resonance frequency, the expression for T_2 includes the frequency-independent term $J(0)$, called as a secular broadening (T_2^{-1}). Frequency-dependent terms of the equations for T_1^{-1} define the so-called spin life time or nonsecular broadening (T_1^{-1}). $T_1/T_1^{\parallel}$ ratio is equal to $10/7$, $10/8$, and $10/5$ for dipole, anisotropic, and isotropic HFIs, respectively, and enables the identification of relaxation mechanism in each specific case by measuring relaxation times at several resonance frequencies [51].

2.3. Spin-packets saturation and saturation transfer effects

The relaxation of a magnetization vector of a single spin-packet to the equilibrium state is mainly described by

the Bloch's equations for a slow resonance passage and saturation absence, when the saturation factor $s = \gamma_e B_1 \tau \ll 1$ (here $\tau = \sqrt{T_1 T_2}$ is the effective relaxation time). In some cases, the lines exhibiting the integral function of spin-packets distribution are observed at modulation method of spectra registration instead of the traditional first derivative of absorption signals or dispersion. This phenomenon was called as passage effect and are widely considered in literature [35,53–57] in terms of fast passage of saturated spin-packets.

The spin-packet shape is assigned by the following set of time characteristics: T_1, T_2, $(\gamma_e \Delta B_{1/2})^{-1}$, ω_m^{-1}, $(\gamma_e B_m)^{-1}$, $(\gamma_e B_1)^{-1}$, and $B_1/(dB/dt)$. The first three of them are stipulated by the origin of the substance and the remaining ones are the instrumental parameters. If the parameters of a spectrum registration satisfy certain inequalities, it becomes possible to analyze the behavior of a magnetization vector $\boldsymbol{M}$ qualitatively.

If the inequality $s < 1$ is valid, τ does not exceed $(\gamma_e B_1)^{-1}$ precession time of vector $\boldsymbol{M}$ about B_1 so the saturation of spin-packets is not realized. The passage effects are not registered in this case, and analytical expressions (8) and (9) for a spin-packet line shape are successfully found. For this case, the analysis of the possible line shape distortion is sufficiently elucidated in literature (see, e.g., Refs. [58,59]).

The saturation of spin-packets is realized, provided that the opposite condition $s \geq 1$ holds.

The qualitative characteristics of passage effects are defined by the time of resonance passage $B_1/(dB/dt)$ to the effective relaxation time τ ratio. If $B_1/(dB/dt) > \tau$, the spin system comes to equilibrium when the sinusoidal modulation field is at one end of its excursion with a sweep rate going to zero. $\boldsymbol{M}$ and $\boldsymbol{B}_0$ vectors are parallel and remain unchanged during a sweep, assuming that adiabatic condition $\gamma_e \omega_m B_m \ll \gamma_e^2 B_1^2$ holds.

The dispersion or absorption signal is detected as the projection of $\boldsymbol{M}$ on $+x$-axis. If the system now comes to equilibrium again at the other end of the sweep, then $\boldsymbol{M}$ will initially be along $+z$-axis, $\boldsymbol{M}$ and $\boldsymbol{B}_{eff}$ will be antiparallel during the passage, and the signal will be the projection of $\boldsymbol{M}$ on $-x$-axis. Thus, the signal from a single spin-packet is $\pi/2$-out-of-phase with respect to the field modulation. The first derivative of the dispersion signal U is generally written as [60]

$$U = u_1 g'(\omega_e)\sin(\omega_m t) + u_2 g(\omega_e)\sin(\omega_m t - \pi) + u_3 g(\omega_e)\sin\left(\omega_m t \pm \frac{\pi}{2}\right) \quad (28)$$

It is obvious, that $u_2 = u_3 = 0$ without microwave frequency (MWF) saturation. The saturation being realized, the relative intensity of u_1 and u_3 components is defined by the relationship between the relaxation time of a spin-packet and the rate of its resonance field passage. If the rate of resonance passage is high and the modulation frequency is comparable or higher than τ^{-1} value, the magnetic field variation is too fast and the spin system does not follow these variations. At adiabatic condition, $\omega_m B_m \ll \gamma_e B_1^2$ such delay leads to that spin can ''see'' only an applied average magnetic field, and the first derivative of a dispersion signal is mainly defined by the $u_2 g(\omega_e)$ and $u_3 g(\omega_e)$ terms of an integral form of Eq. (28), where $u_2 = M_0 \pi \gamma_e^2 B_1 B_m T_2/2$ and $u_3 = M_0 \pi \gamma_e^2 B_1 B_m T_2/(4\omega_m T_1)$.

When the relaxation time does not exceed the modulation period, $\tau < \omega_m$, and $\tau > B_1/(dB/dt)$, the magnetization vector manages to relax to equilibrium state during one modulation period; therefore, the dispersion signal of a spin-packet is independent on the relationship of its resonance field and an external field $\boldsymbol{B}_0$. The sign of a signal is defined by that from what side the resonance is achieved. In this case, the shape of $\pi/2$-out-of-phase component of a dispersion signal also reproduces the shape of the function of spin-packets distribution, and the first derivative of a dispersion signal is mainly defined by $u_1 g'(\omega_e)$ and $u_3 g(\omega_e)$ terms of Eq. (28), where $u_1 = M_0 \pi \gamma_e^2 B_1 B_m$ and $u_3 = M_0 \pi \gamma_e^2 B_1 B_m T_1 T_2/2$. Thus, the times of electron relaxation of a spin system can be estimated by registering the components of a dispersion spectrum of saturated spin-packets at appropriate phase tuning of a phase discriminator.

The molecular processes in polymer systems are often realized with characteristic correlation time $\tau_c \geq 10^{-7}$ s. Such a dynamics is studied by the saturation transfer EPR method [35], which based on the fast passage of saturated spin-packets and broadens the correlation time range up to 10^{-3} s. The most sensitive to such molecular motions are $\pi/2$-out-of-phase first harmonic dispersion and second harmonic absorption spectra. According to the method, the adiabatic condition can be realized for the radicals oriented by, for example, x-axis along $\boldsymbol{B}_0$ and it cannot be realized for the radicals of other orientations. This results in the elimination of the saturation of the spin-packets, whose y- and z-axes are oriented parallel to the field $\boldsymbol{B}_0$ and consequently to the decrease of their contribution to the total ST-EPR spectrum. Therefore, slow spin motion should lead to an exchange of y and z spectral components and to the diffusion of saturation across the spectrum with the average transfer rate [35]

$$\left\langle \frac{d(\delta B)}{dt} \right\rangle = \sqrt{\frac{2}{3\pi^2 T_1 \tau_e}} \frac{\sin\vartheta\cos\vartheta\left(B_\perp^2 - B_\parallel^2\right)}{\sqrt{\left(B_\perp^2 \sin^2\vartheta + B_\parallel^2 \cos^2\vartheta\right)}} \quad (29)$$

where δB is the average spectral diffusion distance, $B_\perp$ and $B_\parallel$ are the anisotropic EPR spectrum components arrangement along the field, ϑ is the angle between $\boldsymbol{B}_0$ and a radical axis.

This method seems to be useful for the registration of anisotropic superslow radical and spin-modified macro-

molecule fragments rotations, provided that a separate registration of all components of their ST-EPR spectra is carried out.

2.4. Spin transfer mechanisms in low-dimensional systems

Electrodynamic properties of conducting polymers whose conductivity can vary by 12–15 orders of magnitude, are defined by various parameters. In a macroscopic conductivity measurement, a superposition of different processes is obviously observed:

(i) 1D conduction along the polymer chains;
(ii) Hopping between the chains;
(iii) Tunneling between conducting regions separated by less conducting parts of fibrils;
(iv) Fluctuation-induced tunneling between fibrils.

It is quite obvious, that the contributions of these processes to the total conductivity depend on the polymer structure, the method of synthesis, and doping level. As the nonlinear excitations, namely solitons, polarons, and bipolarons can have a major effect on the electronic states accessible for electrons, traversing a polymer, they can dramatically affect transport properties.

There are some possible mechanisms of charge transfer in conducting polymers. Kivelson [61] proposed a phenomenological model for phonon-assisted hopping of electrons between soliton sites in undoped and slightly doped polyacetylene (PA). In the frames of this model, charged solitons are coulombically bound to charged impurity sites. The excess charge on the soliton site makes a phonon-assisted transition to a neutral soliton moving along another chain. If this neutral soliton is located near charged impurity at the moment of charge carrier transfer, the energy of the charge carrier remains unchanged before and after the hop. The temperature dependency of the conductivity is then defined by the probability of that the neutral soliton is located near the charged impurity and the initial and the final energies are within k_BT, hence conductivities can be determined at direct current (DC) and at alternating current (AC) measurements [61]

$$\sigma_{DC}(T) = \frac{k_1 e^2 \gamma(T) \xi \langle y \rangle}{k_B T N_i R_0^2} \exp\left(\frac{2k_2 R_0}{\xi}\right) = \sigma_0 T^n \quad (30a)$$

$$\sigma_{AC}(T) = \frac{N_i^2 e^2 \langle y \rangle \xi_\parallel^3 \xi_\perp^2 \nu_e}{384 k_B T} \left[\ln \frac{2\nu_e L}{\langle y \rangle \gamma(T)}\right]^4 = \frac{\sigma_0 \nu_e}{T}\left[\ln \frac{k_3 \nu_e}{T^{n+1}}\right]^4 \quad (30b)$$

where $k_1 = 0.45$, $k_2 = 1.39$, and k_3 are constants, $\gamma(T) = \gamma_0 (T/300\ \mathrm{K})^{n+1}$ is the transition rate of a charge between neutral and charged soliton states, $\langle y \rangle = y_n y_{ch} (y_n + y_{ch})^{-2}$, y_n, and y_{ch} are, respectively, the concentrations of neutral and charged carriers per monomer unit, $R_0 = (4\pi N_i/3)^{-1/3}$ is the typical separation between impurities which concentration is N_i; $\xi = (\xi_\parallel \xi_\perp^2)^{1/3}$, $\xi_\parallel$, and $\xi_\perp$ are dimensionally averaged, parallel, and perpendicular decay lengths for a charge carrier, respectively; L is the number of monomer units per a polymer chain. In this case, a weak coupling of the charge with the polymer lattice is realized when hops between the states of a large radius take place.

In some low-conducting polymers, the charge can be transferred by small polarons. In this case, the relations for AC conductivity depending on the polymer structure can be the following [62]

$$\sigma_{AC}(T) = \sigma_0 \left[k_B T + \frac{4E_H}{\ln(2\nu_{ph}/\nu_e)} \ln\left(1 - \frac{k_B T}{E_H} \ln \frac{2\nu_{ph}}{\nu_e}\right)\right] \quad (31)$$

or

$$\sigma_{AC}(T) = \frac{\sigma_0}{k_B T} (E_H/k_B T)^4 \exp\left(-\frac{E_a + E_H}{k_B T}\right) \quad (32)$$

where E_H and E_a are the hopping and activation energies, respectively, and $\nu_{ph} = \omega_{ph}/2\pi$ is the $2k_F$ lattice optical phonon frequency.

If the coupling of the charge with the lattice is more strong, multiphonon processes dominate. The mobility ultimately becomes simply activated when the temperature exceeds the phonon temperature characteristic of the highest energy phonons with which electron states interact appreciably. In this case, the strong temperature dependency of the hopping conductivity is more evidently displayed in AC conductivity.

A strong temperature dependency for σ_{AC} can be stipulated by a thermal activation of charge carriers from widely separated localized states in the gap to close localized states in the tails of the valence and conducting bands. Both σ_{DC} and σ_{AC} are defined mainly by a number of charge carriers excited to the band tails, therefore [63]

$$\sigma_{DC}(T) = \sigma_0 \exp\left(-\frac{E_a}{k_B T}\right) \quad (33a)$$

$$\sigma_{AC}(T) = \sigma_0 T \nu_e^\gamma \exp\left(-\frac{E_a}{k_B T}\right) \quad (33b)$$

Here $0 < \gamma < 1$ is a constant and E_a is the energy for activation of charge carrier to extended states. As the doping level increases, the dimensionality of the polymer system rises and activation energy of charge transfer decreases. Parneix et al. [64] showed that $\gamma = 1 - k_B T/E_a$ ($E_a = 0.18$ eV) dependency for poly(3-methylthiophene). At the same time, an approximately linear dependency of γ on E_a was registered [65] for other polymers. Therefore, γ value can be varied in 0.3–0.8 range and it reflects the dimensionality of a system under study.

E_a value can depend on the conjugation length and conformation of the polymer chains. Indeed, $E_a \propto n_d$ and $E_a \propto n_d^{1/2}$ dependencies were obtained for *trans*-PA with

different doping level [66,67] (here n_d is the concentration of sp^3-defects in a sample). $E_a \propto (n_\pi + 1)/n_\pi^2$ dependency was estimated [68] for relatively short π-conducting systems having n_π delocalized electrons. In order to reduce the band gap, the planarity of the polymer chains may be increased [69,70], for example, by introducing an additional six-membered ring to a monomer unit [71].

For comparatively high polymer doping levels, the Mott variable range hopping (VRH) model [72] is more appropriate. This model of charge carriers hopping in d dimensions yields

$$\sigma_{DC}(T) = \sigma_0 \exp\left[-\left(\frac{T_0}{T}\right)^{\frac{1}{d+1}}\right] \quad (34a)$$

$$\sigma_{AC}(T) = \frac{2}{3}\pi^2 e^2 k_B T n^2(\varepsilon_F)\langle L\rangle^5 \nu_e \left[\ln\frac{\nu_0}{2\pi\nu_e}\right]^4 \quad (34b)$$

where $\sigma_0 = 0.39\nu_0 e^2[n(\varepsilon_F)\langle L\rangle/(k_B T)]^{1/2}$ at $d = 1$, $\sigma_0 = 1.8\nu_0 e^2 n(\varepsilon_F)T_0/(T\langle L\rangle)$ at $d = 3$, ν_0 is a hopping attempt frequency, $T_0^{-1} = 0.62 k_B n(\varepsilon_F)\langle L\rangle 3$ is the percolation constant or effective energy separation between localized states depending on disorder degree in amorphous regions; $\langle L\rangle = (L_\parallel L_\perp^2)^{1.3}$, $L_\parallel$, and $L_\perp$ are the averaged length of charge wave localization function and its projection in parallel and perpendicular directions, respectively.

Thus, numerous transport mechanisms with different $\sigma_{AC}(\nu_e,T)$ dependencies are realized in conducting polymers. These mechanisms can be directly associated with the evolution of both crystalline and electron structures of the systems. The possibility of soliton-, polaron- and bipolaron-type charge carriers states formation in conducting polymers leads to a variety in transport phenomena, including the contribution of mobile nonlinear excitations to the conductivity.

3. Experimental

The sensitivity of EPR method (i.e., minimum number of the registering spins N_{min}) depends on the registration frequency ν_e as following [33]

$$N_{min} = \frac{k_1 V}{Q_0 k_f \nu_e^2 P^{1/2}} \quad (35)$$

where k_1 is constant, V is sample volume, Q_0 is an unloaded quality factor of a cavity, k_f is cavity filling coefficient, and P is MWF power applied to a cavity input. With k_f and P being constants, $N_{min} \propto (Q_0\nu_e^2)^{-1}$ and $Q_0 \propto \nu_e^{1/2}$, that is, $N_{min} \propto \nu_e^{-\alpha}$, where $\alpha = 1.5$ [33]. In practice, α can be varied from 0.5 to 4.5 [33] depending on spectrometer characteristics, registration conditions, and sample size.

By the present moment, a wide range of frequencies of electromagnetic radiation from several megahertz [73,74] up to few terahertz [75] is successfully used in EPR spectroscopy, that corresponds to 10^2–10^{-6} m wavelengths. However, EPR spectroscopy of 2-mm range required $\nu_e = 140$ GHz and $B_0 \approx 5$ T for $g_e = 2$ provides the highest potential possibilities of the method [37,38]. This waveband EPR technique enables a more complete study of such new effects, attributed to most semiconductor systems, as the dependency of electron spin relaxation on magnetic field strength, specific features of spin resonance excitation at the close values of Zeeman quantum energy and the transitions between the states of localized charge carriers, field dependency of effective mass of charge carriers and many other.

The basic block-scheme of this device is given in Fig. 1.

The spectrometer is assembled as a direct amplification circuit with H_{011} type reflecting cavity, a double SHF T-bridge and a low-temperature n-SbIn ballometer. The main part of the spectrometer includes the microwave solid-state avalanche transit time diode oscillator (11) with some elements of the waveguide section and a cryostat (1) with a superconducting solenoid (2), in whose warm channel the tunable cavity (5) with a sample (6), temperature-sensitive (3) and modulating (4) coils are inserted. A sample in a thin (0.5 mm) quartz capillary (7 mm long) is put into the center of the cavity with the mobile plunger. The microwave cavity with the sample inside is temperature-controlled (6–380 K).

The quality factor Q of the cavity (inside diameter is 3.5 mm, operation height is 1.5 mm) is equal to 2000. The value of microwave field magnetic component B_1 is equal to 20 μT in the center of the cavity. The magnetic field inhomogeneity in the point of sample arrangement does not exceed 10 μT/mm. The absolute point-sample sensitivity of the spectrometer is 5×10^8 spin/mT at room temperature and is unique for EPR spectroscopy (the higher sensitivity is attained only in the specific ''nonsteady state'' experiments with an optical or ''chemical'' signal registration [32,76]). The latter value is two orders of magnitude lower than N_{min} obtained at 3-cm waveband. The concentration sensitivity for aqueous samples is 6×10^{13} spin/(mT cm^3). All experiments are carried out at high (100 kHz) AC modulation frequency.

A quite important problem is to choose the appropriate standards for a precise device tuning, a magnetic field scanning and g-factor scale calibration. The standard must be arranged close to a sample inside a small cavity; therefore, it must produce a sufficiently intensive narrow signal, being of a small size. For example, Mn^{2+} in MgO standard with $I = 5/2$, $a = 8.74$ mT, and $g_{eff} = 2.00102$ satisfies these conditions most of all. The second-order correction to the effective resonance field [77] $\delta B = a^2[I(I + 1) - m^2]/2B_0 = 65$ mT for this standard and does not contribute an essential error to the magnetic parameters

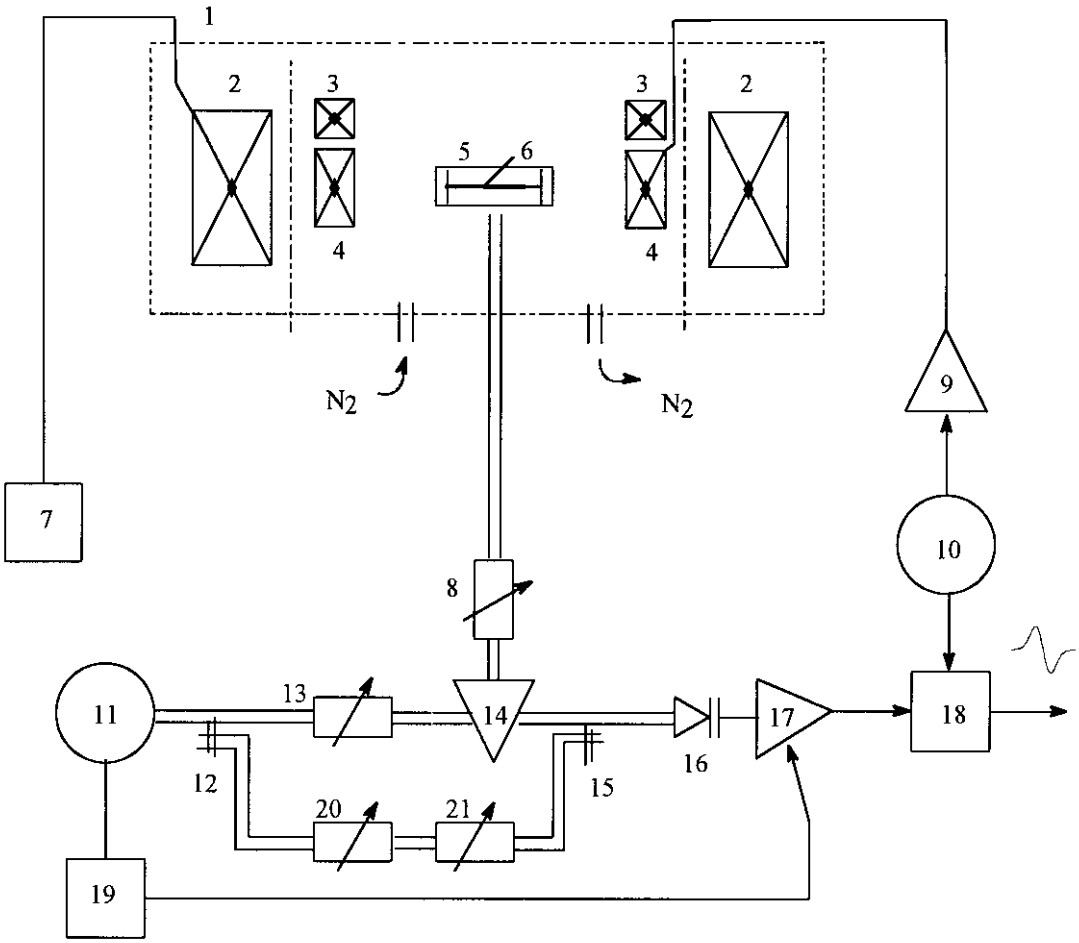

Fig. 1. The sketch of 2-mm waveband EPR spectrometer: 1 — helium cryostat, 2 — superconducting solenoid, 3 — temperature-sensitive coil, 4 — AC modulation coil, 5 — microwave cavity, 6 — sample, 7 — solenoid supply, 8 and 21 — phase shifter, 9 — AC modulator amplifier, 10 — AC oscillator, 11 — diod Hanna solid state oscillator, 12 and 15 — directional MWF couplers, 13 and 20 — MWF attenuators, 14 — MWF circulator, 16 — superlow temperature (4.2 K) barretter, 17 — AC preamplifier, 18 — phase detector and EPR amplifier, 19 — section of auto-adjustment of the MWF clystron oscillator.

measurement. Commonly, MgO powder is attached by a toluene solution of polystyrene to one of the cavity plungers. The signal intensity of this standard is conveniently regulated by plunger rotation about its axis, that is, due to the change of the angle between the B_1 and B_0 directions in the place of its location.

A single crystal of dibenzotetrathiofulvalene platinum hexabromide ($(DBTTF)_3PtBr_6$) with $\Delta B_{pp} = 0.48$ mT and $g = 2.00552$ was found to be suitable for the precise tuning of modulation frequency and MWF phases. This or a similar crystal with a typical size of about 0.1 mm, is attached to a middle of a quartz capillary with a sample. The precise device adjustment in the registration of a real χ' or an imaginary χ'' components of paramagnetic susceptibility χ is obtained by an attainment of the symmetric first and second derivatives of dispersion and absorption standard signals, respectively, in the device output. Modulation frequency phase is most fine adjusted by a minimum $\pi/2$-out-of-phase unsaturated signal of a standard with the following phase change by $\pi/2$. In this case, the $\pi/2$-out-of-phase signal attenuation is not less than 23 dB.

B_1 value is important in the experiments with the application of passage effects and saturation transfer. This value was estimated [38] by the following methods. The first one consisted in the registration of EPR spectrum of $(\text{fluoranthene})_2^+ PF_6^-$ cation-radical salt single crystal depending on MWF power. At 3-cm waveband EPR, this single crystal demonstrates a single narrow (3 μT) signal. Its spectrum becomes multicomponent with $\Delta B_{pp} = 55$ μT individual components width and the splitting between them of 60 μT at 2-mm waveband because of the mosaic structure of the standard. At the maximum MWF power level in the cavity, the components are broadened up to $\Delta B_{pp} \approx 61$ mT. By assuming $\Delta B_{pp}^0 = (\gamma_e T_2)^{-1}$ and $T_1 = T_2$ typical for these salt, the expression $\Delta B_{pp} = \Delta B_{pp}^0 (1 + s^2)^{1/2}$ is correct for a broadened line, from whence $B_1 = 25$ μT. The independent B evaluation, made according to formula $2B_1 = \alpha (QP)^{1/2}$, where $\alpha = 0.2$ is calculating

coefficient and $P = 0.4$ mW is MWF power, drawing by a cavity, yielded $B_1 = 19$ μT.

The accuracy of the measurement of g-factor is not higher than 3×10^{-5} and is attributed in particular to the effects, emerging at a sample freezing, to paramagnetic shielding, etc.

The resolution of EPR method is commonly characterized by $\delta B/B_0$ ratio, where δB is the minimal splitting between two lines registered. This expression is conveniently written as $\delta B/B_0 \propto \delta g/g_e$, where δg is the difference of g-factors of different PCs with equal line width. The magnetic resonance condition (2) and the equality $h\gamma_e = \mu_B g_e$ imply, that these values depend linearly on registration frequency ν_e.

As the probability of energy transfer between individual spin-packets decreases significantly in high fields (see Eq. (27)), the conditions of spin-packets saturation can be realized at quite smaller values of polarizing field B_1. Besides, the electron relaxation time of certain paramagnetic systems can increase with the growth of registration frequency. This is the reason for a more frequent appearance of fast passage effects [53–56] at 2-mm waveband, than at lower frequency EPR bands, on registering PC in polyconjugated systems and other solid state substances. In this case, EPR spectra appear as an integral (almost always Gaussian) distribution function of spin-packets.

The passage effects can be used for simple evaluations of relaxation properties of PC in polymer systems. Besides, the investigation of the passage effects enables the development of 2-mm waveband EPR spectroscopy with saturation transfer. As a spectral resolution at 2-mm band is enhanced, the opportunities of this method in more detail study of superslow molecular motion are expected to be widened. The results of the investigation of different condensed systems using these effects were described in detail in Refs. [38,78–80].

Earlier it was shown [81] that the relaxation times of saturated PC in π-conducting polymers can be determined separately from the analysis of u_1–u_3 components of its dispersion spectrum so then (see Fig. 6)

$$T_1 = \frac{3\omega_m(1+6\Omega)}{\gamma_e^2 B_{1_0}^2 \Omega(1+\Omega)} \tag{36a}$$

$$T_2 = \frac{\Omega}{\omega_m} \tag{36b}$$

(here $\Omega = u_3/u_2$, B_{1_0} is the polarizing field at which the condition $u_1 = -u_2$ is valid) at $\omega_m T_1 > 1$ and

$$T_1 = \frac{\pi u_3}{2\omega_m u_1} \tag{37a}$$

$$T_2 = \frac{\pi u_3}{2\omega_m(u_1 + 11u_2)} \tag{37b}$$

at $\omega_m T_1 < 1$. The amplitudes of u_i components are measured in the central point of the spectra, when $\omega = \omega_e$. It derives from the formulas, that the determination of B_1 value in the cavity center is not required for the evaluation of relatively short relaxation times.

The shape of $\pi/2$-out-of-phase component of the first harmonic of dispersion signal possesses a complex dependency on PC relaxation and anisotropic superslow dynamics. The parameters of the dynamics cannot be determined in general, from the analysis of a line shape of ST-EPR spectra at 3-cm EPR waveband [82,83] because of a low spectral resolution, and the effect of relaxation processes on a signal shape. Therefore, the main problems of ST-EPR method are the separation of the motion and magnetic relaxation effects, and the development of the methods of the determination of the anisotropic molecular motion parameters.

It is important, that the rotation effect on ST-EPR spectra shape is not equivalent to T_1 decrease [38]. Indeed, the spectral diffusion, stipulated by spin reorientation with correlation time τ_c, is proportional to the steepness of magnetic field change $dB(\vartheta)/d\vartheta$, that is, even in the case of isotropic rotation, it is not the same in distinct spectrum ranges, while spin-lattice relaxation, provided that it does not depend on orientation, is the same for all regions of the spectrum. It seems obvious, that the differences indicated are displayed significantly more clearly at 2-mm waveband as compared with 3-cm waveband EPR.

It was shown [38], that the transition to 2-mm waveband enables the estimation separately of characteristic times τ_c, T_1, and T_2 for the radicals, involved in the superslow motion about the different molecular axes, by using their ST-EPR spectra. If PC with anisotropic magnetic parameters moves, say, near molecular x-axis, τ_c^x of such a motion can be calculated from the relative intensities of dispersion u_3 term as following [38]

$$\tau_c^x = \tau_c^0 \left(\frac{u_3^x}{u_3^v} \right)^{-\alpha} \tag{38}$$

where α is a constant determining by an anisotropy of g-factor.

Thus, the EPR spectra of organic radicals become more informative at 2-mm waveband, their interpretation is simplified and the possibility of a more accurate determination of their magnetic resonance parameters (MRPs) change under the effect of different factors, including the change of a radical structure and/or its microenvironment arises. Besides, an independent analysis of relaxation changes in each spectral component and the anisotropic slow molecular rotations study become possible. The configuration of the spin distribution in organic radicals and the registration of several radicals with similar magnetic parameters can be more successfully estimated at this waveband.

As the spectral resolution is enhanced at 2-mm waveband EPR, that makes it possible to obtain more complete and correct information on the structure, conformation, relaxation properties of PC, stabilized in the matrix under

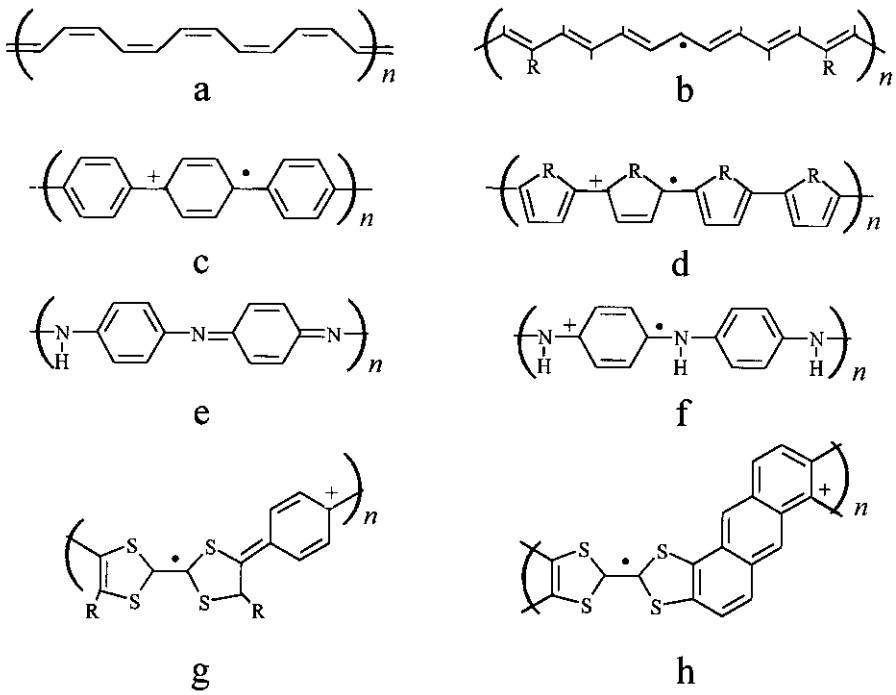

Fig. 2. Schematic representation of *cis*-PA (a), *trans*-PA (R≡H), PATAC (R≡SC_2H_5) (b), PPP (c), PT (R≡S) and PP (R≡NH) (d), PANI base (e), PANI salt (f), PTTF-1 (R≡CH_3), PTTF-2 (R≡C_2H_5) (g), PTTF-3 (h), which were studied by EPR spectroscopy. Spin charge carriers in the polymers are shown.

study, their interactions with own environment. These possibilities of the method are of a especial importance in the identification of the structure and dynamics of such complicated objects, as natural and synthetic polymers, whose properties depend on many factors and are defined by a greater number of parameters.

Section 4 of the present review considers the nature and dynamics of charge carriers and the possible charge transfer mechanisms determined by 2-mm waveband EPR spectroscopy for well-known and new powder- or film-like conducting polymers, namely PA, poly(*p*-phenylene) (PPP), polythiophene (PT), polypyrrole (PP), polyaniline (PANI), poly(*bis*-alkylthioacetylene) (PATAC), and poly(tetrathiofulvalene) (PTTF) (Fig. 2) chemically or electrochemically synthesized from the corresponding monomers.

4. Magnetic, relaxation and dynamic parameters of charge carriers in conducting polymers

As in the case of other π-systems, conducting polymers usually demonstrate a single symmetric line with $g \approx g_e$ and a line width 0.02–1.7 mT in low magnetic fields ($\nu_e \leq 10$ GHz) [28,29]. Deviations from free electron *g*-factor are mainly due to a weak coupling of the electron spin with the orbital angular momentum and are observed when an unpaired electron interacts with heteroatoms, ions of transition or rare-earth metals [52,84–88]. The line width depends on an unresolved hyperfine splitting on the *n*-th monomer site with a_i constant combined with the exchange and motional narrowing which is derived from Eqs. (10)–(12), respectively. The double-integrated intensity of $V_1(\omega)$ signal can be used for the determination of the concentration n of PC, varying within $n = 10^{22}$–10^{27} spins/m^3 for conducting polymers [28,29]. The static electron susceptibility of conducting polymers χ_0 is generally described by Eq. (5).

Another information concerning spin properties of polymer systems comes from the analysis of the line asymmetry factor A/B. Such a Dyson-like line shape is commonly observed in some inorganic substances [89], organic conducting ion-radical salts [90], *trans*-PA [91–94], polythiophene [95], PPP [96], and other conducting polymers [28], but only a few experiments were performed in order to study systematically the evolution of asymmetry factor with various parameters, for example, σ. This is the reason for the lack of the universal behavior for all doped systems, and every case must be analyzed in detail.

4.1. Polyacetylene

In the last years, PA has attracted considerable attention of the investigators due to its own unique electrodynamic properties, which can be a perspective in molecular electronics. So, at introduction donor or acceptor dopants into PA its electroconductivity measured at constant current is

changed by 10–14 orders of magnitude and reaches $\sigma_{DC} = 10^5$–10^7 S/m [5–13]. PA is the simplest conducting polymer in the great family of PPP-like organic conducting compounds of close magnetic and electrodynamic properties, that caused most extensively investigation of its properties using just this compound as an example. It can exist in *cis*- and *trans*-forms (isomers) (Fig. 2a,b), and the latter is thermodynamically more stable [97,98]. The morphology of this polymer mainly depends on the synthesis, structure of the initial monomer, the nature of the introduced dopant and the film thickness. PA is characterized by the chain location parallel to one another, forming a fibril with the thickness of few decades of nanometers and a length of few hundred nanometers. The longitudinal axes of such fibrils are arranged chaotically and can be partially oriented at sample stretching. Each fibril contains close-packed polymer chains, which exhibit crystalline structure. Thus, PA appears as a kind of polycrystal, consisting of ''crystalline'' fibrils. The crystal lattice have the following constants: $a = 0.745$, $b = 0.440$, $c = 0.430$ nm (*cis*-PA) and $a = 0.399$, $b = 0.729$, $c = 0.251$ nm (*trans*-PA) [99,100].

In PA, three of four carbon valence electrons occupy sp^2 hybridized orbitals; two of σ-type bonds constitute 1D lattice, while the third one forms a bond with hydrogen atom. In any isomer, the last valence electron has the symmetry of $2p_z$ orbital, with its charge density oriented perpendicular to the plane defined by the other three electrons. Therefore, s bonds form a low-lying completely filled valence band (VB), while π bonds form a partially filled conducting band (CB). If all bond lengths were equal, pure *trans*-PA would be Q1D metal with a half-filled band. Such a system is unstable with respect to a dimerization distortion, in which adjacent CH groups move towards one another, forming alternating double and longer single bonds. The transition between C–C and C=C bonds does not require energy changing. This Peierls distortion opens up a substantial gap in the Fermi level, so that PA is expected to be a relatively large band gap semiconductor. This twofold degeneration leads to the formation of nonlinear topological excitations, namely solitons on *trans*-PA chains [25], whose energy level is localized at mid-gap thus determining the fundamental properties of PA. The energy required for the soliton formation is equal to 0.42 eV [25].

Su, Schrieffer, and Heeger (SSH) theory [25] predicts that the spin density distribution on the soliton in *trans*-PA, associated with the domain wall in the absence of correlations, is $\rho(n) = A_0 N^{-1} \operatorname{sech}^2(n/N)\cos^2(\pi n/2)$, where n is the index of nucleus site away from the domain wall, $N = 14$ monomer units is the soliton width, and A is a scale constant. According to this theory, a neutral soliton has an effective mass $m_s^* \approx 6m_e$ and activation energy of its 1D motion $E_s = 0.002$ eV. Note, however, that the magnetoreflection measurements [101,102] and ENDOR studies [103] gave $N \approx 50$ and $m_s^* = (0.15–0.4)m_e$.

A single soliton in *trans*-PA has peculiar charge-spin relationship, since a neutral soliton corresponds to a radical with $S = 1/2$, while a negatively or a positively charged soliton loses the spin and becomes diamagnetic. This band becomes completely filled (n-type doping) or empty (p-type doping). At a low doping level y (y implies a number of dopant molecules per monomer), only a part of neutral solitons becomes charged. As the doping increases, all the solitons become spinless and their states start forming a band at mid-gap. The soliton band is suggested to be responsible for the spinless conduction mechanism, which is realized after semiconductor–metal transition. Such conduction mechanism, involving the motion of charged solitons within a filled or empty band, differs significantly from the conduction mechanism in traditional semiconductors. At approximately 10% doping level, the soliton band is found to merge with VB and CB.

In contrast to traditional semiconductors, in PA, except the activation electron transport [63], the phonon-coupled charge tunneling between solitons energetic levels [61] and VRH [72] conductivity, characterizing of different frequency and temperature dependencies $\sigma_{AC}(\nu_e, T)$ are also possible. Such a variety of electron transport in this polymer is associated with a formation of the nonlinear soliton-like excitations and can be directly connected with the evolution of both crystalline and electron structures of the system.

In order to obtain information on interactions of an electron with other electrons or the lattice of *trans*-PA, the electron spin echo or magnetic field modulation technique can be used as well. Since the neutral soliton and polaron have an unpaired electron, which interacts with a hydrogen nuclei, the spin dynamics associated with it can be studied by NMR and EPR methods.

For description of soliton mobility in *trans*-PA, some theoretical conceptions based on either the Brownian 1D-diffusion of solitons interacting with lattice phonons [104] and solitons scattering on optical and acoustic phonons of *trans*-PA [105] have been proposed. One of them predicts square temperature dependence of the 1D-diffusion frequency, $\nu_\parallel = D_{1D} c_\parallel^2$, where D_{1D} is the 1D-diffusion coefficient and $c_\parallel$ is the intrachain hopping length of soliton. In the second case, $\nu_\parallel(T) \propto T^{-1/2}$ and $\nu_\parallel(T) \propto T^{1/2}$ dependencies are predicted for optical and acoustic phonons, respectively. As calculations have shown [106], the extreme velocity of the soliton 1D-diffusion should not exceed $\nu^F = 3.8 \times 10^{15}$ s^{-1} near the Fermi level.

To realize 1D motion, the spin diffusion should be extremely anisotropic in *trans*-PA, because the soliton cannot hop directly from one chain to another. Nevertheless, in real systems, the soliton can hop between the chains with $\nu_\perp$ frequency. The spin diffusion anisotropy in *trans*-PA, $\nu_\parallel/\nu_\perp$ varies approximately in 10^5–10^8 range [74,107].

T_1 of proton nuclei of *trans*-PA was measured by Nechtschein et al. [108] as a function of ν_p for pristine and

AsF_3 doped *trans*-PA. $T_1 \propto \nu_p^{1/2}$ dependency was found for both *trans*-PA samples, which coincides with a characteristic motion spectrum of 1D spin diffusion, and 1D diffusion rate of the neutral soliton was found to be $\nu_\parallel = 6 \times 10^{14}$ s^{-1} (at room temperature) in neutral *trans*-PA and have square temperature dependence. As the valuations shown [108], the diffusion rate can increase by more then three orders of magnitude at introduction of different dopants into the polymer. It should be stressed, however, that the soliton motion influences indirectly the relaxation time of a nuclear spin. As the interaction of a diffusing proton with a immobilized electron spin is also characterized by frequency dependence $T_1 \propto \nu_p^{1/2}$ [109], it can lead to an incorrect interpretation of the results obtained by NMR spectroscopy. So, Masin et al. [110] showed on the base of kinetics of ^{13}C NMR signal fading that *trans*-PA have not a mobile unpaired electrons at all. Ziliox et al. showed [111], however, that such a conclusion can be true only for the specific samples investigated by Masin et al. [110].

Many fundamental properties of PA are determined by the existence of PC localized or/and delocalized along the polymer chains; therefore, most studies of these compounds have been performed by EPR method [28,29,112]. In the study of conducting polymers, the NMR [113] and EPR methods are complementary to one another; however, the latter one allows the direct registration of the pure spin motion [51].

It was shown earlier, that pure *cis*-PA demonstrates no EPR signal according to the SSH model, which does not predict a soliton-like PC in this isomer. However, *cis*-PA samples really contain short *trans*-PA segments (5–10%) on the chains' ends [97] where solitons can be pinned [100] explaining weak and broad (0.7–0.9 mT) line generally observed in EPR spectrum. PCs in *cis*-PA are characterized by $g = 2.00263$ [91] and by **A** tensor with $A_{xx} = -1.16$ mT, $A_{yy} = -3.46$ mT, and $A_{zz} = -2.32$ mT components [114] (*x*-, *y*-, and *z*-axes are directed along *a*, *c*, and *b* crystallographic axes, respectively).

Thermodynamically more stable *trans*-conformation is obtained by thermal, chemical or electrochemical treatment of *cis*-form [97]. EPR spectrum of *trans*-PA may be considered as superposition of contributions of pinned and highly mobile solitons with concentration, respectively, n_1 and n_2, whose ratio changes with temperature, and a contribution of other fixed centers which appearance is connected with the presence of traces of catalyst molecules or/and oxygen molecules. At n- and p-type doping, the concentration of PC in *trans*-PA is monotonic changed at invariable *g*-factor [112], showing the invariable nature of PCs, responsible to the EPR signal. In the case of thermal isomerization, the concentration of unpaired electrons largely increases from $\sim 10^{24}$ spins/m^3 (or one spin per $\sim$ 44.000 CH-units) in *cis*-PA up to $\sim 10^{25}$ spins/m^3 (or one spin per 3.000–7.000 CH-units) in *trans*-PA during the process [112]. This is accompanied by the line width decrease down to 0.03–0.2 mT [28,29]. The latter value depends on the average length of *trans*-chains and demonstrates a linear dependency on concentration of sp^3-defects, n_d [115]. Besides, $\Delta B_{pp} \propto z^{2.3}$ dependency was obtained [116] for PA doped by ions of metals with the atomic number *z*. The line width of partially stretch-oriented *trans*-PA was registered to be sensitive to the direction of the external magnetic field $\boldsymbol{B}_0$: This value is equal to 0.48 mT at $\boldsymbol{B}_0 \| c$ orientation (here *c* is the direction of the stretching) and reduces down to 0.33 mT as $\boldsymbol{B}_0$ direction turns by 90° with respect to *c* direction [117]. Such a tendency was reproduced also by Bartl et al. [115] and by Mizoguchi et al. [118–120]. EPR spectrum of *trans*-PA may be generally considered as the sum of contributions due to highly mobile solitons, to pinned ones, whose number increases with the temperature decreases, and fixed impurities probably related to the presence of traces of catalyst molecules or oxygen after the polymerization process. For most cases, no significant change in *g*-factor of doped (p- or n-type) *trans*-PA was found [28,112]. Being combined with the monotonic variation of a number of PC upon doping, this result suggests that there is no drastic change in the nature of unpaired electrons, affecting EPR signal.

Numerous investigations of the paramagnetic susceptibility of neutral PA showed [112], that both its conformers demonstrate Curie paramagnetism (when inverted temperature dependence, $\chi \propto T^{-1}$ is realized for paramagnetic susceptibility χ at $T < 300$ K). In the same time, Tomkiewicz et al. [121] have shown that the magnetic susceptibility of *cis*-PA does not follow Curie law at temperature region of 4–300 K. The reasons of such disagreement of the results was unclear just so far.

The spin dynamics was studied in *trans*-PA by steady-state [74,118–120] and spin echo [122–124] EPR methods. The analysis of $T_{1,2} \propto \nu_e^{1/2}$ and $\nu_\parallel(T) \propto T^{-2}$ dependencies obtained by the first method at $\nu_e = 5$–450 MHz frequency region evidence on diffusive spin 1D-motion in *trans*-PA with $\nu_\parallel \leq 10^{13}$ s^{-1} and anisotropy $\nu_\parallel/\nu_\perp = 10^6$–$10^7$ at room temperature. The analogous temperature dependence for diffusion rate was found also at higher operation frequencies, $\nu_e = 9$–14 GHz [123,125]. These dependencies were similar to those deduced from ^1H NMR T_1 analyses [113]. However, the detailed spin echo and steady-state EPR measurements of both *trans*-PA and its deuterated analog *trans*-(DH), carried out by Shiren et al. [122], showed a relatively low 1D spin diffusion with $\nu_\parallel \approx 10^{11}$ s^{-1}. This result is in disagreement with SSH theory, which predicted a higher $\nu_\parallel$ value [108,126] and with $\nu_\parallel > 10^{15}$ s^{-1} experimentally obtained from photoconductometry of pristine *trans*-PA [127]. Some data concerning spin dynamics determined by NMR and EPR and by steady-state and spin echo EPR methods are not compatible [122]. In order to explain the discrepancy between the results obtained with complementary magnetic resonance methods, Holczer et al. [128] suggested the exis-

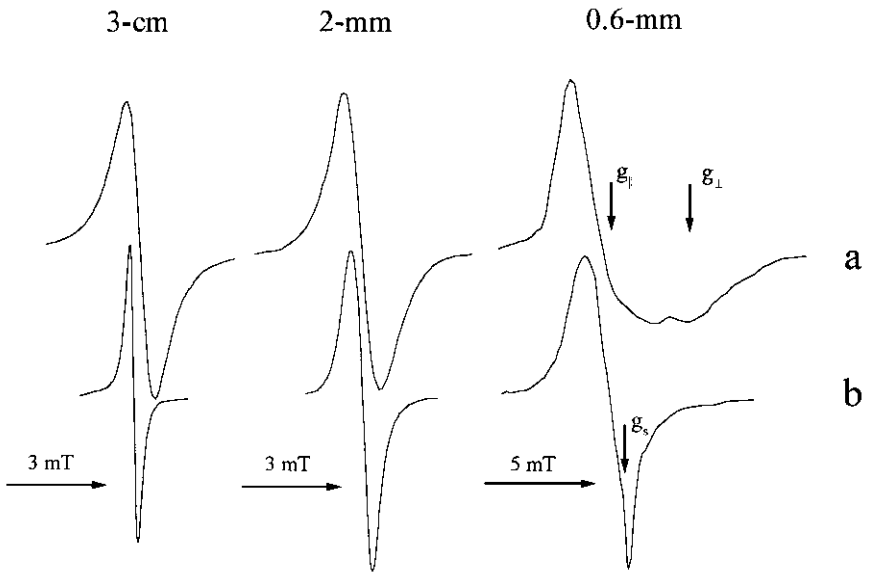

Fig. 3. 3-cm (a,d), 2-mm (b,e), and 0.6-mm (c,f) waveband EPR spectra of *cis*- (a,b,c) and *trans*- (d,e,f) PA registered at room temperature. The position g_s of single line attributed to a neutral soliton in *trans*-PA is shown.

tence of two kinds (diffusive and localized) of PC in *trans*-PA. The dependencies $T_{1,2} \propto \nu_e^{1/2}$ and $\nu_{\|}(T) \propto T^{-2}$ obtained by the first method at $\nu_e = 5$–450 MHz frequency region [29,51] evidence on diffusive spin 1D-motion in *trans*-PA with $\nu_{\|} \geq 10^{13}$ s^{-1} and anisotropy $\nu_{\|}/\nu_{\perp} \geq 10^6$ at room temperature. The analogous temperature dependence for diffusion rate was found also at higher operation frequencies, $\nu_e = 9$–14 GHz [123,125]. However, the rate of the spin diffusion was determined by spin echo EPR method was to be $\nu_{\|} < 10^{11}$ s^{-1} at room temperature with a more complete temperature dependence [122].

Therefore, the data concerning the soliton dynamics in *trans*-PA obtained by same authors and by different methods are very contradictable and sometimes has no simple interpretation. More promising for investigation of the composition and dynamics of the PC seems EPR method, which, however, is limited due to low spectral resolution and high spin–spin exchange at $\nu_e \leq 40$ GHz. This complicates the separate registration of localized and mobile π-radicals with close magnetic parameters in *trans*-PA [128].

In order to study the nature of PC in PA, a series of *cis*- and *trans*-PA samples was investigated at wide frequency (10–430 GHz) EPR bands [129].

Cis- and *trans*-PA samples are characterized by a single symmetric line at 3-cm waveband EPR (Fig. 3a,d), with $g = 2.0026$ and ΔB_{pp} equal to 0.7 and 0.22 mT, respectively (Table 1). *Trans*-PA sample shows ΔB_{pp} values slightly greater than those reported [28,29]. This can be due to a higher content of oxygen molecules in the sample or shorter π-conjugation length. A small EPR line width broadening (0.05–0.17 mT) is observed at 77 K. This is probably due to a smaller libration motion of different parts of the polymer chains. A line width is observed to increase of about of 0.1 mT when the sample is exposed to oxygen.

At 8-mm waveband EPR, an insignificant increase of the line width of PA samples is observed.

At 3-mm waveband, *cis*-PA shows ΔB_{pp} increase up to 0.84 mT with a small broadening of the highfield peak, which is attributed to anisotropy of *g*-factor. *Trans*-PA spectrum shows a line with $g = 2.00270$, $\Delta B_{pp} = 0.37$ mT, and with A/B ratio equal to 1.1.

The decrease of EPR wavelength down to 2-mm leads to the further broadening in ΔB_{pp} of *cis*- and *trans*-PA up to 1.1 and 0.5 mT, respectively. Moreover, the anisotropy of *g*-factor of PC in *cis*-PA and the line asymmetry ($A/B = 1.3$) for *trans*-PA increase (Fig. 3b,e).

Table 1
The linewidth ΔB_{pp} (in mT) and the distance between spin-packets $\Delta\omega_{ij}$ (in 10^{-8} s^{-1}) of PCs in neutral PA at different operating frequencies ν_e (in GHz) at 300 K
I — Solitons localized in *cis*-PA, II — solitons localized in *trans*-PA, III — solitons delocalized in *trans*-PA.

ν_e	ΔB_{pp}			$\Delta\omega_{ij}$		
	I	II	III	I	II	III
9.82	0.70	0.25	0.06[a]	1.7	1.0	0.8[a]
37.5	0.75	0.30	0.11[a]	1.8	1.2	1.3[a]
94.3	0.85	0.45	0.18	1.9	1.4	1.7
139	0.95	0.61	0.30	2.3	2.2	2.2
250	1.82	1.60	0.50	2.8	2.8	2.9
349	2.42	2.52	0.62	3.2	3.5	3.2
428	2.53	1.91	0.81	3.3	3.1	3.7

[a] Determined by extrapolation.

Fig. 4a shows the temperature dependencies of normalized spin susceptibility χ of some *cis*-PA samples, which can be approximated by the following function

$$\chi(T) = a\exp\left(-\frac{E_a}{k_B T}\right) + bT^{-n} \quad (39)$$

where a and b are constants, and E_a is the activation energy. First term of Eq. (39) is determined by librations of polymer chains with activation energy of $E_a = 0.035$–0.055 eV for different samples. The analogous consequence of electron–phonon interaction mainly as energy fluctuation of electron polarization of few millielectronvolts is observed in organic crystal semiconductors [130]. As it is seen from the figure, the activation ordering of the spin magnetic momenta dominates in paramagnetic susceptibility at high temperatures only. At temperature region

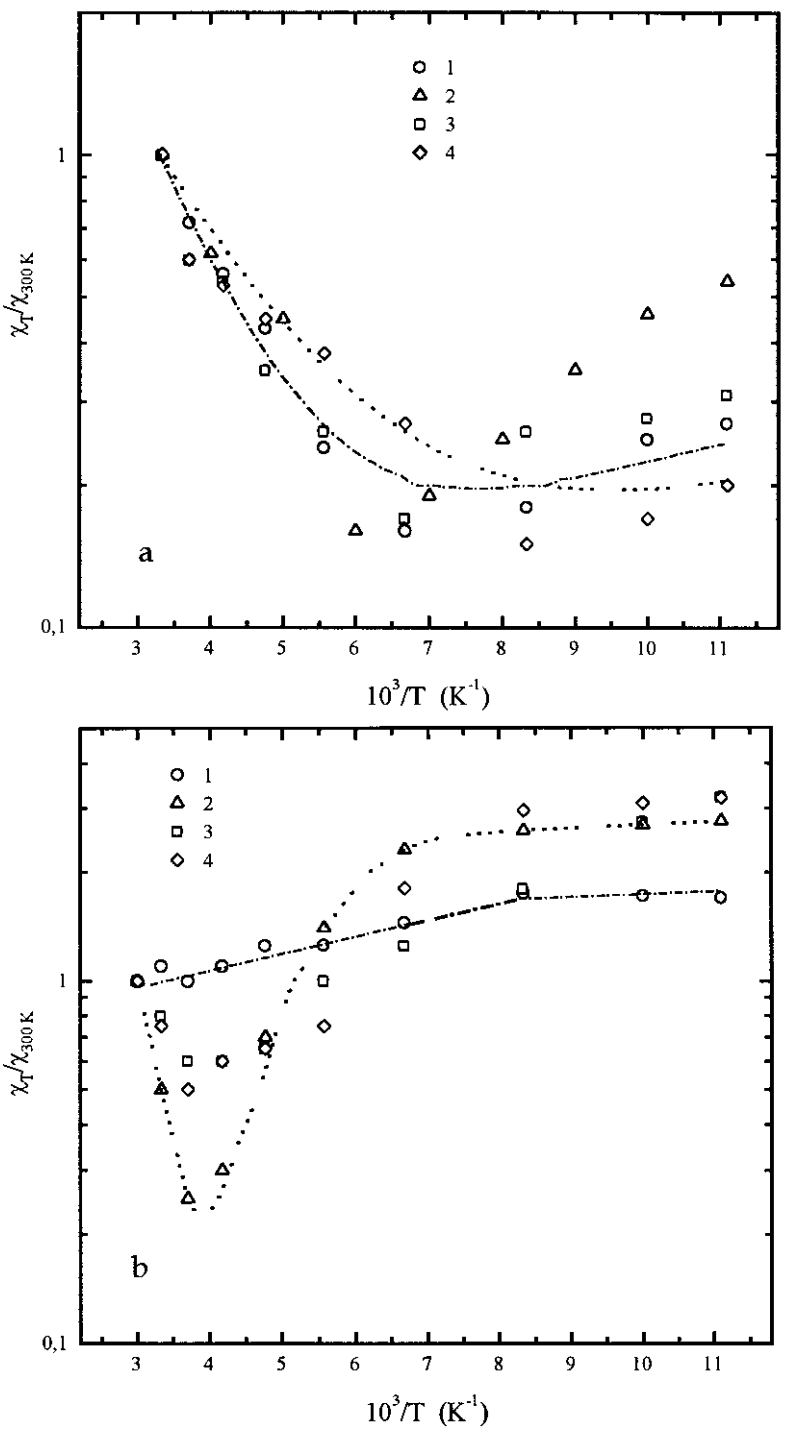

Fig. 4. Temperature dependencies of spin susceptibility χ_T of *cis*- (a) and *trans*-PA (b) numbers 2 (1), 4 (2), 6 (3), and 5 (4) (see Table 2) with respect to that measured at room temperature.

lower then some critical $T_c = 150$ K, this process competes with other ones, following Curie law ($n = 1$) among them. The contributions of these processes of unpaired electrons' magnetic momenta orientation are different for *cis*-PA samples investigated.

The susceptibility of PC in *trans*-PA samples is also characterized by an anomalous temperature dependence (Fig. 4b). As in the case of *cis*-PA, the main contribution to χ of *trans*-PA at high temperature region gives first term of Eq. (39). Higher $E_a = 0.06$–0.19 eV value can be explained by the increase of both rigidity of polymer chains and by its packing density during *cis*–*trans*-isomerization. It probably is a reason for critical temperature shift to $T_c = 250$ K region.

Trans-PA, in contrast to *cis*-PA, is characterized by more sharp primary section of $\chi(T)$ curve at $T < T_c$ (the n value in Eq. (39) is changed from 1 up to 4 for the studied *trans*-PA samples) and flats at $T < 140$ K. The latter fact is analogous to manifestation of so-called magnetic saturation effect. However, such a magnetic saturation can appear if the condition $g\mu_B SB_0 > k_B T$ is valid for a given temperature region, for example, at $B_0 > 100$ T that exceeds significantly the strength of magnetic field $B_0 \leq 5$ T used in our experiments. This effect most probably can be caused by the significant concentration increase of neutral solitons with A amplitude, following the decrease of interradical distance R and a growth of these charge carriers interaction with the probability $W_R \propto A\exp(-2AR)$ [131]. Besides, the defrosting of 1D-diffusion of part of solitons with $\nu_\parallel$ rate leads to an additional increase of intersoliton interaction probability, $W_{ss} \propto \nu_0 T^{-2}$ (see below). The discrete levels of neighboring solitons localized at mid-gap are narrowed due to overlapping of unpaired electrons wave functions and are transformed to soliton band of limited weight. As in the case of *cis*-PA, a, b, and n constants are determined by different properties of *trans*-isomer.

At higher frequencies, the anisotropy of g-factor of PC becomes more evident in *cis*-PA (Fig. 3c). This line shape must be attributed to the localized PC with **g** tensor components: $g_\perp = 2.00283$, $g_\parallel = 2.00236$ ($\pm 5 \times 10^{-5}$) and $\langle g \rangle = 2.00267$. $g_\perp$ value differs from g_e by $\Delta g = 5 \times 10^{-4}$. In a perturbation theory, such a difference corresponds to an unpaired electron transfer from σ_{c-c} orbital to a antibinding π^* orbital with $\Delta E_{\sigma-\pi^*} = 14$ eV. As a matter of fact, $\Delta E_{\sigma-\pi^*}$ value calculated for π-conducting systems, is equal to 14.5 eV in the case of normal C–C bond [132]. The other electron transitions with a greater ΔE_{ij} do not influence Δg. Thus, the spectrum line shape and the agreement between the calculated and measured $\Delta E_{\sigma-\pi^*}$ values support the existence of localized PC in PA.

The line shape of *trans*-PA spectra remains almost unchanged with increasing operation frequency. One only notices the further increase in both line width and asymmetry (Fig. 3f).

To elucidate the dynamic processes in PA more completely, partially stretch-oriented samples were studied [133].

The signals from PC, namely sp^3 and immobile solitons, exhibit weakly axial-symmetric spectra with the abovementioned g-factors and line width $\Delta B_{pp}^{in} = 1.23$ mT for the initial and $\Delta B_{pp}^{str} = 1.45$ mT for the stretch-oriented *cis*-PA samples at room temperature. For the latter one, ΔB_{pp}^{str} value and the other magnetic parameters remain invariable under sample rotation with respect to the direction of an external magnetic field. This value varies nonmonotonically from 0.60 to 0.68 mT for the stretch-oriented *trans*-PA under rotation at room temperature.

The transformation of PA line shape at *cis*–*trans*-isomerization apparently indicates the rise of mobile PC in PA during this process. The proximity of the isotropic g-value of the localized PC and g-value of the delocalized PC shows the averaging of **g** tensor components of delocalized PC due to their mobility with the rate of [33]

$$\nu_\parallel^0 \geq \frac{(g_\perp - g_e)\mu_B B_0}{h} \tag{40}$$

Thus, two types of PC exist in *trans*-PA, that is, there are neutral solitons moving along the long polymer axis with $\nu_\parallel^0 \geq 2 \times 10^8$ s^{-1} rate and neutral solitons pinned on short polymer chains with the relative contribution of 18:1 or 1.1×10^{-3} (1100 ppm) and 6×10^{-5} (60 ppm) spin per carbon atom, respectively. The latter value is two orders of magnitude smaller than that reported by Goldberg et al. [91].

The analysis of *cis*- and *trans*-PA line shape shows, that at $\nu_e \geq 140$ GHz, their lowfield part can be described by a Lorentzian function in the center and by a Gaussian one on the wing. At the same time, the highfield part is Lorentzian. The spin exchange frequency obtained from the analysis is equal to 3×10^7 and to 1.2×10^8 s^{-1} for the localized PC in *cis*- and *trans*-PA, respectively. These values are in agreement with $\nu_{ex} \geq 10^7$ s^{-1} estimated for *trans*-PA by Holczer et al. [128]. Thus, for the frequencies higher than 16 GHz, the condition $\nu_{ex} < \Delta\omega_{ij}$ holds, hence spin-packets become noninteracting, and $\Delta B_\perp^{loc}$ value varies according to Eq. (10).

$\Delta\omega_{ij}$ value obtained for PC in both *cis*- and *trans*-PA samples by using Eq. (10) are also presented in Table 1. The dependencies of line width broadening for both localized and delocalized PC versus ν_e are shown in Fig. 5. It is seen in the figure, that the line width of PC localized in *cis*- and *trans*-PA, changes quadratically with registration frequency, and hence it can be described by the relationship (10). This is an additional evidence for a weak interaction of spin-packets in these samples. At the same time, the line of mobile PC broadens with frequency as ΔB_{pp}^{deloc}. For both types of PC in *trans*-PA, the dependency $\Delta B_{pp}^{deloc} \propto (\Delta B_{pp}^{loc})^\alpha$, where $\alpha = 1.3$–1.4, is valid. It implies, that ΔB_{pp}^{deloc} value reflects 1D spin diffusion in the

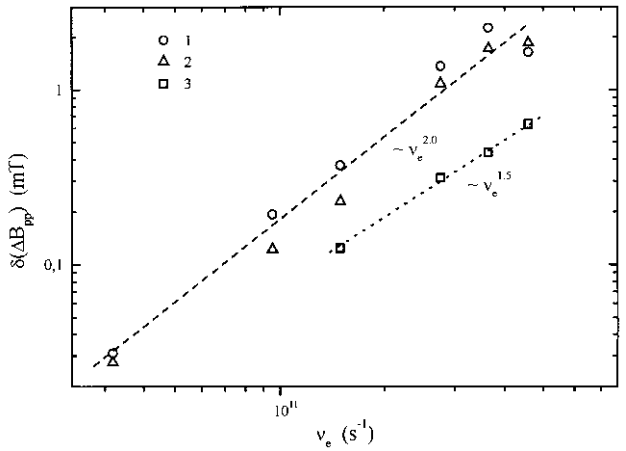

Fig. 5. Logarithmic dependencies of EPR line broadening $\delta(\Delta B_{pp})$ for localized PC in *trans*- (1) and *cis*- (2) PA samples (with respect to ΔB_{pp} value defined at 9.8 GHz) and for delocalized PC in *trans*-PA (3) (with respect to ΔB_{pp} value measured at 93.8 GHz) versus operating frequency at room temperature.

sample in the full frequency range and changes according to Eq. (11).

Considering that $\Delta B_{pp}^{deloc} = 1/(\gamma_e T_2^{deloc})$ at $\nu_e \to 0$ limit, and $T_2(\nu_e \to \infty)/T_2(\nu_e \to 0) = 3.3$ (see Eq. (23b)) and by using spin–spin relaxation time for the delocalized PC $T_2^{deloc} = 0.1$ μs at room temperature [134], it is easy to calculate their zero field line width to be equal to 18 mT. Such a value corresponds to the neutral soliton line width (12–38 mT) proposed by Holczer et al. [128].

Cis–trans-isomerization leads to the increase of both PC concentration in *trans*-PA samples and their spin-lattice relaxation rate. For thick *cis*-PA samples with a smaller packing density, the isomerization takes a course more easily and yields a greater amount of *trans*-PA with more long and rigid π-conducting chains. This is confirmed by the increase in activation energy of chain libration together with the increase of energy transfer from spin system to the lattice [134]. It is interesting to note that this isomerization induces only a small change in E_a. This can be possibly explained by the fact that *cis-trans*-isomerization corresponds not to the noticeable structural changes, but only to the increase of π-conjugation and spin-phonon interaction.

The investigation of *trans*-PA samples, doped by iodine vapor up to $\sigma_{DC} \sim 10$ S/m shows [134] the spectra shape and mobile to localized PC concentration ratio to be nonvarying with doping in *trans*-PA. This fact confirms the assumption proposed by Nechtschein et al. [126] on the existence of both mobile and fixed solitons on a short conducting chain, which become charged and diamagnetic under doping. Thus, during *cis-trans*-isomerization in pristine PA, the concentration of pinned solitons increases remarkably and mobile PC appears. This process leads to the increase in DC conductivity by the same orders of magnitude, probably via motion of the delocalized PC. The difference in $\Delta\omega_{ij}$ and ν_{ex} values for the centers of both type leads to a sharp narrowing in its low-frequency EPR spectrum (e.g., by 4–5 times at $\nu_{ex} \approx 10^{10}$ s^{-1}) under the isomerization. This differs from the opinion existing so far, that such a transformation in spectrum line width is only due to highly mobile neutral solitons [28,29,104,108].

The decrease of the rate of spin–spin exchange in high fields was the cause for the manifestation of the effect of fast passage in *cis*- and *trans*-PA samples (Fig. 6). For these polymers, $\omega_m T_1$ product becomes greater and smaller than unity, respectively, and $U(\nu_e)$ value is therefore defined mainly by u_2, u_3 and u_1, u_3 pairs of terms of Eq. (28), respectively [81,134]. This enables one to calculate independently T_1 and T_2 values for various PA samples of different thicknesses by using Eqs. (36a), (36b), (37a) and (37b) [81,134].

The temperature dependencies of T_1 and T_2 values for some *cis*-PA and *trans*-PA, isomerized from the initial *cis*-PA sample, are presented in Table 2 in the general form $T_{1,2} = AT^{\alpha}$. One can see that spin-lattice relaxation time of both PA isomers is a function decreasing monotonically with temperature, thereby T_2 value demonstrates the different temperature dependencies in these samples. Note, that T_1 and T_2 presented in Table 2 for *trans*-PA samples are effective values of localized and mobile PC. So then one can estimate the relaxation parameters for both types of PC in *trans*-PA from T_1, T_2, n values and n_1/n_2 ratio determined experimentally.

The spin-lattice relaxation rate may be written as $T_1 = An^{-1}\nu_e^{\alpha}T^{\beta}$ where A is a constant, α is equal to 3 and -0.5 for *cis*-PA and *trans*-PA, respectively, and β varies from -1.5 to -3.5 as a function of sample thickness [81,134]. This relation indicates mainly the two-phonon Raman relaxation process in *cis*-PA and the more complicated spin-lattice interaction in *trans*-PA. The dependency mentioned above for the latter sample is probably due to the mixture of 1D Raman modulation and 3D spin-lattice interaction of the immobilized spins with total probability [42] $W_R \propto \nu_e^{-2}T^2 + \nu_e^2 T$, and also to the diffusive modulation of spin-lattice interaction by 1D motion of delocalized centers with the probability [46] $W_D \propto \nu_e^{1/2}$.

It should be noted, that T_1 and T_2 values are the important parameters of PA, characterizing its structural and conductive properties. Thus, a half-year storage of as-prepared *cis*-PA under inert atmosphere results in the sufficient increase in its T_1 (Fig. 7). The analogous change in T_1 is typical for *cis*-PA irradiated by the electron beam with 1 MGy dose. However, T_1 value for this sample irradiated by the electron beam with 0.50–0.75 MGy dose is practically constant during the same period (Fig. 7). After a longer storage of the initial and 1 MGy *e*-irradiated samples, T_1 decreases to a some extent, that can be attributed to a partial degradation and *cis–trans*-isomerization of *cis*-PA. This effect shows the possibility of stabilization and even the improvement of electrodynamic char-

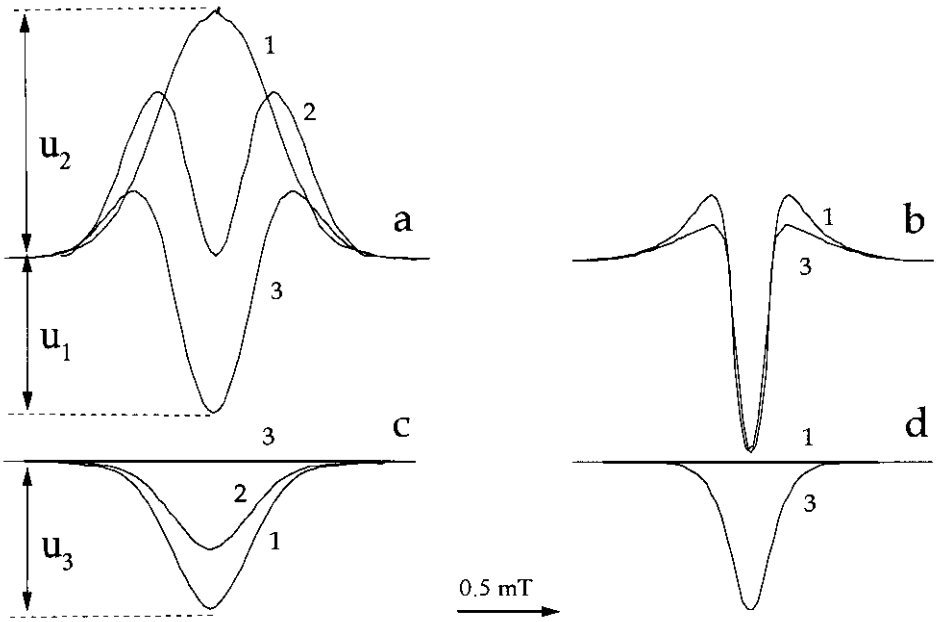

Fig. 6. In-phase (a,b) and $\pi/2$-out-of-phase (c,d) components of the first derivative of dispersion signal of *cis*- (a,c) and *trans*- (b,d) PA registered at 2-mm waveband EPR at $B_1 = 0.2$ μT (1), $B_1 > 0.2$ μT (2), and $B_1 = 20$ μT (3).

acteristics of *cis*-PA irradiated with the optimum dose [81,134].

On moving, a mobile neutral soliton participates in HFI with N protons of a polymer chain. Therefore, by using $\Delta\omega_G \propto N^{1/2}\rho(n)$ dependency for the Gaussian part of soliton line width [44], one can evaluate the relative width of an unpaired electron delocalization in *trans*-PA, provided that $\rho(n) = 1$ and $\rho(n) = N^{-1}$. The analysis of line

Table 2
The relaxation times ($T_{1,2} = AT^{\alpha}$, in s) of different *cis*- and *trans*-PA samples
The samples of different thicknesses were synthesized by different methods.

No.	T_1		T_2		T_1		T_2	
	A	α	A	α	A	α	A	α
	Cis-PA				*Trans*-PA			
1	0.04	−1.6	1.8×10^{-9}	1.2	2.7	−2.6	1.0×10^{-7}	0.5
1[a]	0.37	−2.0	7.7×10^{-9}	1.0	–	–	–	–
2	0.006	−1.4	1.5×10^{-7}	0.5	0.1	−2.2	7.2×10^{-8}	0.3
2[a]	0.77	−2.3	1.0×10^{-7}	0.5	–	–	–	–
3	1.4	−2.3	9.5×10^{-8}	0.5	2.0×10^{-3}	−1.7	1.3×10^{-5}	−0.9
3[a]	290	−3.3	1.7×10^{-8}	0.8	–	–	–	–
3[b]	52	−2.7	1.2×10^{-8}	0.8	–	–	–	–
3[a,b]	6.5	−3.6	4.2×10^{-9}	1.0	–	–	–	–
3[c]	–	–	–	–	62	−3.5	2.1	−3.0
4	0.65	−2.1	9.6×10^{-9}	0.9	4.1×10^{-3}	−1.5	2.9×10^{-6}	−1.0
4[a]	10	−2.6	2.8×10^{-9}	1.1	–	–	–	–
5	27	−2.5	2.4×10^{-7}	0.3	4.0×10^{-4}	−1.2	9.1×10^{-6}	−0.7
5[d]	–	–	–	–	8.3×10^{-4}	−1.3	5.0×10^{-6}	−0.6
6	3125	−3.5	3.4×10^{-8}	0.7	1.7×10^{-4}	−1.1	1.0×10^{-6}	−0.8
7	1587	−2.7	4.2×10^{-9}	1.0	1.1×10^{-2}	−1.9	9.1×10^{-5}	−1.2
8	833	−2.6	9.1×10^{-9}	0.9	2.8×10^{-4}	−1.0	2.2×10^{-5}	−0.7
8[c]	83	−2.7	3.6×10^{-9}	1.1	–	–	–	–

[a] The measurement was carried out at the presence of air.
[b] The measurement was carried out after a half year storage in an inert atmosphere.
[c] The measurement was carried out after doping by J_3 vapor.
[d] The measurement was carried out after an annealing in an inert atmosphere.

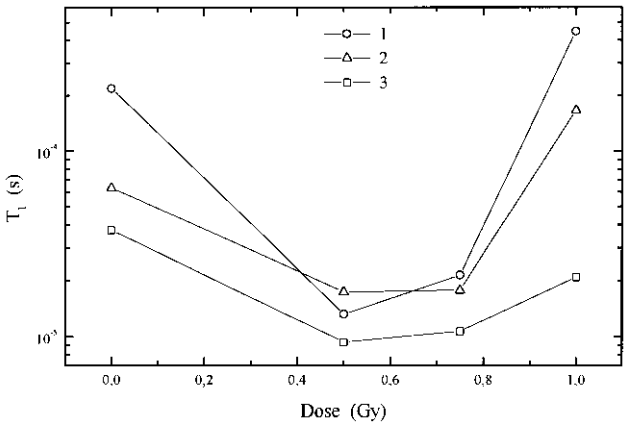

Fig. 7. Dependencies of spin-lattice relaxation time T_1 ($T = 120$ K) on *e*-irradiation dose for the initial *cis*-PA sample number 3 (see Table 2) and that stored during 6 months (1) and 12 months (2).

shape of mobile solitons also yields the frequency and activation energy of small-scale librations of polymer chains [134].

It should be noted that a slight (up to 10 S/m) doping of *trans*-PA sample by iodine vapor leads to a fourfold reduction in total spin concentration and approximately a tenfold decrease of spin-lattice relaxation time (see Table 2). A smaller change (by a factor of two) in the latter value occurs in the presence of oxygen in PA matrix [81]. Taking also into consideration $T_1 \propto n^{-\alpha}$ concentration dependency, where α varies from 0.7 to 1.0 in 330–90 K temperature range, one can postulate both J_3 and O_2 molecules to be the traps for the delocalized PC, and that the introduction of these molecules leads to the decrease of the density of polymer chains packing in PA.

The temperature dependencies of T_1 and T_2 values for the initial and stretch-oriented *cis*- and *trans*-PA samples are shown in Fig. 8 as functions on the angle ψ between the external magnetic field and the stretching directions. These data clearly show that $T_1(T)$ and $T_2(T)$ dependencies of chaotic *cis*- and *trans*-PA and of oriented *cis*-PA samples have a weak sensitivity to angle ψ. Indeed in the case of oriented *trans*-PA, these values are functions changing with ψ. This can be explained by the motion depinning for a part of neutral solitons in *trans*-PA film.

The electron spin relaxation rates, T_1^{-1} and T_2^{-1}, are defined mainly by dipole interaction, and to a certain extent by HFIs between delocalized and fixed spins though 1D diffusion along molecular chains. Therefore, these values can be expressed by Eqs. (24a), (24b), (25a), (25b), (26a) and (26b). The value of n is equal to $n_1 + n_2/\sqrt{2}$ in Eq. (21), where n_1 and n_2 are the spin concentration of localized and mobile PCs per carbon, respectively. The coefficient $1/\sqrt{n}$ in n is used because two solitons diffuse independently with respect to one another. In order to compare these data with the soliton theory and with the results already reported [51,125,135], 1D intrachain diffusion of delocalized PC in *trans*-PA with $\nu_\parallel$ rate and its cutoff by 3D interchain Lorentzian hopping between chains with $\nu_\perp$ frequency is assumed. Since the localized PC predominate in *trans*-PA, the contribution of libration of their chain segments to relaxation mechanism should be also taken into account. The parameters of librations of the chain segments remain almost unchanged at *cis–trans*-isomerization of PA [134]. In order to neglect these librations, the corresponding relaxation rate of *cis*-PA must be therefore subtracted from that of *trans*-PA.

Fig. 9 displays the temperature dependencies of $\nu_\parallel$ (a) and $\nu_\perp$ (b) rates for the chaotic ($A = 0$) and stretch-oriented ($A = 0.07$) *trans*-PA samples calculated from Eqs. (24a), (24b), (25a), (25b), (26a) and (26b) with $P_0 = 4.3 \times 10^{58}$ sin ψ, $P_1 = 4.8 \times 10^{57}$ $(1 - \cos^4 \psi)$, $P_2 = 4.8 \times 10^{57}$ $(1 + 6 \cos^2 \psi + \cos^4 \psi)$, $P_0^\perp = 1.6 \times 10^{58}$, $P_1^\perp = 2.7 \times 10^{57}$, $P_2^\perp = 1.1 \times 10^{58}$ m^{-6}, and $Q = 2.34$ mT, $(\langle I_z \rangle - I_0)/(\langle S_z \rangle - S_0) = 0.078$ [74]. Indeed, the figure shows that both 1D diffusion and 3D hopping rates of the soliton are sensitive to the orientation of the latter sample in an external magnetic field due to 1D soliton motion. It is seen from the figure that the phase of $\nu_\parallel(\psi)$ function for an oriented sample is opposite to that of $\nu_\perp(\psi)$ one. Since *c*-axis orientation remains arbitrary in chaotic *trans*-PA, these values are averaged over angle ψ. Moreover, the averaged $\nu_\parallel$ value is well described by the equation $\langle \nu_\parallel \rangle = \nu_\parallel^\perp \cos^2 \psi + \nu_\parallel^\parallel \sin^2 \psi$, where $\nu_\parallel^\perp$ and $\nu_\parallel^\parallel$ are the extremes of $\nu_\parallel(\psi)$ function. Note that a similar function describes an effective spin diffusion in low-dimensional systems [136,137]. Thus, $\nu_\parallel^\perp \gg \nu_\parallel^\parallel$ inequality displays spin delocalization over a soliton. By taking into account that the soliton is limited in its hopping by the interchain lattice constant and that the value of the average square of its diffusive hopping step along *c*-axis is $\langle N^2 c^2 \rangle$, the soliton width is easily expressed as

$$N^2 = \frac{\nu_\parallel^\perp}{\nu_\parallel^\parallel} \tag{41}$$

Thus, the data obtained [133] confirm the realization of 1D diffusion motion of solitons in *trans*-PA with the rate significantly exceeding $\nu_\parallel^0$ value defined above. Besides, it derives from the analysis of the data, given in Table 1, that relationship (10) holds for the line width in the whole frequency range. This relationship characterizes the narrowing of EPR line of a semiconductor, when 1D spin diffusion motion arises, being the cause of the averaging of **g** tensor components of mobile soliton.

However, the principle evidence for the realization of 1D motion of spins in *trans*-PA is the sensitivity of $\nu_\parallel$ and $\nu_\perp$ values to the orientation of a part of polymer chains in an external magnetic field (Fig. 9).

The analysis of the data presented in Fig. 9 gives $N(T) \propto T^1$ temperature dependence for the soliton width and $2N = 14.8$ cell units at room temperature. This value is in a good agreement with that theoretically predicted by Su et al. [25] and that derived from magnetic resonance

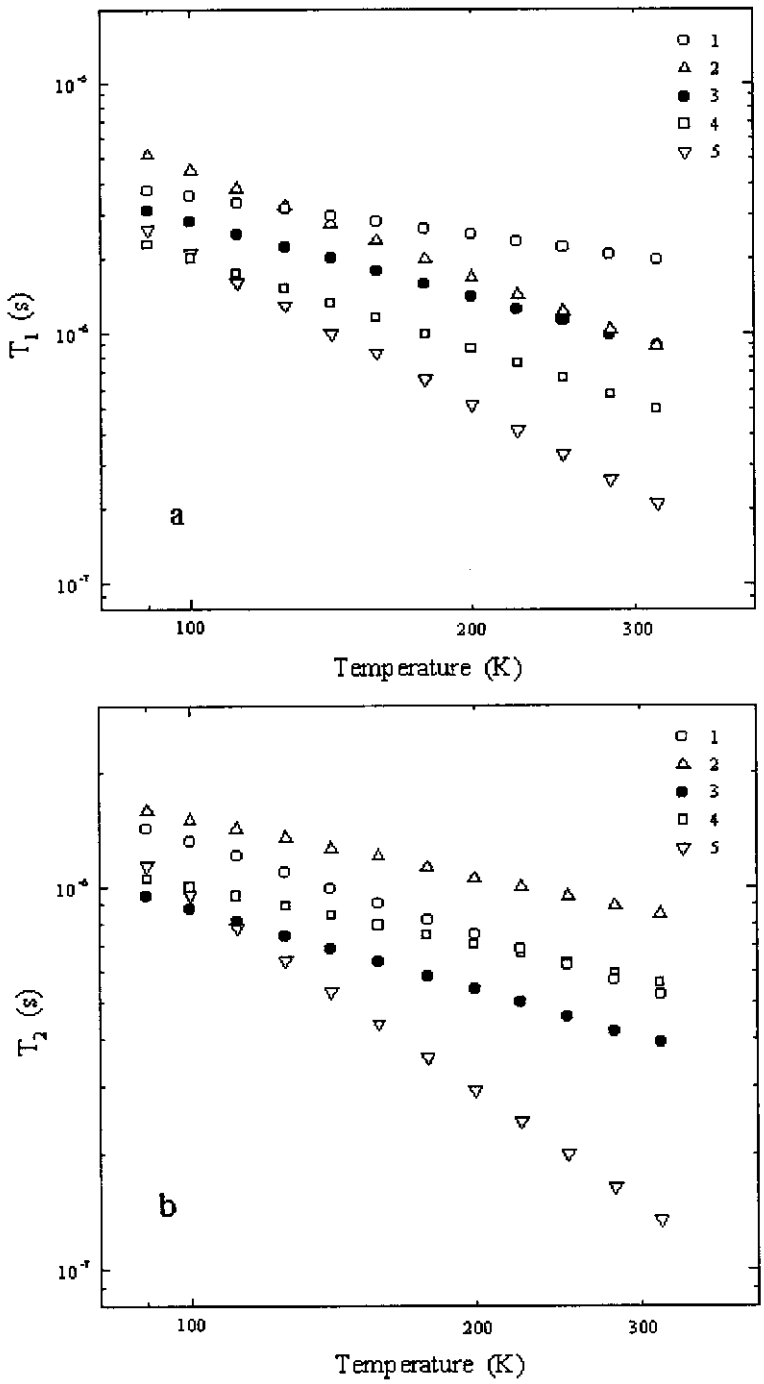

Fig. 8. Temperature dependencies of spin-lattice T_1 (a) and spin–spin T_2 (b) relaxation times for the initial (3) *trans*-PA number 3 (see Table 2) and that stretch-oriented with an orientation degree $A = 0.07$ oriented by lattice *c*-axis with respect to an external magnetic field by $\psi = 90°$ (1), 60° (2), 30° (4), and 0° (5).

experiments [126]. Extrapolation to the low temperature range allows one to determine the temperature ($T = 60$ K), where the soliton width starts to increase.

It is important to stress that at such temperatures, the bend in the experimental $\nu_{\|}(T)$ function together with the difference between the experimental and theoretical results occur [122,126].

The spin dynamics anisotropy, $\nu_{\|}/\nu_{\perp}$ was determined to be almost temperature-independent and equal to 30 for chaotic (initial) and to 45 for stretch-oriented *trans*-PA samples [133]. Note, that if the intra- and interchain spin hopping rates may be written for the chaotic *trans*-PA presented in Table 2 as $\nu_{\|} = AT^{\alpha}$ and $\nu_{\perp} = BT^{\beta}$, the decrease of α values from -2 to -5 is accompanied by

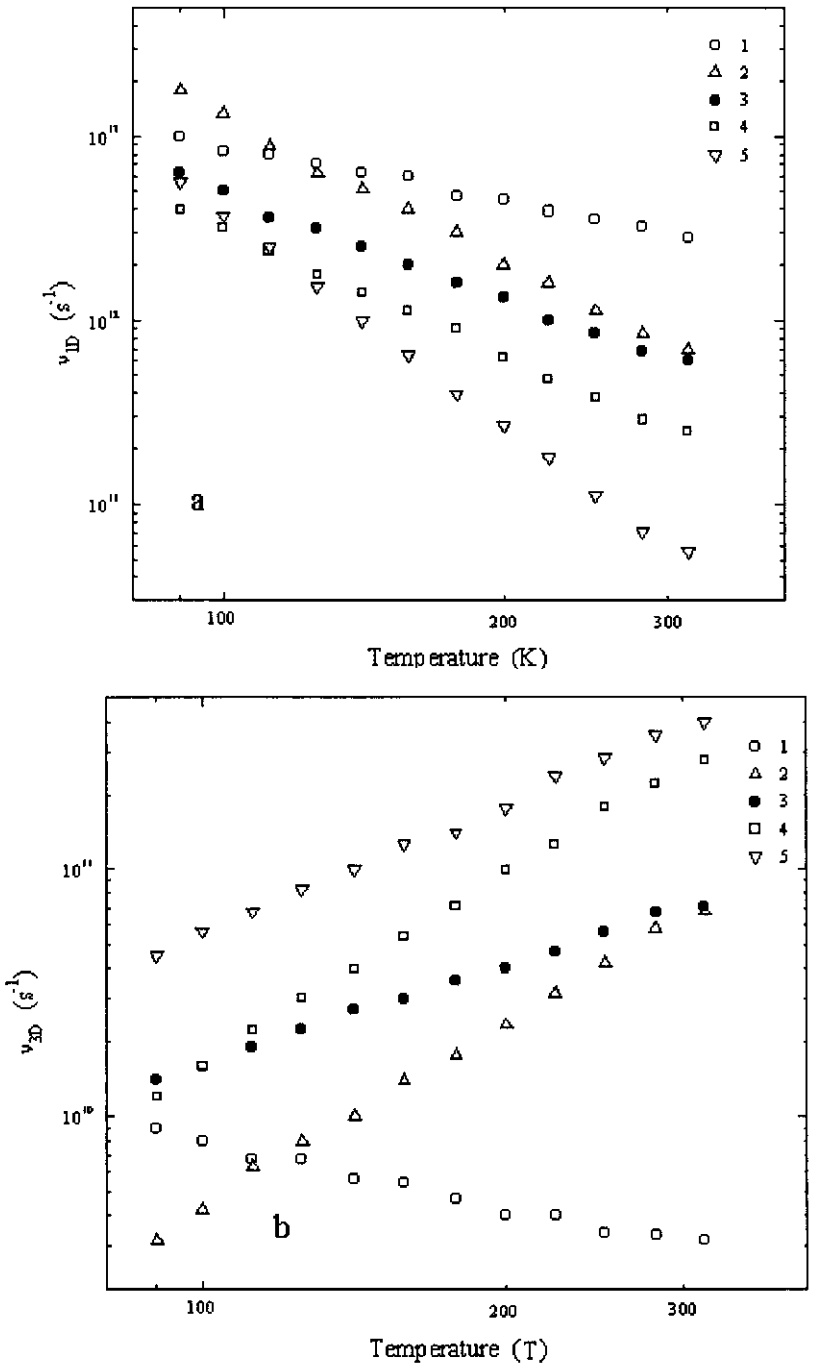

Fig. 9. Temperature dependencies of intrachain diffusion ν_{1D} (a) and interchain hopping ν_{3D} (b) rates for the initial (3) *trans*-PA number 3 (see Table 2) and that stretch-oriented with an orientation degree $A = 0.07$ and oriented by lattice *c*-axis with respect to an external magnetic field by $\psi = 90°$ (1), 60° (2), 30° (4), and 0° (5).

the increase of β value from 0.4 to 7 and by the decrease of anisotropy from 10 to 10^4 at room temperature.

Thus, the experimental data evidence for soliton 1D-diffusion in *trans*-PA with the rate, which exceeds significantly minimum rate $\nu_{\|}^{0}$ calculated above using Eq. (40). This conclusion is also confirmed by the averaging of **g** tensor components of mobile PC at fulfillment of condition (40) and by the *trans*-PA EPR spectral line narrowing according to Eq. (10) at a wide frequency range. However, the more evident evidence for the soliton 1D-diffusion is the sensitivity of $\nu_{\|}$ and $\nu_{\perp}$ values to the orientation of a polymer in an external magnetic field.

The modified well-known Burgers–Korteweg–de Vries equation describing 1D-motion of solitary waves in nonlinear medium is [131]

$$\frac{\partial u}{\partial t} + \left(\nu_{\parallel}^{0} + \varepsilon u\right)\frac{\partial u}{\partial x} - \kappa\frac{\partial^2 u}{\partial x^2} + \beta\frac{\partial^3 u}{\partial x^3} = 0 \qquad (42)$$

where ε, κ, and β are, respectively, the parameters of the medium nonlinearity, dissipation, and ''reactive'' dispersion. In a dissipative system with a small nonlinearity ($\beta \approx 0$), the formation of a mobile front (kink) with $u_2 - u_1$ bounce is possible. The stationary solution of Eq. (42) for such a quasi-particle is the following

$$u(x,t) = \frac{1}{2}(u_1 + u_2) - A\tan h\left[\frac{A\varepsilon(x - \nu_{\parallel}t)}{\kappa}\right] \qquad (43)$$

where $A = 1/2(u_2 - u_1)$, $\nu_{\parallel} = \nu_{\parallel}^{0} + \varepsilon(u_1 + u_2)/2$ and $N = \kappa/(2A\varepsilon)$ are the amplitude, velocity, and width of the kink, respectively. If the dissipation of the system is neglected ($\kappa \approx 0$), the other quasi-particles, solitons can be stabilized in such a system, and for a soliton multitude, Eq. (42) has another integrated solution

$$u(x,t) = A\sec h^2\left[\frac{(x - \nu_{\parallel}t)}{N}\right] \qquad (44)$$

where $\nu_{\parallel} = \nu_{\parallel}^{0}$ and $A\varepsilon/3$ and $N^2 = 3\beta/(A\varepsilon) = \beta/(\nu_{\parallel} - \nu_{\parallel}^{0})$. It is necessary to note that the dependencies analogously to Eqs. (43) and (44) were used for description of nonlinear both lattice deformations and electronic states of *trans*-PA [25].

The functional dependencies $\nu_{\parallel}(T) \propto T^{-n}$ and $N(T) \propto T^{n/2}$ ($n \approx 2$) experimentally obtained [133] give $N^2 \propto \nu_{\parallel}^{-1}$ one for *trans*-PA. It means that if the condition $\nu_{\parallel} \ll \nu_{\parallel}^{F} = 3.8 \times 10^{15}$ s^{-1} holds, the soliton motion in the present sample can be described by Eq. (42) with a stationary solution Eq. (44) which is universal for nonlinear systems. It is obvious, that different *trans*-PA samples can be characterized by different sets of ε, κ, and β constants in Eq. (42), such that the character of a quasi-particle motion in these polymers can deviate from the above described one.

According to the Einstein relation

$$\sigma_{1,3D}(T) = Ne^2\mu = \frac{Ne^2\nu_{\parallel,\perp}c_{\parallel,\perp}^2}{k_B T} \qquad (45)$$

AC conductivity of the doped *trans*-PA should be approximately near to 0.1–1 S/m at room temperature, even if all solitons were participating in charge transfer, in spite of increasing disorder and Coulombic pinning. This value is the same order of magnitude smaller than that usually achieved for highly doped *trans*-PA. Moreover, the slight doping of *trans*-PA causes a decrease of 1D spin diffusion and the increase of 3D hopping rates [138]. Hence, high conductivity of *trans*-PA cannot be achieved with soliton on-chain motion only.

The spin dynamics in slightly doped *trans*-PA sample should be described in terms of the Kivelson theory [61]. The temperature dependencies of AC ($\nu_e = 1.4 \times 10^{11}$ s^{-1}) conductivities, σ_{1D} and σ_{3D} calculated from Eq. (45) for slightly doped 3 *trans*-PA (Table 2) are presented in Fig. 10. For the comparison, the theoretical function $\sigma_{AC}(T)$ calculated by using Eq. (30b) with $\sigma_0 = 2.8 \times 10^{-11}$ S s K/m, $k_3 = 9.3 \times 10^{25}$ s K$^{14.2}$ and $n = 13.2$ and the method described in Ref. [61] is presented in the figure by solid line as well. In fact, the $\sigma_{1D}(T)$ and $\sigma_{3D}(T)$ dependencies seem to be comparable for this sample; however, at γ_0 less then theoretical one. This confirms the applicability of the Kivelson theory for 1D charge transport in *trans*-PA.

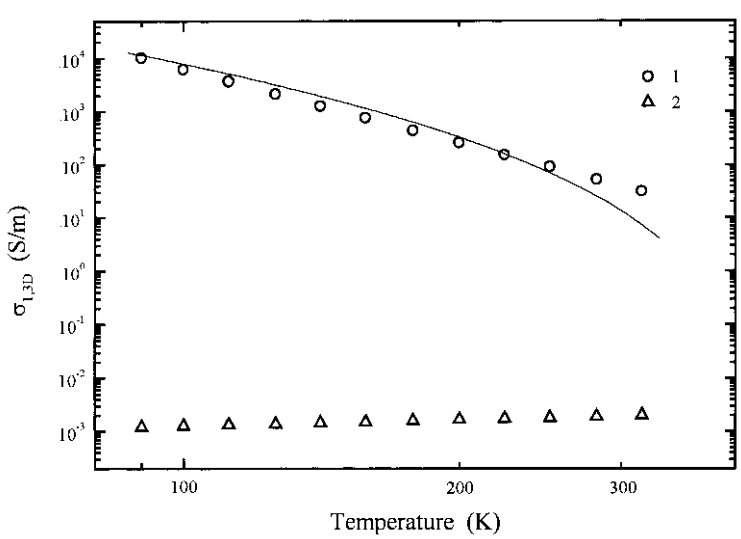

Fig. 10. The temperature dependencies of σ_{1D} (1) and σ_{3D} (2) values calculated from Eq. (45) for slightly doped *trans*-PA number 3 (see Table 2). $\sigma_{AC}(T)$, calculated from Eq. (30b) with $\sigma_0 = 2.8 \times 10^{-11}$ S s K/m, $k_3 = 9.3 \times 10^{25}$ s K$^{14.2}$, $\nu_e = 1.4 \times 10^{11}$ s^{-1} and $n = 13.2$, is shown by solid line.

Hence, the charge transport process in pristine *trans*-PA can be described in the following manner. In *cis*-PA, the solitons trapped in short chains are the dominated spins. The possibility of electron intersoliton hopping is very small being defined only by librations of polymer chains, hence $\sigma_{DC} \sim 10^{-11}$ S/m. The length of π-conducting chains increases in PA during its *cis–trans*-isomerization, and the mobility of about 5% solitons is depinned. This spin mobility causes the drastic increasing in probability of the tunneling electron hopping between the solitons in *trans*-PA and thus in its conductivity up to $\sigma_{DC} \sim 10^{-3}$ S/m. It should be stressed that because the solitons play an auxiliary role, the described charge transport mechanism may be correct, however, only for pristine and slightly doped *trans*-PA. At higher doping levels, the electron intersoliton hopping is unlikely to be the dominant charge transport mechanism and the conductivity is determined mainly by other parallel processes. Thus, charge transfer mechanism and dynamic processes in PA strongly depend on the structure, conformation, packing density, and the length of conducting chains of this polymer.

4.2. Polythiophene

Polythiophene is another known conjugation polymer having crystalline lattice with $a = 0.950$ and $c = 1.22$ nm unit constants [139].

Pristine PT demonstrates a single symmetric line with $g = 2.0026$ and $\Delta B_{pp} \approx 0.8$ mT at 3-cm waveband, showing that the spins do not belong to a sulfur-containing moiety and are localized on the polymer chains [28,29]. The low concentration of PC ($n \approx 66$ ppm or 6.6×10^{-5} spin per monomer unit) is consistent with a relatively high purity of material, containing few chain defects. EPR signal of a slightly doped poly(3-methyl)thiophene was found to be a superposition of Gaussian line with $g_1 = 2.0035$ and $\Delta B_{pp} = 0.7$ mT attributed to the presence of localized PC and a Lorentzian one with $g_2 = 2.0029$ and $\Delta B_{pp} = 0.15$ mT due to delocalized PC [140]. In this sample, the total concentration of PC amounts to about 3×10^{25} spins/m^3, that is, about one spin per 300 thiophene rings. After doping, only one symmetric Lorentzian component of the former spectrum is observed. This line is symmetric at $y \leq 0.25$ and demonstrates a Dyson-like line at higher y [141]. This process is accompanied by a sufficient decrease of electron both spin-lattice and spin–spin relaxation times [140], which may indicate the growth of system dimensionality upon doping process. The analysis of $\chi(y)$ dependency shows that polarons are formed predominantly at low doping level and then start to combine into bipolarons at higher y.

Powder-like PT samples synthesized electrochemically from monothiophene and dithiophene and containing different counterions were studied at 2-mm waveband EPR [95,142].

EPR spectra of PT, synthesized from monothiophene with BF_4^-, ClO_4^-, and J_3^- anions demonstrate a symmetric single line with $g \approx g_e$ and the width, slightly changing in a wide temperature range at 3-cm waveband (Table 3). However, the line width of PT(J_3^-), synthesized from dithiophene, is broadened significantly with the temperature increase.

2-mm EPR spectra of PT demonstrate a greater variety of line shape. Fig. 11 displays 2-mm EPR spectra of powder-like PT samples containing different counterions as a dopant. The figure shows that PC stabilized in PT(BF_4^-) and PT(ClO_4^-) samples demonstrate an axially symmetric spectrum typical for PC localized on polymer chains. The analogous situation seems to be realized also for PT(J_3^-), for which the broadening and overlapping of canonic components of EPR spectrum can take place because of a higher spin-orbit interaction of PC with counterions.

Magnetic parameters, calculated from 2-mm EPR spectra together with an electroconductivity of the abovementioned samples measured at both direct and alternating currents, σ_{DC} and σ_{AC}, and the energies of electron excitation on nearest level, $\Delta E_{\sigma\pi^*}$ are also presented in Table 3. It derives from the analysis of the data, that the energy of an excited configuration $\Delta E_{\sigma\pi^*} \propto \Delta g^{-1}$, increases more than four times within with $J_3^- \rightarrow BF_4^- \rightarrow ClO_4^-$ series. Such a transition also leads to the growth of film conductivity and a sufficient PC concentration change. This may be the evidence for the realization of charge transfer in PT both by polarons and bipolarons, whose concentration ratio depends on the origin of anion, introduced into a polymer. The width of EPR spectral components of PT is more susceptible to the registration frequency change than in the case of PA and some other conducting polymers, indicating a more strong spin–spin exchange in PT.

With the temperature decrease, a Dyson-like line is displayed in the region of a perpendicular component of

Table 3
The concentration of PCs N (in 10^{25} spin/cm^3), electric conductivity σ_{DC} (in 10^3 S/m), linewidth ΔB_{pp} (in mT), **g** tensor components, $g_\parallel$ and $g_\perp$, and the energy of electron excitation state $\Delta E_{\sigma\pi^*}$ (in eV) of PT samples at $T = 300$ K
The linewidths measured at $T = 77$ K are presented within parentheses.

Parameter	PT (J_3^-)	PT (BF_4^-)	PT (ClO_4^-)	PT (ClO_4^-)[a]
N	2	8	5	10
σ_{DC}	0.5	1.2	16	11
ΔB_{pp}^b	0.75 (0.80)	0.23 (0.34)	0.46 (0.52)	0.70 (0.25)
ΔB_{pp}^c	6.52	1.52	2.63	0.51
$g_\parallel$	2.00679[d]	2.00412	2.00230	2.00232[d]
$g_\perp$	2.00232[d]	2.00266	2.00239	2.00364[d]
$\Delta E_{\sigma\pi^*}$	1.6	4.0	7.1	4.5

[a] Synthesized from dithiophene.
[b] Measured at 3-cm waveband.
[c] Measured at 2-mm waveband.
[d] The values are calculated from the equation $\langle g \rangle = 1/3(g_\perp + 2g_e)$.

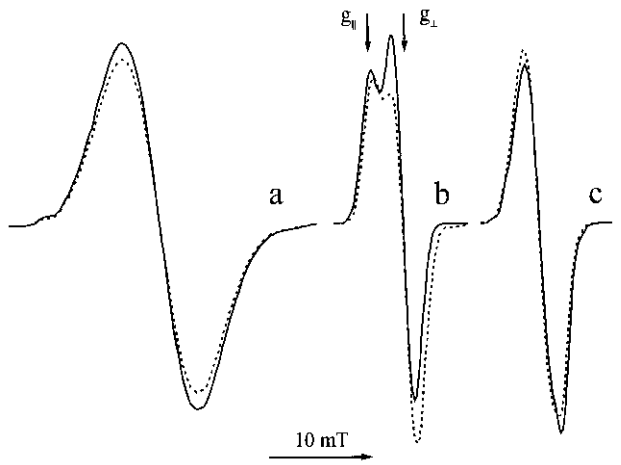

Fig. 11. 2-mm EPR absorption spectra of PT electrochemically synthesized from thiophene and doped by J_3^- (a), BF_4^- (b) and ClO_4^- (c) anions registered at $T = 300$ (solid line) and 200 K (dashed line). The components of **g** tensor are shown.

$PT(BF_4^-)$ EPR spectrum without a noticeable change of signal intensity (Fig. 11b). The further temperature decrease results in the increase of the factor of line asymmetry A/B without reaching the extreme in 100–300 K temperature range, thus being the evidence for the growth of AC conductivity as for the other semiconductors of lower dimensionality. Therefore, AC microconductivity of a sample can be determined knowing the characteristic size of sample particles and using $A/B(\delta)$ dependency, presented in Ref. [89]. Then applying relationship (41), one can determine the mobility $\mu_\parallel$ and the rate of 1D diffusion $\nu_\parallel$ of charge carriers in PT. σ_{AC}, $\mu_\parallel$, and $\nu_\parallel$ values calculated for $PT(BF_4^-)$ amount to 3.6×10^2 S/m, 1.1×10^{-5} m^2 V^{-1} s^{-1}, and 3.2×10^{12} s^{-1}, respectively, at room temperature [95].

3-cm EPR spectrum of $PT(ClO_4^-)$, synthesized from dithiophene, appears as a single symmetric line, whose width decreases smoothly monotonically from 0.7 down to 0.25 mT with the temperature decrease from 300 down to 77 K [142]. At 2-mm waveband EPR, this sample also demonstrates a single EPR line in a wide temperature range, thus indicating the domination of delocalized PC in this polymer. With the temperature rise, a paramagnetic susceptibility of a sample decreases sufficiently down to $T_c = 200$ K and then sharply rises with the further temperature growth (Fig. 12). This is accompanied by the change of line width ΔB_{pp}, the functions $\Delta B_{pp}(T)$ and $\chi(T)$ being in out-of-phase (Fig. 12). This effect can be explained by polaron pairs annihilation into bipolarons at temperature rise from 100 K up to T_c with the following bipolarons break-up to polarons at the further temperature growth probably because of the intensification of polymer chain librations. Assuming a linear dependency for both bipolaron breakup rate and the frequency of polymer chain librations, one can evaluate the activation energy of the latter process to be equal to $E_a = 0.16$ eV at $T > T_c$, by using $\chi(T)$ dependency. Such a complex character of polaron–bipolaron transformation seems to explain the abovementioned unusual broadening of 3-cm EPR spectrum of this sample with the temperature increase.

As in the case of $PT(BF_4^-)$, 2-mm EPR spectrum of this sample demonstrates Dyson-like line at low temperatures, being also the reflection of the change of its electroconductivity. Using the procedure mentioned above in the suggestion that the total concentration of charge carriers of both types is constant, one can establish the temperature dependency of 1D diffusion rate of charge carriers in this sample. It is obvious (Fig. 12) that $\nu_\parallel = 3 \times 10^{13}$ s^{-1} at room temperature and is close on the order of value to that determined earlier for polarons in doped PANI, in which interchain charge transfer dominates. A weak temperature dependency of $\nu_\parallel$, determined for $PT(ClO_4^-)$ is also the evidence for the domination of interchain charge transfer and the growth of dimensionality in this polymer.

4.3. Poly(p-phenylene)

A number of unpaired electrons observed in PPP, strongly depends on the technique used for the polymerization and is varied within 10^{23}–10^{25} spins/m^3 [28]. As in the case of *trans*-PA, the room temperature line width of PPP increases at doping with the increase of atomic number of an alkali metal dopant, a strong interaction between molecule of a dopant and an unpaired electron. The conduction process occurs predominantly via polarons at low doping level and bipolarons at metallic state, similar to that, observed in other highly conducting polymers [143,144]. The lattice constants are $a = 0.779$, $b = 0.562$, and $c = 0.426$ for monoclinic unit [145], and $a = 0.781$, $b = 0.553$, and $c = 0.420$ for orthorhombic unit [146] of PPP.

Some samples of PPP films obtained by electrochemical oxidation of benzene in $BuPyCl–AlCl_3$ melt were studied

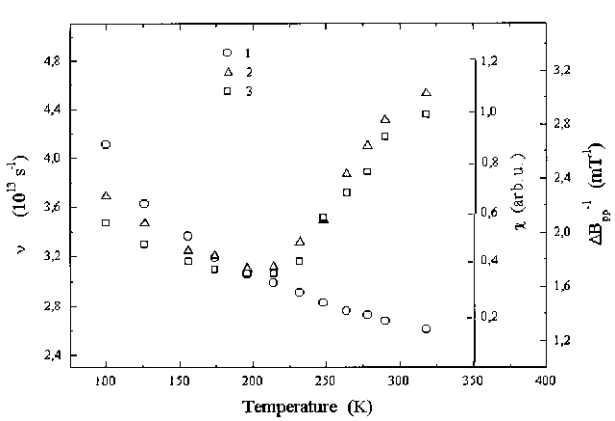

Fig. 12. The plot of intrachain diffusion rate ν_{1D} of charge carriers (1), relative paramagnetic susceptibility χ (2), and inverted linewidth ΔB_{pp} (3) versus temperature for PT electrochemically synthesized from dithiophene and doped by ClO_4^- counterion.

at 3-cm and 2-mm wavebands: a freshly prepared and evacuated PPP(Cl_3^-) film (PPP-1); the same film after a 4-day storage (PPP-2); that exposed for a few seconds to air oxygen (PPP-3); after Cl_3 dopant removal from the PPP-1 sample (PPP-4); and after BF_4 redoping of the PPP-1 film (PPP-5) [96,147].

At 3-cm waveband, PPP-1–PPP-3 samples demonstrate an asymmetric single spectrum with $g = 2.0029$ and a well-pronounced Dyson-like shape (Fig. 13a). The line asymmetry factor A/B (a ratio of amplitude of the positive peak to that of the negative one) is changed depending on the sample conductivity. As dopant Cl_3 is removed, that is, at the transition from PPP-1 film to PPP-4 one, the above spectrum transforms to a two-component one with $g_\perp = 2.0034$ and $g_\parallel = 2.0020$ (Fig. 13b). Such a transition is accompanied by a line broadening and by a drastic decrease in the concentration of spins and charge carriers (Table 4). It is worth noting that in earlier studies of PPP, none of the axially symmetric EPR spectra for π-conducting polymers [28], was registered at 3-cm waveband. With PPP doped by BF_4^- anions (PPP-5), the spectrum shape retains, however, a slight decrease in the concentration of PC, and a change in the sign of its dependency on temperature are observed (Table 4). Using the dispersion $g_\perp - g_\parallel = 1.4 \times 10^{-3}$, the minimum excitation energy of unpaired electron $\Delta E_{\sigma\pi^*}$ is calculated from Eq. (3) to be equal to 5.2 eV. This energy is close to the first ionization potential of polycyclic aromatic hydrocarbons [132]. Consequently, PC can be localized in PPP-4 and PPP-5 samples near cross-linkages which appear as polycyclic hydrocarbons as it was predicted earlier [148].

At 2-mm waveband, the bell-like component $u_2 \cos(\omega_m t - \pi)$ attributed to the manifestation of the fast passage of inhomogeneously broadened line is registered in EPR spectrum of the two latter films (Fig. 13c). Thus, $T_1 = 10^{-4}$ s is correct for dedoped and redoped samples.

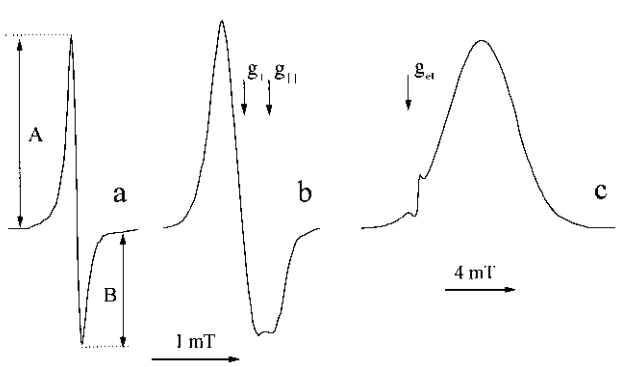

Fig. 13. Typical 3-cm EPR in-phase modulation absorption spectrum of PPP-1–PPP-3 (a) and PPP-4, PPP-5 (b) samples; (c) typical 2-mm EPR in-phase modulation dispersion spectrum of PPP-4 and PPP-5 films (see the text) registered at room temperature. In the latter spectrum, a narrow line of the lateral standard, single crystal $(DBTTF)_3PtBr_6$ with $g_{et} = 2.00411$ is shown.

Table 4
The concentration of PCs N (in 10^{23} spin/cm^3), electric conductivity at constant σ_{DC} and alternating ($\nu_e = 140$ GHz) σ_{AC} current (respectively, in S/m and 10^5 S/m), the line asymmetry parameter (A/B), linewidth ΔB_{pp} (in mT), and spin-lattice relaxation time T_1 (in μs) of PPP samples at $T = 300$ K

Parameter	PPP-1	PPP-2	PPP-3	PPP-4	PPP-5
N	120	320	210	4.1	0.62
σ_{DC}	10^3–10^4	–	–	10^{-6}	1.0
σ_{AC}	3	4	1.4	–	–
A/B	2.3	2.5	1.4	–	–
ΔB_{pp}	0.09	0.12	0.22	0.37[a]	0.47[a]
T_1	0.4	0.5	0.2	≈100	≈100

[a] The width of high-field spectral component.

From the analysis of a line shape of spectra registered at 3-cm and 2-mm wavebands, the rate of spin-packets exchange in neutral and redoped films, $\nu_{ex} = 4 \times 10^7$ s^{-1} was estimated [147]. This value increases up to 1.8×10^8 s^{-1} for doped film due to the PC concentration and mobility increase. Isotropic g-factor, $\langle g \rangle = 1/3(g_\parallel + 2g_\perp)$ of a neutral sample is equal to g-factor of Cl_3^--doped one. This fact shows that **g** tensor components of PC are averaged due to their 1D spin diffusion with the rate (see Eq. (40)) $\nu_\parallel^0 \geq 6.8 \times 10^6$ s^{-1} in doped PPP(Cl_3^-) sample. Indeed, the rate of 1D spin diffusion calculated by using Eq. (11) yields $\nu_\parallel = 9 \times 10^{10}$ s^{-1} at room temperature. The temperature dependency of electroconductivity for PPP-1 film is determined at alternating current from $A/B(T)$ one to be $\sigma_{AC} \propto T^{-1/3}$. Such a dependency seems to indicate the existence of some conductivity mechanisms in doped PPP sample, namely VRH [72] and isoenergetic tunneling of charge carriers. A sharp decrease of PC concentration, the rates of spin exchange and relaxation processes at sample dedoping (at transition from PPP-1 to PPP-4), is the evidence for the annihilation of most polarons, whose 1D diffusion causes electron relaxation of the whole spin system.

Thus, EPR data allow the conclusion that in highly doped PPP-1, the charge is transferred by mobile polarons, whereas in PPP-5, the charge transfer is realized preferably by spinless bipolarons.

At electrochemical substitution of Cl_3^- anion for BF_4^- one, the location of the latter may differ from that of the dopant in the initial PPP sample; the morphology of BF_4^--redoped PPP may be close to that of a neutral film (PPP-4).

As it was established by Goldenberg et al. [96,147], the PPP film synthesized in the BuPyCl–$AlCl_3$ melt is characterized by less number of benzoid monomers and by more number of quinoid units. It leads to a more ordered structure and planar conformation of the polymer that in turn prevents the collapse of the spin charge carriers to bipolaron in highly doped polymer. The anions are removed at dedoping, so then the packing density of the polymer chains grows. It can prevent an intrafibrillous

introduction of BF_4^- anions and lead to the localization of dopant molecules in the intrafibrillous free volume of the polymer matrix. The change of charge transfer mechanism at PPP redoping process is probably a result of such a conformational transition.

4.4. Polypyrrole

The crystal lattice is characterized by $a = 0.820$, $b = 0.735$, and $c = 0.682$ nm unit constants [149].

Neutral PP also exhibits a complex 3-cm EPR spectrum with a superposition of a narrow (0.04 mT) and a wide (0.28 mT) lines with $g \approx 2.0026$ [28], typical for radicals in polyene and aromatic π-systems. The intensities of both lines correspond to one spin per a few hundred monomer units. These features, together with the temperature dependencies of the line width and intensity (the narrow line is thermally activated, while the broad one has a Curie behavior), were interpreted in terms of coexistence of two types of PC with different relaxation parameters in neutral PP. Doped PP sample exhibits only a strong and narrow (~ 0.03 mT) 3-cm EPR spectrum with $g = 2.0028$, which follows Curie law from 300 to 30 K [28]. Most of the preceding results imply that EPR signal does not arise from the same species, which carries the charges, because of the absence of correlations of the susceptibility with concentration of charge carriers and the line width with the carrier mobility. This was interpreted in favor of the spinless bipolaron formation upon PP doping. Thus, EPR signal of doped PP are attributed mainly to neutral radicals and therefore tell little about the intrinsic conducting processes.

The method of spin probe [150] based on the introduction of stable nitroxide radical (NR) into the system under investigation seems to be more effective for these purposes. Only a few papers reported the study of conducting polymers by using spin label and probe at 3-cm waveband [151,152]. However, a low spectral resolution at this band did not allow the registration of all components of **g** and **A** tensors and therefore the separate determination of the magnetic susceptibility of both NR and PC localized on the polymer chain, and the measurement of the dipole–dipole interaction between different PCs. Popypirrole modified during electrochemical synthesis by nitroxide doping anion, as a label covalently joined to the pyrrole cycle, was studied by Winter et al. [151]. However, in spite of a large number of NRs introduced into PP, its 3-cm waveband EPR spectrum did not contain NR lines.

The method of spin probe was found to be more effective at investigation of doped PP at 2-mm waveband EPR [153].

3-cm and 2-mm absorption EPR spectra of 4-carboxy-2,2,6,6-tetramethyl-1-piperidyloxyl NR, introduced as a probe and a counterion into PP and as a probe into a frozen nonpolar model system are shown in Fig. 14. One can see that in spin modified PP 3-cm EPR spectrum, the

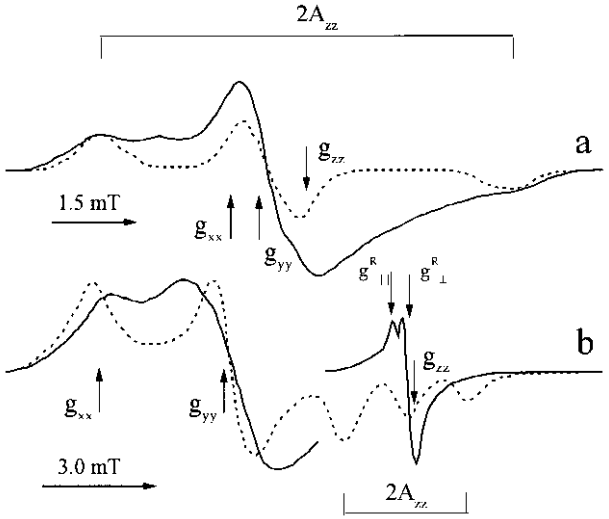

Fig. 14. 3-cm (a) and 2-mm (b) waveband EPR absorption spectra of 4-carboxy-2,2,6,6-tetramethyl-1-oxypiperidiloxyl nitroxide radical introduced into frozen (120 K) toluene (dotted line) and conductive PP (solid line) as a spin probe. The anisotropic spectrum of localized PCs marked by the symbol *R* and taken at a smaller amplification is also shown in the lower figure. The measured magnetic parameters of the probe and radical *R* are shown.

lines of NR with rotating correlation time $\tau_c > 10^{-7}$ s overlap with the single line of PC (R) stabilized in PP (Fig. 14a). Such an overlapping stipulated by a low spectral resolution, hinders the separate determination of MRPs of the probe and radical R in PP together with the dipole–dipole broadening of its spectral components.

Indeed, the spectra of both model and modified polymer systems are expected to be more informative at 2-mm waveband EPR (Fig. 14b). At this band, all canonic components of EPR spectra of the probe are completely resolved in PP and toluene, and consequently all the values of **g** and **A** tensors can be measured directly. Nevertheless, the asymmetric spectrum of radicals R with magnetic parameters $g_{\|}^R = 2.00380$, $g_{\perp}^R >= 2.00235$ and $\Delta B_{pp} = 0.57$ mT is registered in z-component region of the probe spectrum in PP. In nonpolar toluene, the probe is characterized by the following MRP: $g_{xx} = 2.00987$, $g_{yy} = 2.00637$, $g_{zz} = 2.00233$; $A_{xx} = A_{yy} = 0.6$ mT and $A_{zz} = 3.31$ mT. The difference $\Delta g = g_{\|}^R - g_{\perp}^R = 1.45 \times 10^{-3}$ corresponds to an excited electron configuration in R with $\Delta E_{\sigma\pi^*} = 5.1$ eV lying near an energy of electron excitation in neutral PPP. In conducting PP, g_{xx} value of the probe decreases down to 2.00906 and the broadening of its x- and y-components, $\delta(\Delta B_{pp})$ is 4 mT (Fig. 14b). In addition, the shape of the probe spectrum shows the localization of PC R on the polymer pocket of 1 nm size, that is, change is transferred by spinless bipolarons in PP, as it was proposed in the case of PPP(BF_4) and PT(BF_4).

The fragments with a considerable dipole moment are a priori absent in neutral PP. Besides, the dipole–dipole interactions between the radicals can be neglected due to

low concentration of the probe and PC localized on the chain. Therefore, the above change in the probe MRP taking place at transition from model nonpolar system to the conducting polymer matrix may be caused by Coulombic interaction of the probe active fragment with the spinless charge carriers, bipolarons. The effective electric dipole moment of bipolarons nearest to the probe was determined from the shift of g_{xx} component to be equal to $\mu_\upsilon = 2.3$ D. The shift of **g** tensor component g_{xx} of the probe may be calculated within the frames of the electrostatic interaction of the probe and bipolaron dipoles by using the following approach.

The potential of electric field induced by bipolaron in the place of the probe localization is determined as [154]

$$E_d = \frac{k_B T(x \coth x - 1)}{\mu_u} \quad (46)$$

where $x = 2\mu_u \mu_\upsilon (\pi\varepsilon\varepsilon_0 k_B T r^3)^{-1}$, μ_u is the dipole moment of the probe, ε and ε_0 are the dielectric constants for PP and vacuum, respectively, and r is the distance between an active fragment of the radical and bipolaron. By using the dependence of the growth of an isotropic hyperfine constant of the probe under microenvironment electrostatic field, $\Delta a = 7.3 e r_{NO} I^{-1}$ (here r_{NO} is the distance between N and O atoms of the probe active fragment, I is the resonant overlapping integral of C=C bond) and the relation $dg_{xx}/dA_{zz} = 2.3 \times 10^{-3}$ for six-membered NR [155], one can write $\Delta g_{xx} = 6 \times 10^{-3} e r_{NO} k_B T(x \coth x - 1)/(I\mu_u)$. By using $\mu_u = 2.7$ D [156], $\mu_\upsilon = 2.3$ D and $r_{NO} = 0.13$ nm [39], the value of $r = 0.92$ nm is obtained.

The spin–spin relaxation rate which stipulates the radical spectral line width can be written as $T_2^{-1} = T_{2(D)}^{-1} + T_{2(0)}^{-1}$, where $T_{2(0)}^{-1}$ is the relaxation rate of the radical noninteracting with the environment and $T_{2(D)}^{-1} = \gamma_e \delta(\Delta B_{x,y})$ is the growth in the relaxation rate due to dipole–dipole interactions. The characteristic time τ_c of such an interaction can be calculated from the broadening of the spectral lines using Eq. (23b) with $J(\omega_e) = 2\tau_c/(1 + \omega_e^2 \tau_c^2)$. The inequality $\omega_e \tau_c \gg 1$ is valid for most condensed systems of high viscosity, so then averaging over angles, $\sum\sum(1\text{-}3\cos^2\vartheta)^2 r_1^{-3} r_2^{-3} = 6.8 r^{-6}$ [44] and using $r = 0.92$ nm calculated above and $\gamma_e \delta(\Delta B_{pp}) = 7 \times 10^8$ s^{-1}, one can determine $T_{2(D)}^{-1} = 3\langle \omega^2 \rangle \tau_c$ or $\tau_c = 8.1 \times 10^{-11}$ s. Taking into account, that the average time between the translating jumps of charge carriers is defined by the diffusion coefficient D and by the average jump distance equal to a product of lattice constant $c_\parallel$ on half-width of charge carrier $N_p/2$, $\tau_c = 1.5\langle c_\parallel^2 N_p^2 \rangle D^{-1}$, and by using then $D = 5 \times 10^{-7}$ m^2/s typical for conducting polymers, one can determine $\langle c_\parallel N_p \rangle = 3$ nm equal approximately to four pyrrole rings. This value lies near to a width of the polaron in both PP and PANI, but, however, is smaller considerable then N_p obtained for polydithiophene [157].

Thus, the shape of the probe spectrum displays a very slow motion of the probe due, probably, to a enough high pack density of polymer chains in PP. The interaction between spinless charge carriers with an active fragment of the probe results in the redistribution of the spin density between N and O nuclei in the probe and therefore in the change of its MRP. This makes it possible to determine the distance between the radical and the chain along which the charge is transferred together with a typical bipolaron length in doped conducting polymers.

4.5. Poly(tetrathiofulυalene)

3-cm EPR spectra of powder-like PTTF samples in which TTF units are linked via phenyl (PTTF-1,2) or tetrahydroanthracene (PTTF-3) bridges (Fig. 2) are a superposition of a strongly asymmetric spectrum of immobilized PC with $g_{xx} = 2.0147$, $g_{yy} = 2.0067$, $g_{zz} = 2.0028$ and a symmetric spectrum caused by mobile polarons with $g = 2.0071$ [86,87]. A relatively high value of **g** tensor evidences for the interaction of an unpaired electron with sulfur atom having large spin-orbit coupling constant. The temperature dependency of T_1 of an undoped PTTF-2 sample was determined by Roth et al. [86,87] to be $T_1 \propto T^{-\alpha}$ where $\alpha = 2$ at $100 < T < 150$ K and $\alpha = 1$ in $150 < T < 300$ K range. The addition of a dopant causes the change of a line shape of PTTF-2 referring to the appearance of a greater number of mobile PC. Such a change in the magnetic and relaxation parameters was attributed to the conversion of the bipolarons into the paramagnetic polarons induced by the doping process or/and temperature increase. In neutral and slightly doped polymers, the charge is transferred by small polarons [62]. However, it was found impossible to carry out the detailed investigation of doped PTTF samples, having low concentration of the immobilized PC and to analyze the contributions of PC of both types to electrodynamic and relaxation parameters at 3-cm waveband EPR.

The nature, composition, and dynamics of PC in initial and iodine-doped PTTF samples were studied at 2-mm waveband EPR more completely [88,158–160].

Typical 2-mm waveband EPR absorption spectra of the samples are shown in Fig. 15. They allow one to determine more correctly all canonic components of the anisotropic **g** tensor and to separate the lines attributed to different PCs. Computer simulation shows that the signals are a superposition of a strongly asymmetric spectrum with temperature-independent magnetic parameters. The anisotropic EPR spectrum of PTTF-1 consists of two lines of PC, namely R_1 with $g_{xx} = 2.01189$, $g_{yy} = 2.00544$, $g_{zz} = 2.00185$, and more mobile R_2 one with $g_{xx} = 2.00928$, $g_{yy} = 2.00632$, $g_{zz} = 2.00210$. The spectrum of PTTF-2 is characterized by the magnetic parameters $g_{xx} = 2.01424$, $g_{yy} = 2.00651$, $g_{zz} = 2.00235$, whereas PCs with nearly symmetric spectrum are registered at $g^p =$

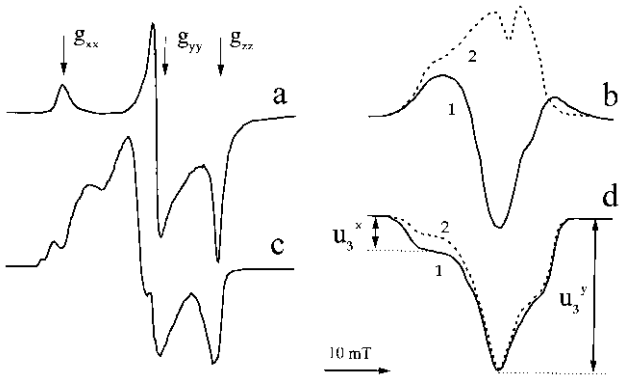

Fig. 15. Typical 2-mm EPR in-phase absorption spectra (a,c) and in-phase (b) and $\pi/2$-out-of phase (d) components of dispersion signal of the initial (a) and doped (b–d) PTTFs registered at room temperature. The dispersion spectra of the polymers registered at $T \leq 150$ K (2) and $B_1 = 20$ μT are shown.

2.00706. The canonic components of **g** tensor of PC localized in PTTF-3 are $g_{xx} = 2.01292$, $g_{yy} = 2.00620$, $g_{zz} = 2.00251$, whereas PCs with weakly asymmetric spectrum are characterized by the following parameters $g_{\|}^{p} = 2.00961$ and $g_{\perp}^{p} = 2.00585$. PCs of different types are present in the sample with the concentration ratio of 20:1 in neutral PTTF-1, 1:1.8 in PTTF-2, and 3:1 in neutral PTTF-3.

As g^{p} value is close to the average g-factor of immobile PC, PC of two types with approximately equal magnetic parameters exist in PTTF, namely polarons moving along the polymer long axis with the rate (see Eq. (40)) of $\nu_{\|}^{0} \geq 5 \times 10^{9}$ s^{-1} and polarons pinned on traps or/and on short polymer chains. The comparatively large ions of iodine soften the polymer matrix at doping, so the mobility of its polymer chains increases. It is just a reason for the growth of a number of delocalized polarons (Fig. 15). The components of **g** tensor of part of PC are averaged completely due to its mobility in PTTF-2, whereas such an averaging takes place only partially in the case of PTTF-3. This fact can be explained by a different structure and conformation of the polymers' chains.

The line width ΔB_{pp}^{imm} of EPR spectral components of immobile polarons in, for example, PTTF-2 is weakly temperature-dependent; however, increases from 0.28 to 0.38 mT and then to 3.9 mT, while the operation microwave frequency ν_e increases from 9.5 to 37 and then to 140 GHz, respectively. At the same time, the line width ΔB_{pp}^{mod} of mobile polarons increases from 1.0 to 1.12 and then to 17.5 mT, respectively, at such a transition. The fact, that the mobile PCs have a broader line than the pinned ones, can be explained by their stronger interaction with a dopant. This is typical for conducting polymers [38,95]; however, it disagrees with the data obtained for PTTF-2 at 3-cm waveband EPR [86,87].

The decrease of the spectrum line width of the mobile polarons in PTTF samples with the temperature decrease indicates the mobility of polarons to become more intensive. Such a change in ΔB_{pp}^{mod} is analogous to the line narrowing of spin charge carriers in classic metals.

Since the line widths of PC increases according to Eq. (10) with the increase of ν_e in $37 \leq \nu_e \leq 140$ GHz range, this evidences for a weak interaction between spin-packets in this polymer. This is a reason for the saturation of PC in PTTF at comparatively small B_1 values at 2-mm waveband EPR and therefore for the manifestation of the effects of fast passage in both in-phase and $\pi/2$-out-of-phase components of its dispersion signal (Fig. 15). $\omega_m T_1 < 1$ inequality is realized for doped PTTF samples, so that the first derivative of its dispersion signal is determined mainly by u_1 and u_3 terms of Eq. (28). On the other hand, $\omega_m T_1 > 1$ condition is actual for the undoped PTTF-3 sample; therefore, its dispersion signal is determined by u_2 and u_3 terms of the above equation.

The simulation of the dispersion spectra showed them to be a superposition of a predominant asymmetric spectrum with $g_{xx} = 2.01189$, $g_{yy} = 2.00564$, $g_{zz} = 2.00185$ (undoped PTTF-1); $g_{xx} = 2.01356$, $g_{yy} = 2.00603$, $g_{zz} = 2.00215$ (PTTF-2); $g_{xx} = 2.01188$, $g_{yy} = 2.00571$, $g_{zz} = 2.00231$ (undoped PTTF-3) of immobile polarons and a spectrum, attributed to mobile polarons (Fig. 15). The components u_i^x, u_i^y, and u_i^z of the dispersion signal U corresponding to the parts of a strong asymmetric spectrum are caused by the g-factor anisotropy.

The effective relaxation times of PC in PTTF samples determined from their 2-mm EPR spectra using Eqs. (36a), (36b), (37a) and (37b) are summarized in Table 5. T_1 value was shown to change with temperature like $T^{-\alpha}$, where $\alpha \geq 3$ for pinned and mobile polarons. The exponent α determined from 2-mm waveband EPR is larger than that measured for immobile radicals by using 3-cm spin echo technique [86]. A small difference between T_1^{mob} and T_1^{imm} can be caused, for example, by a strong interaction between different PCs.

Table 5
The relaxation times ($T_{1,2} = AT^{\alpha}$, in s) of PCs in PTTFs as a function of the doping level y and temperature
T_2 values of PTTF-1 samples are presented for $100 \leq T \leq 180$ K temperature range.

Sample	y	T_1		T_2	
		A	α	A	α
PTTF-1	0.00	8.9×10^{10}	−6.6	1.6×10^{-12}	2.8
	0.02	8.8×10^{5}	−4.7	2.5×10^{-9}	1.3
	0.04	205	−3.3	2.1×10^{-8}	0.8
	0.08	4.9	−2.7	7.3×10^{-8}	0.7
PTTF-2	0.12	2.4	−2.5	6.9×10^{-4}	−1.3
PTTF-3	0.00	17.8	−2.7	8.4×10^{-8}	0.6
	0.10[a]	3.6×10^{-6}	−0.3	9.1×10^{-8}	0.2
	0.10[b]	1.1×10^{-3}	−1.4	9.1×10^{-8}	0.2

[a] Measured at $100 \leq T \leq 160$ K temperature range.
[b] Measured at $160 \leq T \leq 300$ K temperature range.

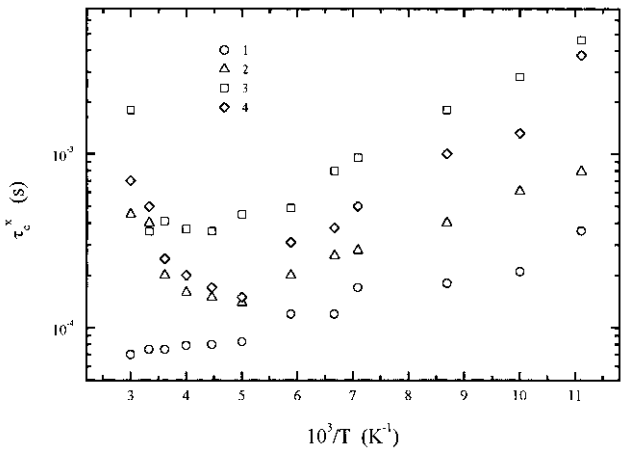

Fig. 16. The Arrhenius dependencies of correlation time τ_c^x of x-anisotropic libration of polymer chains in PTTF-1 with $y = 0.00$ (1), 0.02 (2), 0.05 (3), and 0.08 (4) evaluated from their ST-EPR spectra.

Let us consider the possibility of application of 2-mm waveband EPR spectroscopy for an investigation of molecular mobility in PTTF and other conducting polymers, in which PCs have a significant anisotropy of magnetic parameters. The macromolecular motion in PTTF, similarly to ordinary ones, is a priori strongly anisotropic with the correlation time $\tau_c \geq 10^7$ s^{-1} [138]. A widely used, ''linear'' EPR method in which the in-phase absorption signal is registered is not sensitive to such molecular processes. Therefore, ST-EPR method [35] based on the abovementioned saturation effect can be used.

The ST-EPR method is based on the introduction of nitroxide label or probe into the system under investigation and on the registration of this radical spectrum in a condition of fast passage of a saturated signal. Earlier, it was shown [38] that the components ratio of $\pi/2$-out-of-phase term of the dispersion signal U, $K_{mov} = u_3^x/u_3^y$ is the more sensitive parameter to the anisotropic molecular dynamics. The sensitivity of the method depends also on an anisotropy of magnetic parameters of PC and on an operation frequency (see Eq. (29)). Taking into account that PC, localized on a polymer chain, are themselves paramagnetic labels and are characterized by a considerable magnetic parameters anisotropy, one could hope that this method would be efficient in the investigation of conducting compounds at 2-mm waveband EPR.

As it is seen from Fig. 15, the heating of PTTF leads to the growth of its $K_{mov} = u_3^x/u_3^y$ parameter. It can be a result of an anisotropic librational reorientations of the pinned polarons near main x-axis of the polymer chains. The Arrhenius dependencies of correlation times of such molecular motions in PTTF-1 samples calculated from Eq. (38) by using the method described in Ref. [38] are shown in Fig. 16. The maximum value of τ_c is approximately 10^{-4} s at $T = 75$ K when $K_{mov} = 0.07$. This value follows $\tau_c = 9.8 \times 10^{-6}$ exp(0.02 eV/k_BT) law for PTTF-2, $\tau_c = 5.2 \times 10^{-6}$ exp(0.02 eV/k_BT) for undoped PTTF-3, and $\tau_c = 2.4 \times 10^{-6}$ exp(0.04 eV/k_BT) for doped PTTF-3 samples. The activation energy of librational motion is comparable with that of interchain charge transfer in doped PTTF samples [86,87], which indicates the interaction of pinned and mobile polarons in this polymer matrix.

In order to compare experimental results with the polaron theory, 1D diffusion motion of mobile PC in PTTF with the rate of $\nu_\parallel$ and their 3D hopping between the chains with the frequency of $\nu_\perp$ was assumed.

The temperature dependencies of $\nu_\parallel$ and $\nu_\perp$ calculated for PC in PTTF samples by using Eqs. (23a) and (23b) and the data presented in Table 5 are shown in Figs. 17–19. Assuming that the spin delocalization over the polaron in PTTF occupies approximately five monomer units [157],

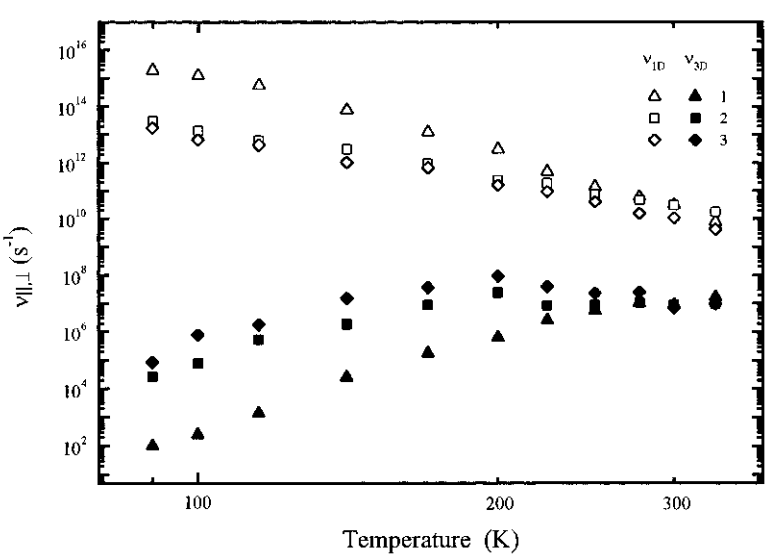

Fig. 17. Temperature dependencies of spin intrachain diffusion ν_{1D} and interchain hopping ν_{3D} rates determined for PTTF-1 with $y = 0.02$ (1), 0.05 (2), and 0.08 (3) from Eqs. (23a) and (23b) and the data presented in Table 5.

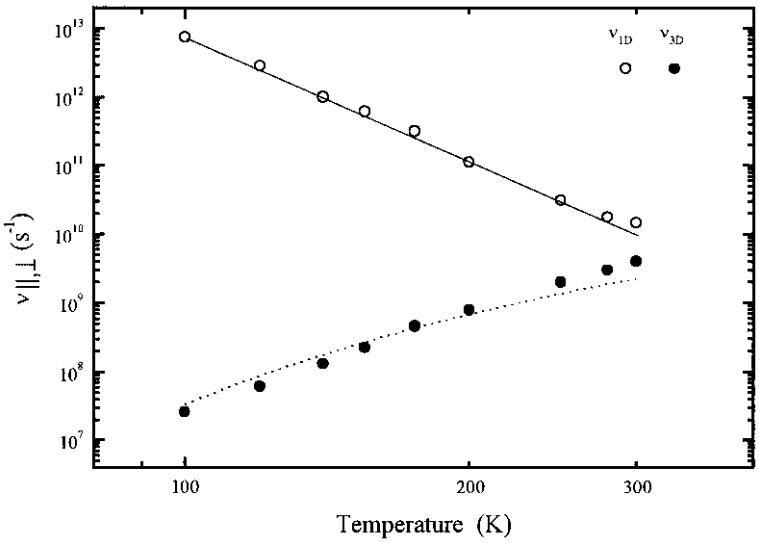

Fig. 18. Temperature dependencies of spin intrachain diffusion ν_{1D} and interchain hopping ν_{3D} rates determined for PTTF-2 sample doped up to $y = 0.12$ from Eqs. (23a) and (23b) and the data presented in Table 5, and AC conductivity σ_{AC} calculated from Eq. (30b) (solid line) and Eq. (33b) (dotted line), respectively.

the maximum value of $\nu_{\parallel}$ does not exceed 1×10^{10} s^{-1} for PTTF-1, 2×10^{10} s^{-1} for PTTF-2, and 2×10^{12} s^{-1} for undoped PTTF-3 samples at room temperature. This value is at least two orders of magnitude lower than that determined earlier by low-frequency magnetic resonance methods for polarons in polypyrrole [161] and polyaniline [157] but higher then $\nu_{\parallel}^{0}$ above calculated. The anisotropy of spin dynamics in PTTF is $\nu_{\parallel}/\nu_{\perp} > 10$ at room temperature.

It is obvious, that the spin dynamic plays a sufficient role in the charge transfer process. Assuming the equal diffusion coefficients for both spin and charge carriers and $n_2 = 6.9 \times 10^{-5}$, the components of PTTF-2 conductivity were calculated by using Eq. (45) to be $\sigma_{1D} \approx 0.1$ and $\sigma_{3D} \approx 4 \times 10^{-3}$ S/m at room temperature. The former value is at least two orders of magnitude larger than $\sigma_{DC} \approx 10^{-3}$ S/m for PTTF-2 [86]. In fact, the electrical conductivity, which is a macroscopic value, is limited by hopping processes between segments, while the microscopic conductivity which is probed by EPR method is higher because $\nu_{\parallel} >> \nu_{\perp}$. Taking into account the difference in temperature behavior of σ_{1D} and σ_{3D} for PTTF-2

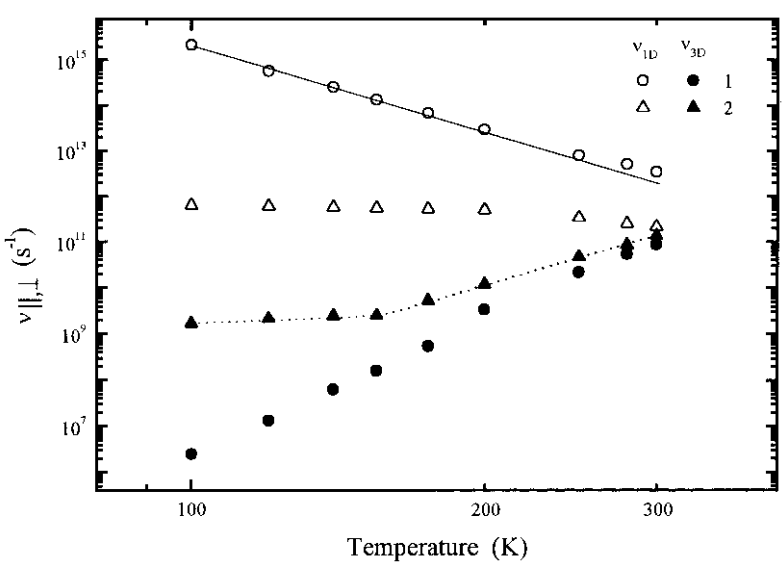

Fig. 19. Temperature dependencies of spin intrachain diffusion ν_{1D} and interchain hopping ν_{3D} rates determined for undoped (1) and doped up to $y \approx 0.1$ (2) PTTF-3 samples from Eqs. (23a) and (23b) and temperature dependencies of AC conductivity σ_{AC} calculated for these samples from Eq. (30b) (solid line) and Eqs. (33b) and (34b) (dotted line).

and that the charges are transferred by polarons of small radius in PTTF [62], one can suggest the isoenergetic mechanism of charge transport in PTTF.

The $\nu_{\parallel}(T)$ dependency for PTTF-2 was shown (Fig. 18) to be good correlated with $\sigma_{1D}(T) = 2.4T^{-1}(25.6–4.3 \ln T)^4$ one, calculated by using Eq. (30b) in terms of the Kivelson's isoenergetic interchain electron hopping formalism [107]. According to Eq. (30a), isoenergetic charge transport should lead to a temperature dependence $\sigma_{DC}(T) \propto T^{12.6}$; however, $\sigma_{3D}(T)$ experimentally obtained follows Eq. (33b) [86]. Therefore, the most acceptable spin dynamic process can be suggested within the thermally activated polaron hopping in conduction band tails.

Indeed, the temperature dependence of $\sigma_{\perp}$ of PTTF-2 is good approximated by function (33b) at $\sigma_0 = 8.3 \times 10^{-14}$ S s m^{-1} K^{-1}, $\nu_e = 1.4 \times 10^{11}$ s^{-1}, $\gamma = 0.8$ and $E_a = 0.04$ eV (Fig. 18). The activation energy obtained corresponds to that of interchain charge transfer at low temperatures, $E_a = 0.03$ eV [86,87]. Besides, this value is approximately equal to the above determined activation energy for PTTF chains libration, $E_a = 0.02$ eV. These facts lead to the conclusion that the conductivity of PTTF is determined mainly by interchain phonon-assisted hopping of polarons.

The probability of charge transfer depends upon the strength of the interaction of a lattice with an electron, which interchain transfer is accompanied with the absorption of minimum number m of lattice phonons. Fig. 18 demonstrates, that interchain hopping rate increases in PTTF-2 with temperature and can be approximated by the power law $\nu_{\perp} \propto T^{4.7}$. On the other hand, the spin-lattice relaxation rate of PC in the polymer has $T^{2.5}$ dependency (Table 5) and reflects a multiphonon process. Thus, by using the averaged $\langle m \rangle = 3.6$ and $E_a^1 = mh\nu_{ph}$ relation, the frequency $\nu_{ph} = 2.5 \times 10^{13}$ s^{-1} for phonons in PTTF-2 can be determined. Thus, the polymer conductivity is initiated by the librations of a polymer chain and is defined by the multiphonon processes due to the strong electron–lattice coupling.

Figs. 17–19 show, that $\nu_{\parallel}$ value increases at room temperature by at least one to two orders of magnitude at transition from PTTF-1,2 to PTTF-3 samples due probably to more planar chains conformation of monomer units of PTTF-3 sample. Indeed, the variation of g_{xx} value is $\Delta g_{xx} = 1.32 \times 10^{-3}$ at such a transition. Assuming, that the overlapping integral of macromolecule depends on dihedral angle θ (i.e., the angle between p-orbits of neighboring C-atoms) as $I \propto \cos\theta$, and that spin density on sulfur atom ρ_s depends as $\rho_s \propto \sin\theta$ [132], one can calculate from Eq. (3) the difference $\Delta\theta$ at such a transition to be $\Delta\theta = 22°$. Note, that analogous change in θ takes place at transition from benzoid to quinoid form of PPP [162] and at transition from emeraldine base to salt form of PANI [163].

Assuming, that somewhat number of bipolarons with 2e charge exists in PTTF, one can describe the conductive properties of PTTF-3 in the frames of the phenomenological approach of isoenergetic phonon-assisted charge hopping between soliton states proposed by Kivelson [61,107] for charge transfer in *trans*-PA. Later, he pointed out [164] that such a process might also be relevant in the other 1D semiconductors in which charge is transferred by soliton-like excitations or even in *cis*-PA with lightly nondegenerate ground states. In this case, the charge hopping would occur between bound soliton–antisoliton pairs such as polarons and bipolarons.

So that $n = 12.2$ and $y_{ch} = y_{bp} = 7.5 \times 10^{-5}$ in Eq. (30b) can be determined from the slope of $\nu_{\parallel}(T)$ dependency shown in Fig. 19. By using $N = 2 \times 10^{23}$ m^{-3}, $c_{\parallel} = 1.2$ nm and the data presented in Fig. 18, $\sigma_{1D} = 1.8$ S/m at room temperature is obtained from Eq. (45). Then using $\xi_{\parallel} = 6$ nm, $\xi_{\perp} = 0.6$ nm, $y_n = y_p = 6.7 \times 10^{-4}$, and $\sigma_{DC} = 2 \times 10^{-6}$ S/m [86], one can obtain $R_0 = 4.1$ nm, $\gamma(T) = 4.0 \times 10^{-23} T^{13.2}$ and $N_i = 3.3 \times 10^{24}$ m^{-3} from Eqs. (30a) and (30b). $\sigma_{AC}(T)$ function calculated for the initial PTTF-3 sample by using Eq. (30b) is presented in Fig. 19. The figure shows a good correlation of both $\nu_{\parallel}(T)$ and $\sigma_{AC}(T)$ dependencies.

It is seen in Fig. 19, that the rate of polaron diffusion increases linearly with temperature up to $T = 160$ K and then changes more strongly at higher temperatures. Such a peculiarity can be explained in terms of the model of VRH small polarons at low temperatures with a contribution of an activation charge transfer at high temperatures. By using the equality $\xi = \langle L \rangle$ and $\nu_0 = \nu_{ph} = 2.5 \times 10^{13}$ s^{-1} for PTTF determined above, $n(\varepsilon_F) = 2.6 \times 10^{-3}$ states/eV and $T_0 = 7.8 \times 10^7$ K are evaluated from Eqs. (34a) and (34b).

The high-temperature part of $\nu_{\perp}(T)$ dependency is well described by Eq. (33b) with $\gamma = 0.8$ and $E_a = 0.035$ eV (Fig. 19). This value is close to those of superslow PTTF chain librations and of interchain charge transfer in PTTF-2. This evidences for the interaction of molecular and charge dynamics in PTTF. It confirms also the supposition given earlier [165], that the fluctuations of lattice oscillations, librations among them, can modulate the electron interchain transfer integral in conducting compounds. PTTF-2 has more soft chains as compared with PTTF-3; therefore, such a modulation is realized at sufficiently lower temperatures in this polymer (Figs. 17 and 18).

The rise of libron–exciton interactions evidences for the formation of a complex quasi-particle, namely molecular-lattice polaron [130] in doped PTTF. According to this phenomenological model, molecular polaron, which is characterized by the mobility of $\mu_m \propto T$ type, is additionally covered by lattice polarization. As the lattice polaron mobility μ_l is temperature-activated, the resulting mobility of such a quasi-particle becomes the sum of mobilities of molecular and lattice polarons

$$\mu(T) = \mu_m(T) + \mu_l(T) = aT + b\exp\left(-\frac{E_a}{k_B T}\right) \qquad (47)$$

where a and b are constants. Assuming the formation energy of molecular polaron in PTTF to be close to that in polyacene crystals, namely $E_{pm} \approx 0.15$ eV [166], one can determine the same value for molecular-lattice polaron in PTTF as $E_{pml} = E_{pm} + E_{pl} = 0.19$ eV. Therefore, the relaxation time, necessary for polarization of both atomic and molecular orbits of polymer, is equal to $\tau_p \approx 2\pi h E_{pml} = 3.5 \times 10^{-15}$ s at room temperature. This value is more than two orders of magnitude smaller than intra- and interchain hopping times for charge carriers in PTTF (Figs. 17–19). This leads to the conclusion, that the hopping time for the charge carriers in PTTF sufficiently exceeds the polarization time for charge carriers' microenvironment in the polymer, that is, $\tau_h \gg \tau_p$. This inequality is a necessary and sufficient condition for electronic polarization of polymer chains by a charge carrier.

The Fermi velocity v_F was determined for PTTF samples to be near to 1.9×10^5 m/s [159]. So the mean free path l_i of a charge was determined to be $l_i = \nu_{\|} c_{\|}^2 v_F^{-1} = 10^{-2}$–$10^{-4}$ nm for different PTTF samples. This value is too small to consider this polymer as Q1D metal.

Thus, 1D and 3D spin dynamics is realized in PTTF affecting the processes of charge transfer. The results show that both the diffusive on-chain and hopping interchain spin dynamics processes occur in PTTF. The conductivity of the polymer is shown to be dominated by interchain electron transfer. However, the analysis of the transport properties of PTTF should include also 1D diffusion of spin and spinless charge carriers.

4.6. Poly(bis-alkylthioacetylene)

The analogue of *trans*-PA, PATAC (Fig. 2b), is also an insulator in neutral form. From ^{13}C NMR study [167], the conclusion was made that PATAC has sp^2/sp^3-hybridized carbon atom ratio typical for PA; however, in contrast with the latter, pristine polymer has a more twisted backbone. The DC conductivity of PATAC at chemical doping increases from $\sigma_{DC} \approx 10^{-12}$ S/m up to $\sigma_{DC} \approx 10^{-8}$–$10^{-2}$ S/m depending on the structure of an anion introduced into the polymer in liquid or gas phase. Roth et al. [168] have shown that at irradiation of PATAC by argon ion laser with $\lambda = 488$ nm, the conductivity increases up to $\sigma_{DC} \approx 10^{-8}$–$10^{-2}$ S/m depending on the absorbed dose. Hall coefficient measurements [168] have shown that the charge carriers are from p-type and the mobility depends on the condition of the sample preparation. In highly laser-modified PATAC, the hall mobility μ is a function of the temperature as $\mu = \mu_0 T^{\alpha}$ with $0.25 \le \alpha \le 0.33$ at $80 \le T \le 300$ K and lies within 10^{-5}–8×10^{-4} m^2/Vs interval at room temperature. The unexpected high latter value is near to $\mu = 2 \times 10^{-4}$ m^2/Vs obtained for *trans*-PA [169].

It is proposed [168] that in laser-modified PATAC, the electronic p-type conductivity is realized by polarons and bipolarons. In conducting PATAC, the temperature increase leads to the decrease of the bipolaron mobility and to the increase of its concentration. The product of both processes lead to extremal low temperature coefficient of PATAC conductivity, $\sigma_{DC} = \sigma_0(1 + \alpha T)$ with 3×10^{-4} $K^{-1} \le \alpha \le 2 \times 10^{-3}$ K^{-1}.

2-mm waveband EPR study of pristine (sample PATAC-1) and that treated by means of a medium power argon ion laser at $\lambda = 488$ nm up to 5, 20, and 80 J/cm^2 doses (respectively, samples PATAC-2, PATAC-3, and PATAC-4) has shown [170,171] that two types of PC exist in PATAC, namely a polaron localized on short π-conducting polymer chain (R_1) with $g_{xx} = 2.04331$, $g_{yy} = 2.00902$, $g_{zz} = 2.00243$, and line width $\Delta B_{pp} = 6.1$ mT, and polaron moving along longer π-conducting polymer chain (R_2) with $g_{xx} = 2.00551$, $g_{yy} = 2.00380$, $g_{zz} = 2.00232$ ($2g_{\|} = g_{xx} + g_{yy}$, $g_{\perp} = g_{zz}$) and $\Delta B_{pp} = 2.6$ mT (Fig. 20). Since g-factor of the PATAC samples is higher considerably than that of most PPP-like conducting polymers [28,29,112], one can conclude that unpaired electron in the polymer interacts with a sulfur atom that is typical for PTTF [158–160] and benzo-trithioles [172,173] in which sulfur atoms are involved into the conjugation. In this case, the shift of g-factor from g_e is expressed by modified Eq. (3)

$$g_{ii} - g_e = \frac{g_e \lambda_s \rho_s(0)}{\Delta E_{nj}} \frac{(1 - \cos\Theta)}{(1 + k_1 \cos\Theta)} \tag{48}$$

where $\rho_s(0)$ is the spin density on the sulfur nuclei, $\lambda_s = 0.0474$ eV [45] is the constant of spin-orbit interaction of the electron spin with sulfur nuclei, and k_1 is a constant. In sulfur containing solids, PCs in which electrons are localized directly on the sulfur atom, their isotropic g-factor will lie in the region of $2.014 \le g_{iso} \le 2.020$ [38,79,172,173]. In tetrathiofulvalene (TTF) derivatives, an unpaired electron is localized in a monomer unit with 12 or more carbon atoms and four sulfur atoms that leads to the decrease of $\rho_s(0)$ and g_{iso} values [79]. Because additional fast spin motion takes place in the PTTF [38,79], this leads to a further decrease in spin density $\rho_s(0)$, and to the decrease of the isotropic g-factor down to $2.007 \le g_{iso} \le 2.014$ depending on the structure and effective polarity in PTTF samples. Due to the smaller g-factor in PATAC, one can expect a higher spin delocalization in pristine and laser-modified PATAC as compared with the abovementioned organic semiconducting solids involving sulfur atoms into conjugation.

Assuming $\Delta E_{n\pi^*} \approx 2.6$ eV as typical for benzo-trithioles and PTTF [38,174], then the g-factor components of the initial PATAC yields by Eq. (3) to $\rho_s(0) = 1.1$ and $\Delta E_{n\sigma^*} = 15.6$ eV for the PC in unmodified PATAC. This means that in the initial polymer, the spin is localized within one monomer unit.

If one supposes that the doping of PATAC leads to the polaron formation and spin delocalization onto approximately five polymer units [157], so then $\rho_s(0)$ value deter-

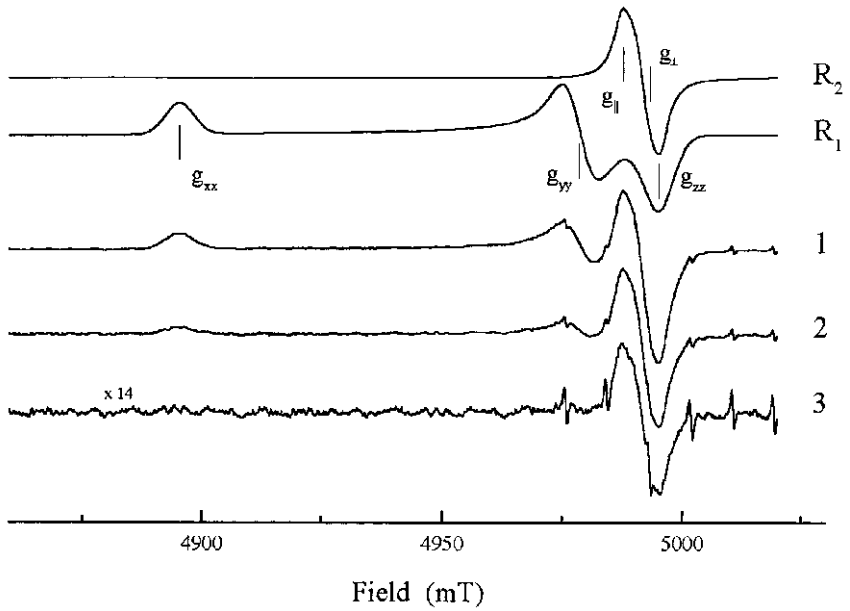

Fig. 20. 2-mm waveband EPR absorption spectra of the PATAC-2 (1), PATAC-3 (2), and PATAC-4 (3) samples registered at 100 K. The calculated spectra of radical R_1 with $g_{xx} = 2.0433$, $g_{yy} = 2.00902$, $g_{zz} = 2.00243$, and R_2 with $g_{xx} = 2.00551$, $g_{yy} = 2.00380$, $g_{zz} = 2.00232$ are shown as well.

mined above should decrease down to 0.22. This fits very well with the measured *g*-factor for the PATAC-2 sample. Further spin delocalization during polymer laser modification can be accompanied by the decrease of the Θ value and consequently by an additional acceleration of spin diffusion along polymer chain. The decrease in $\rho_s(0)$ and Θ values calculated from Eq. (48) for PC on polaron in PATAC-4 are approximately equal to 0.032° and 21.3°, respectively. The latter value is close to $\Delta\Theta = 22–23°$, realised, for example, at transition from benzoid to quinoid form in PPP [175], at transition from PTTF with phenyl bridges to PTTF with tetrahydroanthracene ones (see above), and at transition from emeraldine base to emeraldine salt form of PANI (see below). That is, the evaluation of the changes in the *g*-factor support the assumption from Roth et al. [168] that laser irradiation leads to a more planar structure of the polymer chains. Such an effect leads to higher spin delocalization and therefore to higher conductivity of PATAC.

The concentration ratio $[R_2]/[R_1]$, being equal near to 1:2 for the insulating PATAC-1, increases during the laser modification up to 2:1, 4:1, and 10:1, respectively, for the PATAC-2–PATAC-4. This means that the laser treatment leads to the formation of mobile polarons in conductive PATAC. The total spin concentration increases strongly at the polymer treatment from about 2.7×10^{20} spins/m^3 (PATAC-1) [168] up to 5.2×10^{24} spins/m^3 (PATAC-2); however, decreases during further laser modification down to 3.2×10^{24} spins/m^3 (PATAC-3) and down to 3.4×10^{23} spins/m^3 (PATAC-4). On the other hand, the concentration of charge carriers was determined from Hall and DC conductivity studies to change by more than 15 orders of magnitude reaching $N \sim 10^{25}$ m^{-3} at relatively strong laser irradiation of the polymer [168]. This means that, analogously to some other conducting polymers, the charges are predominantly paramagnetic polarons in an initial and slightly modified PATAC and the polarons are mainly transferred to diamagnetic bipolarons in highly irradiated polymer. As the number and mobility of spin charge carriers increases and the chains become more planar under the polymer modification, most polarons collapse into diamagnetic bipolarons. The latter seems to be the dominant charge carriers in highly modified PATAC.

Spin susceptibility in PATAC depends not only on laser irradiation, but also on the temperature. Fig. 21 presents the temperature dependencies of effective spin susceptibility for the PATAC-2–PATAC-4 samples. The figure shows that the spin susceptibility decreases with the temperature

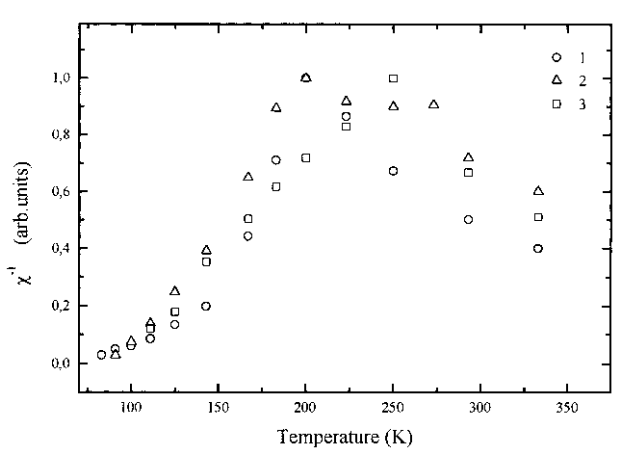

Fig. 21. The temperature dependencies of inverted and normalized to a maximum value paramagnetic susceptibility of PATAC-2 (1), PATAC-3 (2), and PATAC-4 (3) samples.

decrease in the temperature region from room temperature down to about 250 K and then increases as temperature becomes lower than some critical temperature $T_c \approx 220$–250 K. The decrease in the magnetic susceptibility with temperature lowering in high temperature region can be a result of the conversion of some paramagnetic polarons into bipolarons or of the formation of antiferromagnetic microphases in the polymer solid. Assuming an activation character for the process which reduces the spin susceptibility at $T > T_c$, one can evaluate from Fig. 21 the energies $E_a = 0.04$, 0.06, and 0.07 eV for activation of such a process in the PATAC-2–PATAC-4, respectively. The observed increase of the magnetic susceptibility at temperatures lower than T_c can be due the formation of spin glass phases with ferri- or ferromagnetic behaviors. Another interpretation possibility is that as an effect of a structural phase transition, a partly separation of bipolarons into polarons takes places.

As in the case of PA, 2-mm waveband dispersion EPR spectra of PATAC contain bell-like contribution (Fig. 22). For the modified PATAC samples, inequality $\omega_m T_1 > 1$ is realized; therefore, their dispersion spectra are determined mainly by the two last terms of Eq. (28).

It is seen from Fig. 22 that the heating of modified PATAC sample leads to the growth of its u_3^x/u_3^y parameter. As in the case of other conducting polymers, the comparatively slow macromolecular reorientation in the PATAC samples can be determined by means of the EPR signal of the localized polaron R_1 by the ST-EPR method [35] analyzing the u_3^x/u_3^y ratio (Fig. 22) from Eq. (38). The temperature dependence for the correlation time of macromolecular librations in PATAC-2 was determined [171] from its ST-EPR spectra to be $\tau_c^x = 6.3 \times 10^{-6} \exp(0.04\ \text{eV}/k_B T)$. The dynamics of the pinned spins and with it the polymer segments dynamics depends also on the level of the polymer treatment. At laser irradiation, the polymer matrix becomes more rigid, resulting in a stronger temperature dependence of the correlation time, with $\tau_c^x = 3.1 \times 10^{-6} \exp(0.06\ \text{eV}/k_B T)$ of these librations in PATAC-3.

The decrease in an isotropic g-factor at PATAC by laser modification apparently indicates the rise of polarons moving along the polymer chains. This value was determined from 2-mm waveband EPR spectra using Eq. (40) to be $\nu_\parallel \geq 3.2 \times 10^9\ \text{s}^{-1}$ at room temperature for mobile polarons in PATAC-2 sample.

1D spin diffusion along the polymer chain and its 3D hopping between the chains with rates $\nu_\parallel$ and $\nu_\perp$, respectively, accelerate spin relaxation. It should lead to $\Delta B_{pp}^{-1} \propto T_2 \propto \nu_e^{1/2}$ dependence [46] which is realized for conducting polymers with heteroatoms [38,79]. Multifrequency EPR studies have shown approximately twofold increase in PATAC line width at transition from 3-cm to 8-mm and from 8-mm to 2-mm waveband EPR [171]. This means that just above relations are valid also for PATAC.

The rates $\nu_\parallel$ and $\nu_\perp$ of spin motion in PATAC-2 were determined separately from Eqs. (23a) and (23b) using spin relaxation data [171] (Fig. 23). The figure shows also the contribution of the polarons to AC conductivity (at 140 GHz) of PATAC-2 determined from Eq. (45) with $d_\parallel = 0.25$ nm and $d_\perp \approx 0.36$ nm. It is seen, that the interchain spin diffusion can be interpreted in the framework of activation of spin charge carrier to extended states according Eq. (33b) with $\gamma = 0.8$ and $E_a = 0.035$ eV. The break

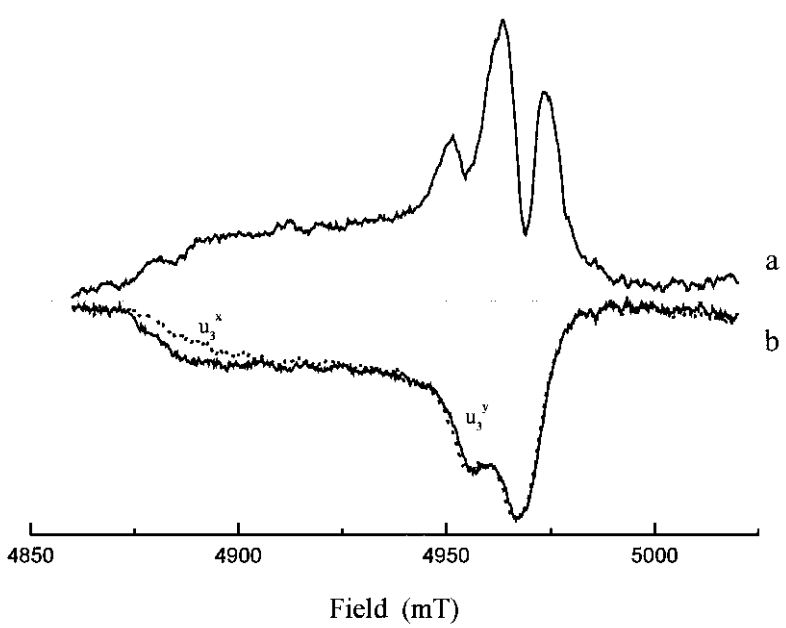

Fig. 22. 2-mm waveband in-phase (a) and $\pi/2$-out-of-phase (b) dispersion spectra of the PATAC-2 sample registered at 280 K (solid lines) and 143 K (dashed line).

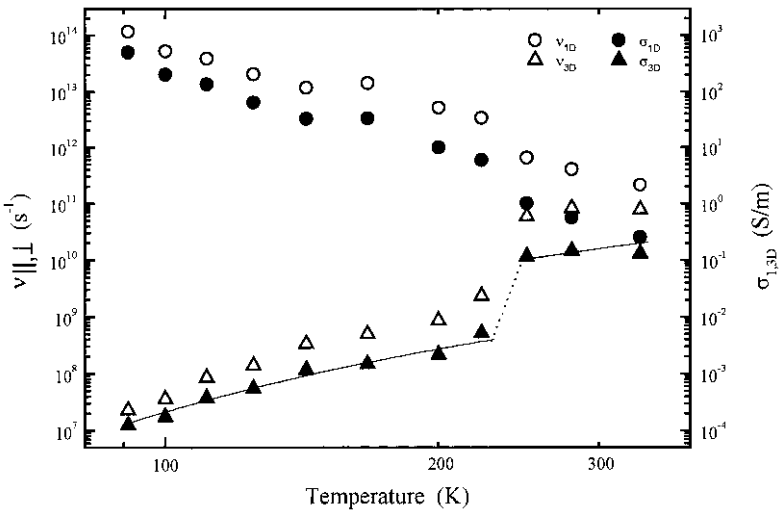

Fig. 23. Temperature dependencies of intrachain diffusion ν_{1D} (open circles) and interchain hopping ν_{3D} (open triangles) rates of mobile PCs in PATAC-2 sample determined using Eqs. (23a) and (23b) and of AC (140 GHz) conductivities σ_{1D} (filled circles) and σ_{3D} (filled triangles) calculated from Eq. (45) with $N = 3.5 \times 10^{24}$ spin/m^3, $d_{1D} = 0.246$ nm and $d_{3D} = 0.359$ nm. By solid line is shown the dependence calculated from Eq. (33b) with $\sigma_0 = 1.0 \times 10^{-13}$ Ss/mK (low temperatures), $\sigma_0 = 2.2 \times 10^{-12}$ Ss/mK (high temperatures), $\nu_e = 1.4 \times 10^{11}$ s^{-1}, and $E_a = 0.035$ eV.

in $\sigma_{3D}(T)$ function should be attributed to a change in conformation or to the polaron/bipolaron transition in the system at $T_c \cong 230$ K. The latter value is near to that of the analogous structural transitions in other conducting polymers [38,78,79].

The activation energy necessary for the charge carriers hopping between polymer chains is near to those obtained above from the PATAC paramagnetic susceptibility data and polymer chains' librations. Therefore, one can conclude that at low temperatures in modified PATAC samples, spin charge carriers thermal-activated hop and their interaction with lattice optical phonons increase sharply when the phonon energy becomes comparable with $k_B T_c \cong 0.02$ eV. The spin motion between chain segments and the intrinsic conductivity of the sample depend also on the macromolecular dynamics, because the interaction of the spins and charge transfer integral can be modulated by PATAC lattice librations as we detected it also in other organic semiconductors [38]. $\sigma_{3D}(T)$ function follows $1/\tau_c^x(T)$ [171]; therefore, one can conclude that the polymer chain librations indeed modulate spin exchange and consequently the charge transfer integral. Assuming that polaron is covered by electron and excited phonon clouds, we can propose that both spin relaxation and charge transfer should be accompanied by the phonon dispersion.

DC conductivity and Hall study of PATAC [168] has given $\sigma_{DC} \cong 2 \times 10^3$ S/m and charge carriers' mobility $\mu \cong 4 \times 10^{-4}$ m^2/Vs for highly irradiated polymer at room temperature. So then the values $n_2 \cong 3 \times 10^{-2}$ and $\sqrt{\nu_\parallel \nu_\perp} \approx 10^{13}$ s^{-1} can be evaluated from these data. These values are higher by approximately two orders of magnitude than $\nu_{\parallel,\perp}$ calculated above and n_2 obtained for PATAC-2 and PATAC-3 samples. This means that conductivity in highly conducting PATAC is determined mainly by dynamics of spinless bipolarons which concentration exceeds the number of mobile polarons by approximately two orders of magnitude.

4.7. Polyaniline

The PANI family is known for its remarkable insulator-to-conductor transition as a function of protonation or oxidation level [176]. This polymer differs from other conducting ones in several important aspects. It has no charge conjugation symmetry in contrast with PA and other PPP-like polymers. Besides, both carbon rings and nitrogen atoms are involved in the conjugation. The benzenoid rings of PANI can rotate or flip, significantly altering the nature of electron–phonon interaction. This results in difference in its electrical and magnetic properties compared with other PPP-like polymers. Stronger spin-orbit and spin-lattice interactions of the polarons diffusing along the chains is also characteristic of PANI. Finally, upon protonation or oxidation of the insulating emeraldine base form of PANI (PANI-EB) (Fig. 2), its conductivity increases by 10 orders of magnitude, while a number of electrons on the polymer chains remains constant in the emeraldine salt form of PANI (PANI-ES) (Fig. 2) [177]. The lattice constants are $a = 0.765$, $b = 0.575$, $c = 1.020$ nm for PANI-EB [178] and $a = 0.705$, $b = 0.860$, and $c = 0.950$ nm for HCl-doped PANI-ES [179] units. An analysis of experimental data on the temperature dependencies of DC conductivity, thermoelectric power, and Pauli-like susceptibility allowed Zuo et al. [180] and Epstein and MacDiarmid [181] to show that PANI-EB is completely amorphous insulator in which 3D granular

metal-like domains of characteristic size of 5 nm are formed in the course of its transformation into PANI-ES. A more detailed study of the complex microwave dielectric constant, EPR line width, and electric field dependence of conductivity of PANI-ES [179,182–185] allowed them to conclude that both chaotic and oriented PANI-ES consist of some parallel chains strongly coupled into ''metallic bundles'' between which 1D VRH charge transfer occurs and in which 3D electron delocalization takes place. The intrinsic conductivity of these domains was evaluated using Drude model [186] as $\sigma_{AC} = 10^9$ S/m [187] which was very close to value expected by Kivelson and Heeger for the metal-like domains in highly doped Naarmann *trans*-PA [188]. However, an experimentally obtained AC conductivity of the sample does not exceed 7×10^4 S/m at 6.5 GHz [187].

It was mentioned above that the metallic properties of conducting polymers strongly depend on their structure, morphology, and quality [22,23]. Indeed, from an optical (0.06–6 eV) reflectance study and from the analysis of the band structure of HCl^-, $H_2SO_4^-$, and camphor-sulfonic-acid-(CSA) doped PANI-EB, Lee et al. [189] have shown that the quality and therefore metallic properties of the polymer increases in PANI–HCl → PANI–H_2SO_4 → PANI–CSA series.

The oxidation or protonation of PANI-EB leads to the approximately linear increase of PC concentration accompanied with the line narrowing from 0.2 to 0.05 mT at 3-cm waveband [190,191]. Lapkowski and Genies [191] and MacDiarmid and Epstein [192] showed the initial creation of Curie spins in EB, indicating a polaron formation, followed by a conversion into Pauli spins, which shows the formation of the polaron lattice in high conductive PANI-ES [163,193]. As for PANI-CSA, Sariciftci et al. [194,195] have reported that in EPR susceptibility, the Curie law was predominant in PANI–CSA powder; on the other hand, in the PANI–CSA film cast from *m*-cresol solution with the same powder, they observed the Pauli-like behavior down to 50 K and then a change to a Curie-like behavior below 50 K. The temperature-independent susceptibility is observed in less qualitative PANI–HCl [69,157] as well.

EPR and NMR studies of spin dynamics in PANI–HCl were performed by Mizoguchi et al. [135,196,197]. The dependencies $T_1 \propto \omega_p^{1/2}$ and $\Delta B_{pp} \propto \omega_e^{1/2}$ obtained, respectively, for nuclear and electron spins were interpreted in terms of 1D polaron diffusion with the rate of $\nu_{\|} = 10^{12}$–10^{14} s^{-1} in separated chains of PANI-ES. The anisotropy of this motion, $\nu_{\|}/\nu_{\perp}$ varies from 10^4 in PANI-EB down to 10 in PANI-ES at room temperature. If the rate of on-chain spin motion is characterized by weak dependency on y value, $\nu_{\perp}$ value of PANI-ES depends on y and correlates with corresponding DC and intrinsic conductivities. This fact was attributed to the existence of the conducting clusters as a solitary single polymer chains even in heavily doped PANI, which corresponds to the data [198,199], but contradicts with the concept of metal-like islands diluted in an amorphous phase of the polymer [182,183]. Therefore, the discrepancy exists in interpretation of different experimental data on electronic processes taking in PANI.

The more detailed results of investigation of magnetic, electrodynamics properties of PANI-EB (sample I) and PANI-ES with $y = 0.01$, 0.03, 0.22, 0.41, and 0.50 (respectively, samples II–VI) [163,200–204] are summarized below.

PCs in PANI at 3-cm waveband demonstrate a Lorentzian single symmetrical spectra which ΔB_{pp} value depends on both doping level and temperature (Fig. 24a). The line width of PC in undoped and lightly doped PANI is practically temperature-independent at this waveband (Fig. 24a), whereas this value of IV–VI PANI-ES samples demonstrates bell-type temperature dependence with critical temperature $T_c \approx 200$ K. Such an extremality becomes more evident at the growth of y, especially for the heavily doped PANI-ES. ΔB_{pp} value was observed to increase approximately linearly with temperature at $T \leq T_c$ and to decrease at lower temperatures.

In addition to unresolved averaged HFS, EPR spectrum of PANI indicates also a HFI of a small part of the spins with both hydrogen and nitrogen nuclei. As an example, the central regions of the second derivatives of 3-cm waveband absorption signals of IV and VI PANI-ES samples are shown in Fig. 25. In the first sample, an unpaired electron interacts with four nearly equivalent neighboring hydrogen atoms of the lateral benzoid circles possessing nuclear spin $I = 1/2$ and with the central nitrogen nucleus with $I = 1$ resulting for the appearance of the equidistant well-resolved lines with the relative intensities of 1:5:11:14:11:5:1 (Fig. 20b). In addition to these nuclei, an unpaired electron in sample VI interacts also with the fifth nonequivalent hydrogen nucleus located at N atom. This leads to the appearance of an additional splitting in the spectrum (Fig. 20a). The measured constants of HFI of an unpaired electron with H and N atoms and calculated spin densities on their nuclei are summarized in Table 6.

The typical 2-mm waveband absorption and dispersion EPR spectra of PC in PANI-EB and PANI-ES samples are shown in Fig. 26. At this waveband, the PANI EPR spectra became Gaussian with higher line width compared with 3-cm waveband spectra as it occurs in case of other conducting polymers [78,79]. In the dispersion spectra of undoped and lightly doped PANI, the bell-like components are registered. As in the case of other conducting polymers, the appearance of such a component is attributed to the effect of adiabatically fast passage of the separated and saturated spin-packets by a modulating magnetic field.

The plots of ΔB_{pp} versus temperature and doping level for PANI samples are shown in Fig. 24b. As in the case of 3-cm waveband, ΔB_{pp} depends on both temperature and conductivity of the sample, however, with a higher susceptibility to both parameters.

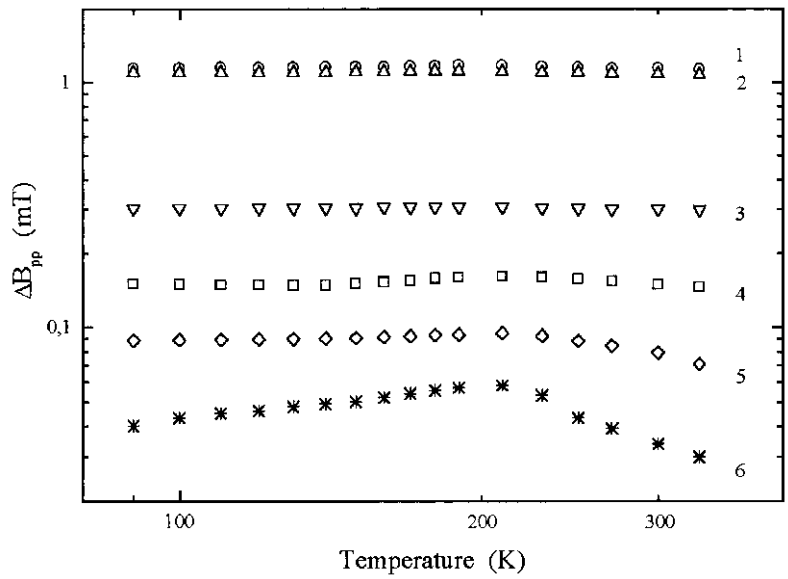

Fig. 24. The plots of peak-to-peak linewidth of 3-cm waveband EPR in-phase absorption spectrum of PCs in I (1), II (2), III (3), IV (4), V (5), and VI (6) PANI samples versus temperature.

The analysis shows that at least two types of PC are stabilized in PANI-EB, namely PC R_1 (Fig. 26a) with $g_{xx} = 2.00535$, $g_{yy} = 2.00415$, $g_{zz} = 2.00238$, $A_{xx} = A_{yy} = 0.33$ mT, $A_{zz} = 2.3$ mT and R_2 with $g_{\perp} = 2.00351$, $g_{\parallel} = 2.00212$. The relative concentration ratio of PC R_1, $n_1/(n_1 + n_2)$ is equal approximately to 0.3 and decreases with the temperature and doping level increase. This can be explained by the increase of a number of spin mobile charge carriers and by the creation of polaron lattice in PANI at high polymer doping.

PC R_1, which exhibits strongly asymmetric EPR spectrum, is attributed to –(Ph–$N^{\cdot +}$–Ph)– radical, localized on a polymer chain. The magnetic parameters of this radical differ weakly from those of Ph–$N^{\cdot}$–Ph one [39] probably because of a smaller delocalization of an unpaired electron on nitrogen atom ($\rho_N^{\pi} = 0.39$) and of more planar conformation of the latter. The contribution of CH-groups of such radicals to g_{xx} value is sufficiently small, that is, $\Delta g_{xx} \approx 1.7 \times 10^{-5}$ [39], and thus may be neglected. Assuming $A_{xx} = A_{yy} = 1.25$ mT [205] for PC in pernigrani-

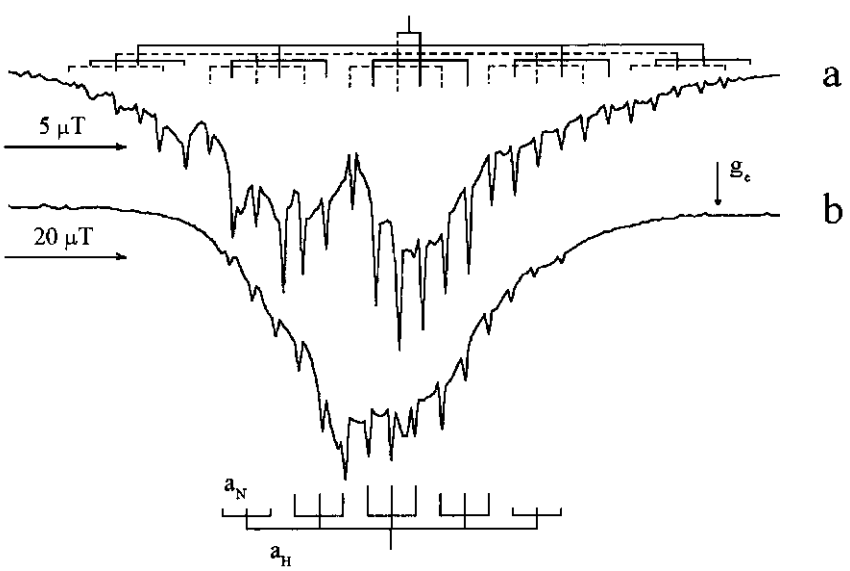

Fig. 25. The center section of 3-cm waveband in-phase second harmonic absorption spectra of VI (a) and V (b) PANI powders registered at room temperature. The hyperfine structures, constants of the hyperfine interaction of an unpaired electron with H (a_H) and N (a_N) nucleus, and the position of *g*-factor of free electron ($g_e = 2.00232$) are shown.

Table 6
The values calculated for central H atom are marked by the * symbol. The ρ_i values were calculated using the McConnell relation (4) with Q proportionality constant equal to 2.25 and 2.37 mT [39,45] for H and N atoms, respectively.

Parameter	I	II	III	IV	V	VI
a_H	0.41	0.31	0.28	0.024	0.014	5.3×10^{-3}
a_H^*	–	–	–	–	–	9.5×10^{-4}
a_N	0.14	0.10	0.092	7.6×10^{-3}	4.6×10^{-3}	1.8×10^{-3}
ρ_H	182	138	124	107	6.22	2.36
ρ_H^*	–	–	–	–	–	0.422
ρ_N	59.1	42.2	38.8	3.21	1.94	0.760

line base and McConnell proportionality constant for HFI of the spin with nitrogen nucleus $Q = 2.37$ mT [39], the spin density on heteroatomic nucleus $\rho_N(0) = (A_{xx} + A_{yy} + A_{zz})/(3Q) = 0.62$ can be estimated. Using the above-mentioned values of the **g** tensor components, the constant of spin-orbit coupling of electron with ^{14}N nucleus and λ_N equal to 9.4 meV [45], the energies of the lowest induced electron excited transitions in R_1 were calculated from Eq. (3) to be $\Delta E_{n\pi^*} = 3.8$ eV and $\Delta E_{\sigma\pi^*} = 6.3$ eV.

The averaged g-factors of the radicals R_1 and R_2 are almost similar. Hence, the spectrum of radical R_2 can be attributed to polaron diffusing along the polymer chain with the effective rate (see Eq. (40)) $\nu_\perp^0 \geq 10^9$ s^{-1}.

The decrease of line width and the decrease of g-factor of radical R_1 with the y growth can be associated with the decrease of spin density on nitrogen atom and with the change in polymer chains conformation. The angle between the rings, Ph-N-Ph, may increase by 22° at transition from PANI-EB to PANI-ES [69]. However, the calculation evidences that this increase results in the change of g_{xx} value only by several percentages. Moreover, the decrease of dihedral angle θ between the planes of a benzene rings seems to take place as y increases. Transfer integral I_{C-N} between nitrogen and carbon p_z orbits at *para*-position of benzene rings of PANI has $I_{C-N} \propto \cos\theta$ dependency [206], typical for other aromatic hydrocarbons [132]. By taking $\theta = 56°$ for undoped EB [206], the effective dihedral angle and the spin density on nitrogen atom were calculated for ES with $y = 0.2$ from Eq. (3) to be $\theta = 33°$ and $\rho_N^\pi = 0.42$. This θ angle decrease causes the increase of spin density on benzene rings due to I_{C-N} integral increase. Thus, the change in magnetic parameters can evidence for a higher degree of spin delocalization along the polymer chain and for a more planar conformation of the chains at PANI oxidation.

It is important to note, that drastic temperature dependency of line shape of radical R_2 in IV is registered at 300 K. If the inequality $g_\perp > g_\parallel$ holds for the smaller y and $T < 300$ K, the opposite inequality $g_\perp < g_\parallel$ holds at $y = 0.22$ and $T > 300$ K (Fig. 26). The latter condition remains invariable for samples IV–VI at $90 < T < 330$ K. The analogous effect was observed by Lubentsov et al. [202] upon the treatment of PANI sample with water vapor. It was interpreted with essential conformational distortion of radical R_2 due to H_2O-bridges formation between the polymer chains. The above change of line shape can be probably explained by a structural transformation of polymer chains as well.

The investigation of PANI samples at 2-mm waveband EPR shows that as conditions $\gamma_e \omega_m B_m \ll \gamma_e^2 B_1^2$ and $s = \gamma_e B_1 \sqrt{T_1 T_2} \leq 1$ are valid, their spectra demonstrate the effects of fast adiabatic passage of resonance conditions (Fig. 26c,d). Fig. 27 presents the temperature dependencies of effective relaxation parameters of I–III PANI samples. The figure demonstrates that the increase of doping level of EB causes the simultaneous decrease of T_1 value, so that $T_1 \propto nT^l$ ($l = 3$–4 at $y < 0.03$ and $l = 0.3$ at $0.03 < y < 0.22$). This fact can be associated with the increase of spin–spin exchange between PC on the neighboring polymer chains due to the grow of the number and size of metal–like domains in PANI–ES. Moreover, this indicates the sharp change of energy transfer from spin ensemble to polymer lattice and the change of charge transport mechanism during the PANI oxidation process.

As in case of PTTF, both the intensity and the shape of the dispersion signal U of PANI depend not only on a spin exchange and on an electron relaxation, but also on a comparatively slow macromolecular reorientation in the samples. Such molecular processes can be studied by using the ST–EPR method [35].

The $K_{mov} = u_3^x/u_3^y$ parameter of PANI changes with the temperature (Fig. 26c). As in the case of PANI, this evidences for anisotropic librational reorientations of the pinned polarons near x-axis of the polymer chains. So then the correlation time, $\tau_c^x = 3.5\times10^{-5}\ \exp(0.015\ \text{eV}/(k_B T))$ of macromolecular librations in I sample was determined from its ST-EPR spectra by using Eq. (38)

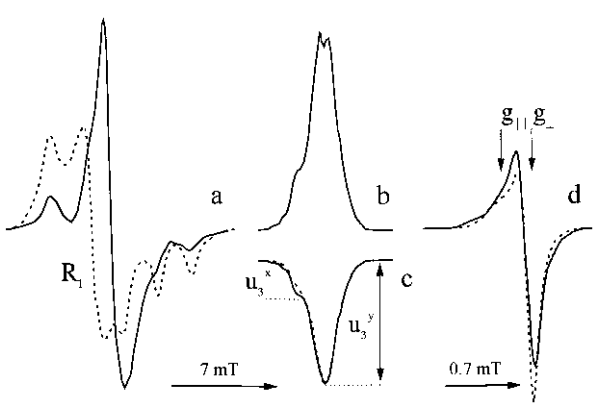

Fig. 26. 2-mm waveband in-phase absorption (a,d), in-phase dispersion (b), and $\pi/2$-out-of-phase dispersion (c) spectra of I (a,b,c) and VI (d) PANI samples registered at room temperature in an inert atmosphere. The simulated spectrum of the PCs R_1 (a) and the spectra registered at 200 K (c,d) are shown by dotted lines. The components u_3^x and u_3^y of the $\pi/2$-out-of-phase dispersion spectrum (c) and the components $g_\parallel$ and $g_\perp$ of the PCs R_1 (d) are shown as well.

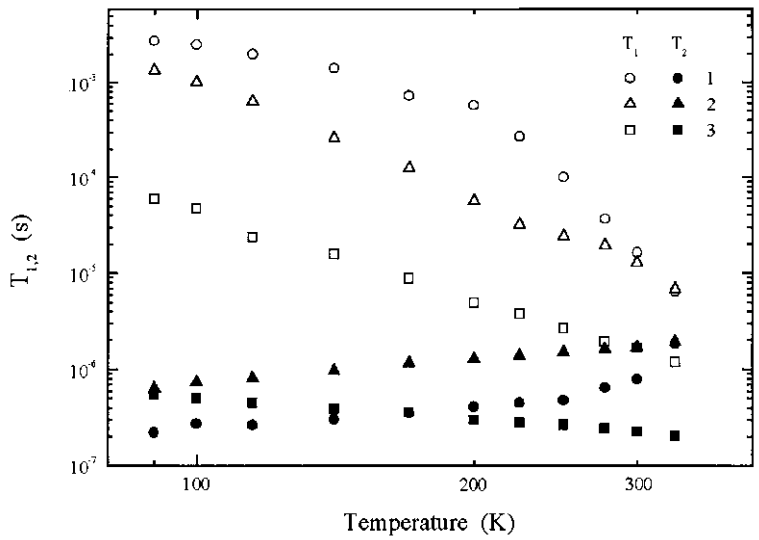

Fig. 27. Temperature dependence of effective spin-lattice T_1 (open points) and spin–spin T_2 (filled points) relaxation times of the PCs in I (1), II (2), and III (3) PANI samples.

with $\tau_0 = 5.4 \times 10^{-8}$ s and $m = 4.8$. Similar dependencies were also obtained for II and III samples. τ_c^{max}, calculated using Eq. (29), $\theta = 45°$, $B_1 = 0.01$ mT [207], g_{xx} and g_{zz} values measured for R_1 center, is equal to $\tau_c^{max} = 1.3 \times 10^{-4}$ s and corresponds to $K_{mov} = u_3^x/u_3^y = 0.22$ (see Eq. (38)) at 125 K.

As PANI is characterized by $T_{1,2} \propto n\omega_e^{1/2}$ dependency [135,196], the experimental results shown in Fig. 27 can also be interpreted in the terms of modulation of spin relaxation by both intrachain 1D diffusion of polaron and its interchain 3D hopping transfer with the rates $\nu_\parallel$ and $\nu_\perp$, respectively.

Fig. 28 shows the temperature dependencies of $\nu_\parallel$ and $\nu_\perp$ values of PC in I–III samples at spin delocalization over five repeating units of polaron. These constants were obtained to be $\nu_\parallel \sim 10^{11}$ s and $\nu_\perp \sim 10^8$ s at room temperature. The first value is lower by approximately two orders of magnitude then that earlier reported for $y = 0.05$ PANI sample [135,196], but considerably higher then $\nu_\perp^0$ calculated above. At comparatively high doping level ($y > 0.2$), T_1 is approximately equal to T_2 and they have a weak temperature dependency because of a strong spin–spin exchange in metal-like domains and the growth of the system dimensionality. The accuracy of the estimation of

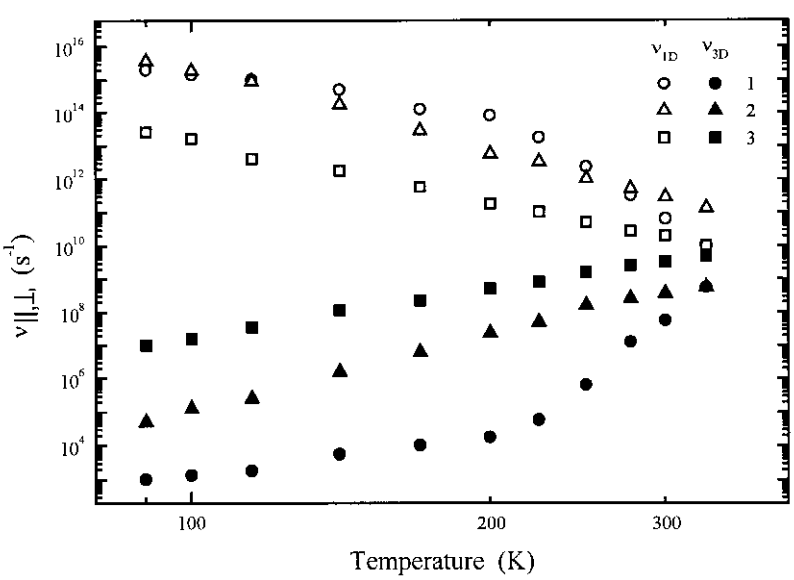

Fig. 28. Temperature dependence of in-chain diffusion ν_{1D} (open points) and interchain hopping ν_{3D} (shaded points) rates of mobile PCs in I (1), II (2), and III (3) PANI samples determined by using Eqs. (23a) and (23b).

spin diffusion frequencies decreases at $y > 0.1$; however, the rate of spin motion can be evaluated from Eqs. (23a) and (23b) assuming $2T_1^{-1} = T_2^{-1}$ to be $\nu_{\|} = 1.6 \times 10^{12}$ s. This value is considerably smaller then that obtained for PANI by the magnetic resonance methods at low operation fields [135].

Mizoguchi et al. [135] showed, that anisotropy of spin diffusion in PANI is high enough up to $y = 0.6$ at room temperature. However, Fig. 28 demonstrates, that $\nu_{\|}/\nu_{\perp}$ ratio is high only for I–III samples. It was shown [201,203,204], that the dimensionality of PANI grows at $y > 0.2$ and spin motion becomes almost isotropic as it occurs in 3D-semiconductors. This fact indicates clearly the formation of massive metal-like domains accompanied with the growth of crystallinity of PANI-ES samples with doping. This must result in the decrease of the concentration of traps for electrons and thus in the decrease of the relativity of electron scattering on the phonons of the lattice. This must also result in the decrease of temperature dependency for both relaxation and electrodynamic processes during PANI doping (Figs. 27 and 28) as it occurs in classic amorphous semiconductors [24].

By assuming that the diffusion coefficients D of spin and diamagnetic charge carriers have the same values, one can obtain from Eq. (45) $\sigma_{1D} = 10$ S/m and $\sigma_{3D} = 1 \times 10^{-3}$–0.5 S/m at room temperature for a sample with $0 < y < 0.03$. At $\nu_{\|} \approx \nu_{\perp}$, these values were determined to be $\sigma_{1D} = (5–18) \times 10^3$ and $\sigma_{3D} = (3–10) \times 10^3$ S/m. Thus, the conclusion can be drawn, that σ_{3D} grows more strongly with y, that is, the evidence for the growth of a number and a size of 3D quasi-metal domains in PANI.

Let us consider the charge transfer mechanisms in the PANI samples. Instead of the dependence $\sigma_{DC}(T) \propto T^{13.5}$ typical for *trans*-PA [63], PANI-EB have some stronger temperature dependence, $\sigma_{DC}(T) \propto T^{22}$ at high temperatures (Fig. 29). The slope of this dependence is approximately the same evaluated from the high-temperature data for PANI-EB reported earlier by Zuo et al. [208] and seems to be too strong to describe the charge transport in this sample as isoenergetic interpolaron hopping [61,107]. Attempts to analyze quantitatively conductivity data of the low conductive PANI samples in the framework of Mott's VRH conventional model for disordered semiconductors [72] always resulted in quite unreasonable values for Mott's parameters, in contrast to the heavily doped case [208]. So another conduction mechanism should be motivated.

The interchain AC conductivity of the initial PANI-EB sample can be calculated from Eq. (45) and the data presented in Fig. 28. Fig. 29 shows the temperature dependence of $\sigma_{AC}(T)$ calculated from Eq. (45) with $N = 9.5 \times 10^{23}$ m^{-3} and $c_{\|} = 0.439$ nm [202] compared with experimental $\sigma_{DC}(T) = 1.4 \times 10^{-62} T^{22}$ one of the sample. These dependencies are quite similar at least at $T \geq T_c \approx 200$ K temperature region. It is evident that there are two temperature regions divided by the critical temperature $T_c = h\nu_{ph}/k_B$ (here ν_{ph} is the $2k_F$ optical phonon frequency) with different slopes of the functions $\sigma_{AC}(T)$. Such a behavior can be explained by pure distance-dependent charge carriers hopping at temperatures $T \leq T_c$ and by their both energy- and distance-dependent hopping at $T \geq T_c$ in the framework of the model of ''small polaron'' tunneling [62].

The temperature dependencies of σ_{AC} calculated using Eq. (31) with $\sigma_0 = 1.3 \times 10^{-6}$ S/(m eV), $h\nu_{ph} = 0.017$ eV, $E_H = 0.073$ eV and Eq. (32) with $\sigma_0 = 1450$ S eV/m, $E_H = 0.073$ eV, and $E_a = 0.40$ eV are presented in Fig. 29.

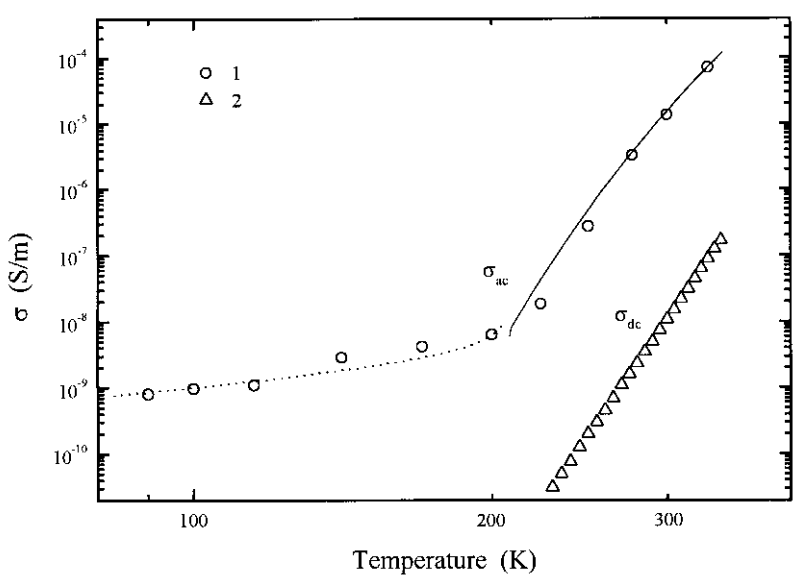

Fig. 29. Temperature dependencies of AC (1) conductivity of I PANI-EB sample determined using Eq. (45) and data presented in Fig. 23, and DC (2) one. AC conductivities calculated from Eq. (31) with $\sigma_0 = 1.3 \times 10^{-6}$ S/(m eV), $h\nu_{ph} = 0.017$ eV, and $E_H = 0.073$ eV (dotted line) and Eq. (32) with $\sigma_0 = 1450$ S eV/m, $E_H = 0.073$ eV, and $E_a = 0.40$ eV (solid line) are shown as well.

The figure evidences for well experimental and theoretical data correlation; therefore, one can conclude that the charges are transferred mainly by mobile small polarons in this sample. Note that similar $\sigma_{AC}(T)$ functions were obtained earlier for undoped PANI [208] at comparatively low registration frequencies and for lightly doped PTTFs [62,159] at different frequencies.

As in the case of PTTF, in order to explain experimental data on lightly doped samples, the model of isoenergetic phonon-assisted charge hopping between soliton-bound states proposed by Kivelson for charge transfer in *trans*-PA [61,107] may also be used.

If the conductivity is dominated by interpolaron hopping, $\sigma_{DC}(T)$ should follow $\sigma_{DC}(T) \propto T^n$ power law, according to Eq. (30a). Such a behavior is really observed for the lightly doped PANI samples (Fig. 30). Therefore, one may state that the measured $\sigma_{DC}(T)$ in these samples better follows T^n law predicted by Eq. (30a) than Mott's $T^{-1/2}$ one.

The concentration of mobile spins in II PANI sample is $y_p = 1.2 \times 10^{-4}$ per two benzoid rings. Therefore, taking into account that each bipolaron possesses dual charge, $y_{bp} = 2.3 \times 10^{-3}$ and $\langle y \rangle = 4.6 \times 10^{-2}$ can be obtained. The concentration of impurity is $N_i = 2.0 \times 10^{25}$ m^{-3}, so then $R_0 = 2.28$ nm is obtained for this polymer as well. The prefactor γ_0 in Eqs. (30a) and (30b) is evaluated from the $\sigma_{DC}(T)$ dependence to be 3.5×10^{19} s^{-1}. Assuming spin delocalization over five polaron sites [157] along the polymer chain with a lattice constant $c_{\parallel} = 0.95$ nm [179], $\xi = 1.19$ nm is obtained as well. The perpendicular component $\xi_{\perp}$ of ξ value can be determined from the relation [61]

$$\xi_{\perp} = \frac{c_{\perp}}{\ln(\Delta_0 / t_{\perp})} \tag{49}$$

where $2\Delta_0$ is the band gap and $t_{\perp}$ is the hopping matrix element estimated as [209]

$$t_{\perp} = \frac{h^4 \nu_{3D} \nu_{ph}^3}{2\pi E_p} \exp\left(\frac{2E_p}{h\nu_{ph}}\right) \tag{50}$$

where E_p is the polaron formation energy. Using $2\Delta_0 = 3.8$ eV [210], typical for π-conducting polymers $E_p = 0.1$ eV [209], $\nu_{\perp} = 3.6 \times 10^8$ s^{-1} determined from experiment, $\nu_{ph} = 4.2 \times 10^{12}$ s^{-1} obtained below, $t_{\perp} = 7.1 \times 10^{-3}$ eV, $\xi_{\perp} = 0.079$ nm, and $\xi = 0.2$ nm are obtained for II PANI sample. The similar procedure gives $\langle y \rangle = 7.9 \times 10^{-2}$, $\gamma_0 = 2.1 \times 10^{17}$ s^{-1}, $\xi_{\perp} = 0.087$ nm, and $\xi = 0.21$ nm for III PANI sample with $y_p = 1.1 \times 10^{-3}$ and $y_{bp} = 1.2 \times 10^{-2}$.

The conductivities of II and III PANI samples were calculated from Eq. (30a) to be $\sigma_{DC}(T) = 2.3 \times 10^{-42} T^{15.2}$ and $\sigma_{DC}(T) = 1.2 \times 10^{-32} T^{12.1}$, respectively. Fig. 30 shows these dependencies in comparison with an experimentally determined function. $\sigma_{AC}(T)$ calculated using Eq. (45) with $N = N_i$ and data presented in Fig. 28 and those calculated using Eq. (30b) with $n = 15.2$ and $n = 12.1$, respectively, for II and III samples are shown in this figure as well. As it can be seen from Fig. 30a, there is insufficient coincidence of the theory and experiment in case of II PANI sample. Moreover, the prefactor γ_0 determined for this polymer is higher by approximately two orders of magnitude compared with $\gamma_0 = 1.2 \times 10^{17}$ s^{-1} estimated by Kivelson for *trans*-PA [61]. The better fitting of an experimental data to the Kivelson's theory is realized in the case of III PANI sample (Fig. 30b) for which the value of prefactor γ_0 is approximately the same as that for *trans*-PA. It can be explained by the increase of number and mobility of the mobile charge carriers in higher doped polymer that leads to the increase of a probability of charge hopping between the chains. Therefore, charge transport in an initial polymer is determined by the mobility of small polarons. This process is replaced by an isoenergetic charge hopping between the polaron sites at an optimum polymer doping. At lower oxidation of the sample, charge transfer is realized in the framework of both superposing mechanisms.

Studying DC conductivity and thermoelectric power Wang et al. [183,184] have found that the charge transport mechanism in PANI-ES samples of different doping levels seems to be 1D VRH at low temperatures. They have assumed that crystalline fraction of the samples consists of ''bundles'' of well-coupled chains with 3D extended electron states. Since such domains may be considered as a large-scale cluster of chains, 1D charge transfer between them seems to dominate in the macroscopic conductivity of the polymer. A similar charge transfer is probably realized in the heavily doped PANI-ES samples under study.

Fig. 31 shows that DC conductivity of IV–VI PANI-ES samples follows well Mott's $T^{-1/2}$ law for 1D VRH charge transport (see Eqs. (34a) and (34b)). T_0 values evaluated from the slopes of the $\sigma_{DC}(T)$ dependencies (Fig. 31) and the averaged localization lengths $\langle L \rangle$ of a charge in the samples determined from $n(\varepsilon_F)$ are presented in Table 7. Using the method proposed by Wang et al. [184], $L_{\parallel}$ and $L_{\perp}$ components of $\langle L \rangle$ value are obtained as well (Table 7). Prefactor ν_0 is calculated using Eqs. (34a) and (34b) to vary in $(3.4–4.8) \times 10^{12}$ s^{-1} region that is near to $\nu_0 = 1.6 \times 10^{13}$ s^{-1} evaluated from the data obtained by Wang et al. [182,183] for PANI-ES. So then, the phonon frequency can be obtained from the equation $\nu_{ph} = k_B T_c / h = 4.2 \times 10^{12}$ s^{-1} to fall into region for ν_0 determined above.

As dipole interaction between the spin-packets strongly increases at polymer doping due to formation of the metal-like domains, therefore, an effective relaxation time of PC becomes considerably smaller then ω_m, so that sensitivity of the saturation methods to a spin relaxation and dynamics decreases. In this case, the charge mobility in high-conductive PANI-ES can be evaluated from the analysis of the polymer absorption line containing Dyson

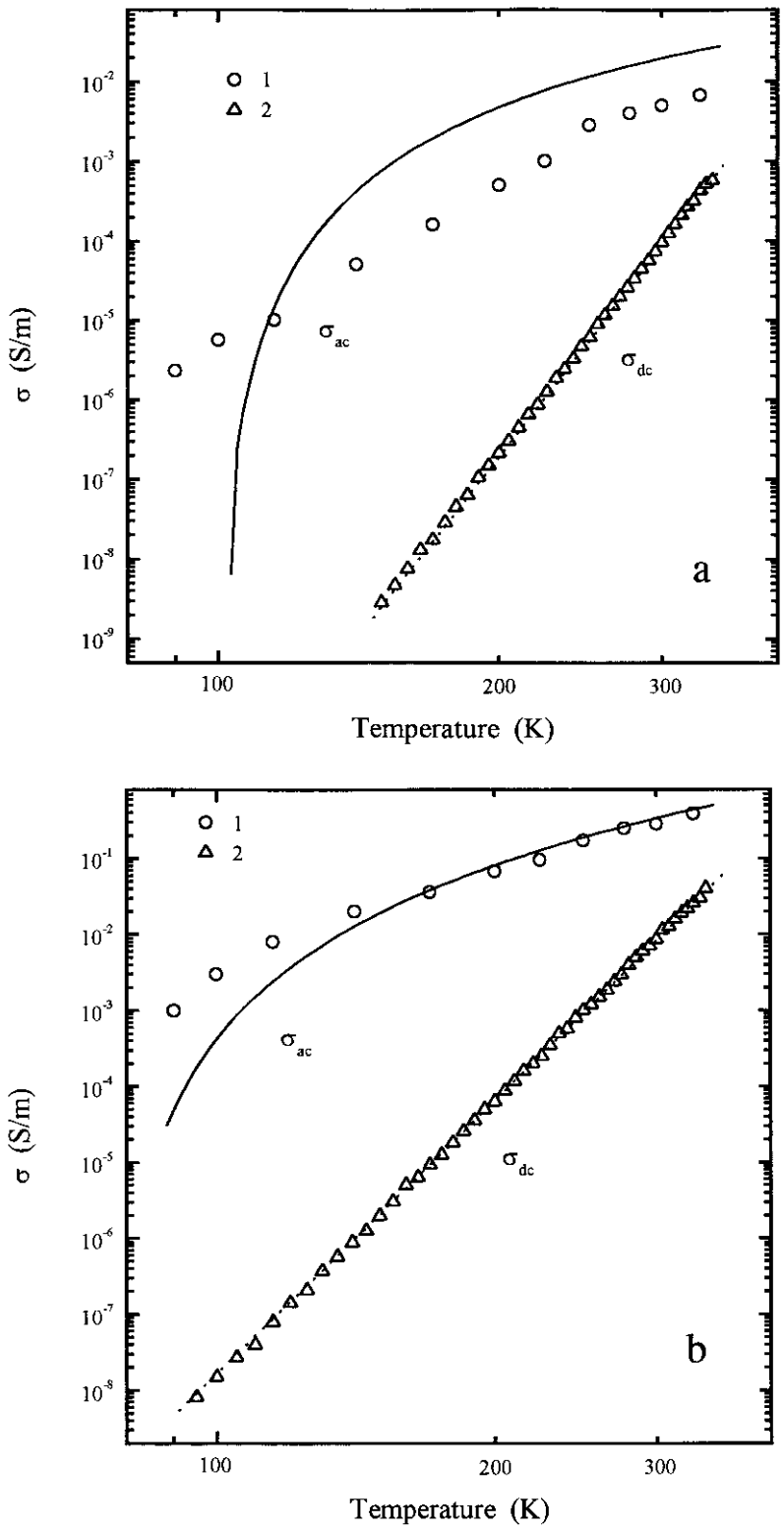

Fig. 30. Temperature dependencies of AC (1) and DC (2) conductivities of II (a) and III (b) PANI-ES samples determined using Eq. (45) and data presented in Eqs. (23a) and (23b). The solid and dotted lines show, respectively, AC and DC conductivities calculated using Eqs. (30a) and (30b) with $n = 15.2$, $\langle y \rangle = 0.046$, $\xi_\perp = 0.079$ nm, $\gamma_0 = 3.5 \times 10^{19}$ s^{-1} (a) $n = 12.1$, $\langle y \rangle = 0.081$, $\xi_\perp = 0.087$ nm, $\gamma_0 = 2.1 \times 10^{17}$ s^{-1} (b), $\xi_\parallel = 1.19$ nm, and $\nu_e = 140$ GHz.

contribution. As one can see from Fig. 26d, the asymmetry of an absorption line of the heavily doped PANI-ES sample is changed with temperature demonstrating the Dyson behavior [48]. This fact indicates the decrease of a

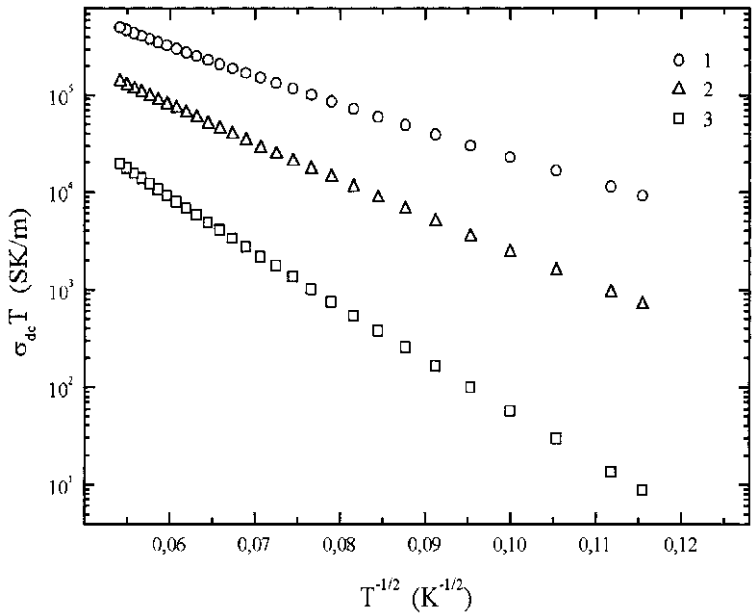

Fig. 31. The dependencies of $\sigma_{DC}T$ product versus $T^{1/2}$ for VI (1), V (2), and IV (3) PANI-ES samples.

thickness of skin-layer δ on the polymer surface due to the growth of the domains' intrinsic conductivity. Therefore, the intrinsic 3D conductivity σ_{AC} of metal-like domains in PANI-ES can be determined according to the method proposed by Wilamovski et al. [89] for the amorphous semiconductors of lower dimensionality from Eq. (13).

The temperature dependencies of the intrinsic conductivity of some PANI-ES samples are shown in Fig. 32. The figure exhibits a maximum of $\sigma_{AC} = 1.2 \times 10^6$ S/m lying near the critical temperature $T \approx 200$ K determined above for the samples of lower doping levels. Maximum σ_{AC} is higher by approximately two orders of magnitude then that determined by Joo et al. [187] at 6.5 GHz for $y = 0.50$ PANI-ES. This evidences additionally for 1D electron localization (semiconductive behavior) at $T \leq T_c$ and its 3D delocalization (metallic behavior) in the domains at higher temperatures. It is important to note, that the temperature dependencies of thermoelectric power S, σ_{AC}, and $\nu_\perp$ of some conducting polymers reported earlier [183,197,211–215], $T_1(T)$, and $\nu_\parallel$(T) for PANI-EB and $\Delta B_{pp}(T)$, presented, respectively, in Figs. 28 and 19, demonstrate similar temperature behavior at the same temperature region.

Table 7
The percolation constant T_0 (in 10^3 K), spin concentration N (in 10^{25} spin/m^3), the density of states $n(\varepsilon_F)$ at the Fermi level ε_F (in eV^{-1} mol^{-1}), the averaged $\langle L \rangle$, parallel $L_\parallel$, and perpendicular $L_\perp$ lengths (in nm) of charge wave function localization in the PANI samples

Parameter	I	II	III	IV	V	VI
N	0.20	0.37	2.1	18	76	153
T_0	–	–	–	10.2	3.76	1.65
$n(\varepsilon_F)$	–	–	–	0.6	1.7	3.8
$\langle L \rangle$	–	–	–	2.02	1.91	1.92
$L_\parallel$	–	–	–	7.1	6.9	7.0
$L_\perp$	–	–	–	1.1	1.0	1.0

At low temperature region, when $T \leq T_c$, $\sigma_{AC}(T)$ dependence follows to Mott's VRH Eq. (34b) [72,216] (Fig. 32). At $T \geq T_c$, the conductivity is determined by phonon scattering according to undimerized SSH model proposed for intrinsic conductivity in *trans*-PA and other conducting polymers [188,217]

$$\sigma_{AC} = \frac{Ne^2 c_\parallel^2 M t_0^2 k_B T}{8\pi\hbar^3\alpha^2}\left[\sin h\left(\frac{2\pi\hbar\nu_{rh}}{k_B T}\right) - 1\right] \qquad (51)$$

where M is the total mass of CH group, $t_0 \approx 2$–3 eV is the π-electron hopping matrix element, and α is the electron–phonon coupling constant. As it is seen from Fig. 32, Eqs. (34b) and (50) well approximate the $\sigma_{AC}(T)$ dependence experimentally obtained for VI PANI-ES at $\langle L \rangle = 1.64$ nm, $c_\parallel = 0.95$ nm [179], and $\alpha = 41$ eV/nm [188]. Room temperature intrinsic conductivity of heavily doped *trans*-PA and PANI-ES was calculated in the framework of the undimerized SSH model and the Drude model, respectively, to be approximately equal to 10^8 S/m [188] and 10^9 S/m [187], respectively. The analysis of our data, however, shows that such a conductivity should be achieved at sufficiently massive (some hundreds of M) polymer units. Therefore, we can conclude that in highly doped PANI-ES sample, charge carriers variable-range hop at low temperatures and are scattered on lattice optical phonons when the phonon energy becomes comparable with $k_B T_c = k_B T$.

Aasmundtveit et al. [218] have shown that 3-cm waveband line width and consequently spin–spin relaxation rate of PC in PANI depend directly on its DC conductivity.

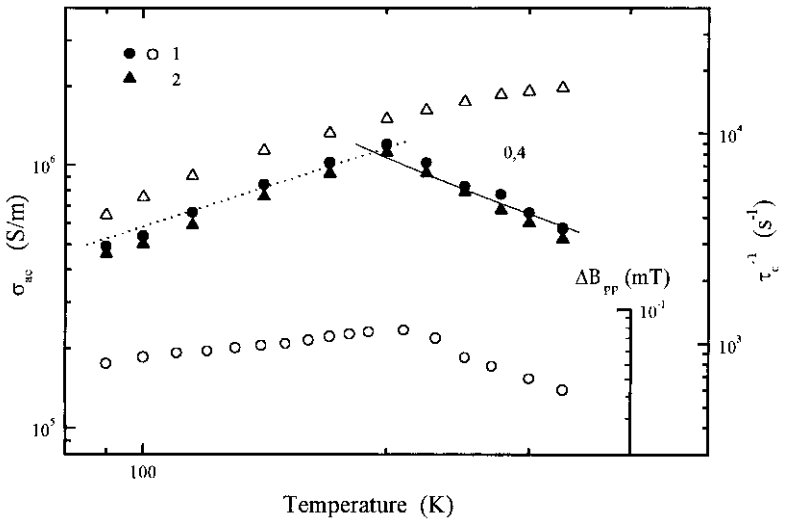

Fig. 32. Temperature dependencies of the intrinsic conductivity σ_{AC} of the VI (1) and V (2) PANI samples (filled points) determined from their EPR line asymmetry and Eq. (13), and those calculated from Eq. (34b) with $\langle L \rangle = 1.64$ nm (dotted line), and from Eq. (51) with $c = 0.950$ nm, and $\alpha = 41$ eV/nm (solid line). For the comparison, the temperature dependence of the polymer chains libration frequency (open triangles) and that of ΔB_{pp} value for VI PANI-ES polymer given from Fig. 24 (open circles) are also shown.

The comparison of $\sigma_{AC}(T)$ and $\Delta B_{pp}(T)$ functions presented in Fig. 32 demonstrate the additivity of these values at least at $T \geq T_c$ region. Besides, Khazanovich [219] have found that spin–spin relaxation depends on the number of spins on each polymer chain N_s and on the number of neighboring chains N_c with which these spins interact as following

$$T_2^{-1} = \frac{4\langle \Delta\omega^2 \rangle}{5\nu_0 N_s}\left[21 \ln\frac{\nu_0}{\nu_e} + 18 \ln N_c\right] \qquad (52)$$

Using $T_2 = 1.7 \times 10^{-7}$ s, $\sum_{ij} = 1.2 \times 10^{51}$ m^{-6}, and $\nu_0 = 4.2 \times 10^{12}$ s^{-1} determined from experiment, a simple relation $N_c \approx 55 \exp(N_s)$ of these values is obtained from Eq. (52). This means that at $L_{\|} = 7.0$ nm at least seven interacting spins exist on each chain as spin-packet and interact with $N_c = 20$ chains, that is, spin and charge 3D hopping does not exceed distance more than $3c_{\perp} < L_{\perp}$.

The spin motion and the intrinsic conductivity of the sample depend also on the macromolecular dynamics, because the interaction of the spins and charge transfer integral can be modulated by PANI lattice librations as it happened in other organic crystalline semiconductors [130]. One can see from Fig. 32, that $\sigma_{AC}(T)$ dependence for the domains follows $1/\tau_c^x(T)$ one for the polymer chain librations determined above at least at $T \leq T_c$. This means that the lattice librations indeed modulate the interacting spin exchange and consequently the charge transfer integral. Assuming that polaron is covered by electron and excited phonon clouds, we can propose that both spin relaxation and charge transfer should be accompanied with the phonon dispersion. Such cooperating charge-phonon processes seems to be more important for the doped polymers whom high-coupled chains constitute 3D metal-like domains.

The velocity of the charge carriers at the Fermi level, $v_F = 4c_{\|}/[hn(\varepsilon_F)]$ is equal to 2.5×10^5 m/s for highly doped PANI-ES, so that the rate of the interchain charge hopping can be determined as $\nu_{\perp} = v_F/L_{\perp} = 2.4 \times 10^{14}$ s^{-1} that gives (see Eq. (45)) $\sigma_{3D} = 1.3 \times 10^6$ S/m at $L_{\perp} = 1.0$ nm (see Table 7) and $T_c \approx 200$ K. The conductivity obtained is close to AC conductivity evaluated from EPR spectra of the sample (Fig. 32). This fact confirms additionally the existence of metal-like domains with three dimensionally delocalized electrons in PANI-ES polymer. Therefore, as in the case of the usual metals, we can calculate the effective mass m^* of charge carries from the relation [24] $m^* = (3\pi^2 N)^{1/3}\hbar v_F^{-1}$, equal approximately to two free electron masses. The mean free path l_i of the carriers is calculated for this samples [24] $l_i = \sigma_{AC} m^* v_F/(Ne^2)$ to be as approximately long as 8.0 nm at T_c. This value is somewhat smaller than that estimated for oriented *trans*-PA [188,220,221], but however, evidences for extended electron states in this polymer as well.

Thus, in undoped PANI, the charge carriers are transferred mainly by small polarons, which hopping probability strongly depends on the lattice phonon energy. In lightly doped PANI, the distribution of site energies is narrow compared with $k_B T$ and isoenergetic hopping dominates. Both $\sigma_{DC}(T)$ and $\sigma_{AC}(T)$ can be described by modified Kivelson's model for polarons and bipolarons bound to charged impurities. This is in agreement with the intersoliton charge hopping in lightly doped PA and with the VRH among pinned solitons in moderately doped PA. A similar change probably occurs upon doping of the PANI samples. The polaron states are broadened at the PANI doping, so in this case, the distribution of the site

energies is much broader then k_BT and the VRH charge transport dominates.

As the doping level increases and as the percolation transition takes place the conducting single chains become crystallization centers for the formation of the massive metal-like domains. This process is accompanied with the increase of the electron–phonon interaction, crystalline order and interchain coupling. The latter factor plays an important role in stabilization of the metallic state, when both 1D electron localization and ''Peierls instability'' are avoided. Besides, charge transfer is modulated by the macromolecular librations in PANI-ES, which chains are strongly coupled and form metal-like domains. These domains consist of the packed polymer chains with the joint conducting electrons, which are three dimensionally delocalized between and along them. This is in agreement with the metal-like ''bundles'' concept, but contradicts with the existence of many solitary conducting chains in PANI-ES.

5. Conclusions

The data presented show the variety of electronic processes, realized in the organic conducting polymers, which are stipulated by the structure, conformation, packing, and the degree of ordering of polymer chains, and also by a number and the origin of dopants, introduced into the polymer. Among the general relationships, peculiar to these compounds are the following ones.

Spin and spinless nonlinear excitations may exist as charge carriers in organic conducting polymers. The ratio of these carriers depends on various properties of the polymer and dopant introduced into it. With the increase of doping level, the tendency of molecular polaron collapse with bipolaron formation is observed. However, such a process can be embarrassed in some polymers due to the structural–conformational peculiarities of the polymer. Doping process leads to the change of charge transfer mechanism. Conductivity in neutral or weakly doped samples is defined mainly by interchain charge tunneling in the frames of the ''small polarons'' or Kivelson formalisms, which is characterized by a high enough interaction of spins with several phonons of a lattice and by the relation between 1D spin motion and interchain charge transfer. These mechanisms cease to dominate with the increase of doping level and the charge can be transferred due to thermal activation of the carriers. Therefore, complex quasi-particles, namely the molecular-lattice polarons are formed in some polymers due to the libron–phonon interactions analogously to that it is realized in organic molecular crystals. It should be noted that as conducting polymers have a priori a lower dimensionality as compared with molecular crystals, their dynamics of charge carriers is more anisotropic. In heavily doped samples, the dominating is the interchain Mott charge transport, characterized by complete interaction of electrons with lattice phonons.

The spectral resolution, achieved at 2-mm waveband EPR, is quite enough for a separate registration of individual spectral lines of most organic free radicals with different radical structure or orientation in a magnetic field. This is realized not only for PCs with comparatively strong spin–orbit coupling (e.g., nitroxide or sulfuric radicals), but also for localized π-radicals. In high fields, the interaction between spin-packets decreases significantly in paramagnetic systems, and they may be considered as noninteracting. Therefore, 2-mm waveband EPR enables one to obtain more correct and complete information on molecular and electronic processes, realized in polymer and other condensed systems.

2-mm waveband EPR reveals the anisotropic character of superslow molecular motions and the mobility of charge carriers in low-dimensional organic semiconductors; it broadens the range of measurements of characteristic times of molecular and electronic processes. High spectral resolution at 2-mm waveband provides the unique possibility of the registration of fine structural and conformational transitions and electronic processes in various systems with their following interpretation in the frames of the present theories.

Acknowledgements

The author expresses his gratitude to Prof. S.A. Brazovskii, Prof. Dr. H.-K. Roth, Prof. Dr. E. Fanghänel, Prof. Dr. K. Luders, Prof. Y.S. Lebedev, and Prof. Dr. G. Hinrichsen for fruitful discussion. This work was in part supported by the Russian Foundation for Basic Researches, Grant No. 97-03-33707.

References

[1] K. Tanigaki, in: H.S. Nalwa (Ed.), Handbook of Organic Conductive Molecules and Polymers, Vol. 1, Wiley, Chichester, 1997, pp. 293–331.
[2] J.M. Williams, J.R. Ferraro, R.J. Thorn, K.D. Carlson, U. Geiser, H.H. Wang, A.M. Kini, M.-H. Whangboo, Organic Superconductors (Including Fullerenes): Synthesis, Structure, Properties and Theory, Prentice-Hall, Englewood Cliffs, NJ, 1992.
[3] P. Day, in: T.E. Scotheim (Ed.), Handbook of Conducting Polymers, Vol. 1, Marcel Dekker, New York, 1986, p. 117.
[4] G.E. Wnek, in: T.E. Scotheim (Ed.), Handbook of Conducting Polymers, Vol. 1, Marcel Dekker, New York, 1986, p. 205.
[5] J.L. Brédas, R. Silbey (Eds.), Conducting Polymers, Kluwer Academic, Dordrecht, 1991.
[6] H. Kiess (Ed.), Conducting Polymers, Vol. 102, Springer-Verlag, Berlin, 1992.
[7] M. Aldissi (Ed.), Intrinsically Conducting Polymers: An Emerging Technology, NATO ASI Series, Kluwer Academic Publishing, Dordrecht, 1992.

[8] A. Echte, Handbuch der Technischen Polymerchemie, VCH Verlag, Weinheim, 1993.
[9] J.P. Farges (Ed.), Organic Conductors Fundamental and Applications, Marcel Dekker, New York, 1994.
[10] A.F. Garito, A.K.-Y. Jen, C.Y.-C. Lee, L.R. Dalton (Eds.), Electrical, Optical and Magnetic Properties of Organic Solid State Materials, Vol. 328, Materials Research Society Symposium Proceeding, Materials Research Society, Pittsburgh, 1994.
[11] S. Roth, One-Dimensional Metals — Physics and Material Science, VCH, Weinheim, 1995.
[12] J.C. Salamone (Ed.), Encyclopedia of Polymeric Materials, CRC Press, Boca Raton, 1996.
[13] H.S. Nalwa (Ed.), Handbook of Organic Conductive Molecules and Polymers, Vols. 1 to 4, Wiley, Chichester, 1997.
[14] F.L. Carter (Ed.), Molecular Electronic Devices, Vols. 1 and 2, Marcel Dekker, New York, 1982 and 1987.
[15] J.-L. Brédas, R.R. Chance (Eds.), Conducting Polymeric Materials: Opportunities in Electronics, Optoelectronics, and Molecular Electronics, NATO Advanced Study Series, Kluwer Academic Publishing, Dordrecht, 1990.
[16] W.R. Salaneck, D.T. Clark, E.J. Samuelsen (Eds.), Science and Applications of Conducting Polymers, Adam Hilger, New York, 1991.
[17] G.J. Ashwell (Ed.), Molecular Electronics, Wiley, New York, 1992.
[18] B. Scrosati (Ed.), Application of Electroactive Polymers, Chapman & Hall, London, 1993.
[19] J.-P. Farges (Ed.), Organics Conductors: Fundamentals and Applications, Marcel Deccer, New York, 1994.
[20] J.A. Chilton, M.T. Gosey (Eds.), Special Polymers for Electronic and Photonic Applications, Chapman & Hall, London, 1995.
[21] H.S. Nalwa, S. Miyata (Eds.), Nonlinear Optics of Organic Molecules and Polymers, CRC Press, Boca Raton, 1997.
[22] R. Menon, C.O. Yoon, D. Moses, A.J. Heeger, in: T.A. Skotheim, R.L. Elsenbaumer, J.R. Reynolds (Eds.), Handbook of Conducting Polymers, Marcel Dekker, New York, 1997, pp. 27–84.
[23] B. Wessling, in: H.S. Nalwa (Ed.) Handbook of Organic Conductive Molecules and Polymers, Vol. 3, Wiley, Chichester, 1997, pp. 497–632.
[24] G.S. Blakemore, Solid State Physics, Cambridge Univ. Press, Cambridge, 1985.
[25] W.P. Su, J.R. Schrieffer, A.J. Heeger, Phys. Rev. B 22 (1980) 2099.
[26] R.R. Chance, D.S. Boudreaux, J.L. Brédas, R. Silbey, in: T.E. Scotheim (Ed.), Handbook of Conducting Polymers, Vol. 2, Marcel Dekker, New York, 1986, p. 825.
[27] R.E. Peierls, Quantum Theory of Solids, Oxford Univ. Press, London, 1955.
[28] P. Bernier, in: T.E. Scotheim (Ed.), Handbook of Conducting Polymers, Vol. 2, Marcel Dekker, New York, 1986, p. 1099.
[29] K. Mizoguchi, S. Kuroda, in: H.S. Nalwa (Ed.), Handbook of Organic Conductive Molecules and Polymers, Vol. 3, Wiley, Chichester, 1997, p. 251.
[30] W.M. Mims, in: S. Geschwind (Ed.), Electron Paramagnetic Resonance, Plenum, New York, 1972, p. 263.
[31] K.M. Salikhov, A.G. Semenov, Yu.D. Tsvetkov, Electron Spin Echo and its Utilization (Russian), Nauka, Novosibirsk, 1976.
[32] S. Geschwind, in: S. Geschwind (Ed.), Electron Paramagnetic Resonance, Plenum, New York, 1972, p. 353.
[33] Ch.P. Poole, Electron Spine Resonance, International Science Publication, London, 1967.
[34] L. Kevan, L.D. Kispert, Electron Spin Double Resonance Spectroscopy, Wiley, New York, 1976.
[35] J.S. Hyde, L.R. Dalton, in: L. Berliner (Ed.), Spin Labeling: Theory and Application, Vol. 2, Academic Press, New York, 1979, p. 1.
[36] W. Karte, E. Wehrsdorfer, J. Magn. Reson. 33 (1979) 107.
[37] O.Y. Grinberg, A.A. Dubinski, Y.S. Lebedev, Uspekhi Khimii (Russian) 52 (1983) 1490.
[38] V.I. Krinichnyi, 2-mm Wave Band EPR Spectroscopy of Condensed Systems, CRC Press, Boca Raton, 1995.
[39] A.L. Buchachenko, A.M. Wasserman, Stable Radicals (Russian), Khimija, Moscow, 1973.
[40] S.V. Vonsovskii, Magnetism (Russian), Nauka, Moscow, 1971.
[41] H.-K. Roth, F. Keller, H. Schneider, Hochfrequenzspectroskopie in der Polymerforschung, Academie Verlag, Berlin, 1984.
[42] S.P. Kurzin, B.G. Tarasov, N.F. Fatkullin, R.M. Aseeva, Visokomol. Soedin. A (Russian) 24 (1982) 117.
[43] L.A. Blumenfeld, V.V. Voevodski, A.G. Semenov, Application of Electron Paramagnetic Resonance in Chemistry (Russian), Izdat, SO AN USSR, Novosibirsk, 1962.
[44] Ya.S. Lebedev, V.I. Muromtsev, EPR and Relaxation of Stabilized Radicals (Russian), Khimija, Moscow, 1972.
[45] F. Carrington, A.D. McLachlan, Introduction to Magnetic Resonance with Application to Chemistry and Chemical Physics, Harrer and Row Publishers, New York, 1967.
[46] M.A. Butler, L.R. Walker, Z.G. Soos, J. Chem. Phys. 64 (1976) 3592.
[47] P.D. Krasicky, R.H. Silsbee, J.C. Scott, Phys. Rev. B 25 (1981) 5607.
[48] F.J. Dyson, Phys. Rev. B 98 (1955) 349.
[49] A. Abragam, The Principles of Nuclear Magnetism, Clarendon Press, Oxford, 1961.
[50] H.C. Torrey, Phys. Rev. 92 (1953) 962.
[51] K. Mizoguchi, Macromol. Chem., Macromol. Symp. 37 (1990) 53.
[52] S.A. Altshuler, B.M. Kozirev, Electron Paramagnetic Resonance of Compounds of Elements of Intermediate Groups (Russian), Nauka, Moscow, 1972.
[53] A.A. Bugai, Fiz. Tverd. Tela (Ashkhabad, USSR) 4 (1962) 3027.
[54] E.E. Salpeter, Proc. Phys. Soc. 63A (1950) 337.
[55] G. Feher, Phys. Rev. 114 (1959) 1219.
[56] M. Weger, J. Bell. Syst. Technol. 39 (1960) 1013.
[57] C.A.J. Ammerlaan, A. van der Wiel, J. Magn. Reson. 21 (1976) 387.
[58] Ch.P. Pool, Electron Spin Resonance: A Comprehensive Treatise on Experimental Techniques, Wiley, New York, 1983.
[59] A. Lösche, Kerninduction, VEB Deutscher Verlag, Berlin, 1957.
[60] P.R. Gullis, J. Magn. Reson. 21 (1976) 397.
[61] S. Kivelson, Phys. Rev. B 25 (1982) 3798.
[62] J. Patzsch, H. Gruber, in: H. Kuzmany, M. Mehring, S. Roth (Eds.), Electronic Properties of Polymers (Springer Series in Solid State Sciences, Vol. 107), Springer-Verlag, Berlin, 1986, p. 121.
[63] A.J. Epstein, in: T.E. Scotheim (Ed.), Handbook of Conducting Polymers, Vol. 2, Marcel Dekker, New York, 1986, p. 1041.
[64] J.P. Parneix, M. El Kadiri, in: H. Kuzmany, M. Mehring, S. Roth (Eds.), Electronic Properties of Conducting Polymers (Springer Series in Solid State Sciences, Vol. 76), Springer-Verlag, Berlin, 1987, p. 23.
[65] M. El Kadiri, J.P. Parneix, in: H. Kuzmany, M. Mehring, S. Roth (Eds.), Electronic Properties of Polymers and Related Compounds (Springer Series in Solid State Sciences, Vol. 63), Springer-Verlag, Berlin, 1985, p. 183.
[66] D. Schäfer-Siebert, C. Budrowski, H. Kuzmany, S. Roth, in: H. Kuzmany, M. Mehring, S. Roth (Eds.), Electronic Properties of Conducting Polymers (Springer Series in Solid State Sciences, Vol. 76), Springer-Verlag, Berlin, 1987, p. 38.
[67] D. Schafer-Siebert, S. Roth, Synth. Met. 28 (1989) D369.
[68] H. Meier, Topics in Current Chemistry, Vol. 61, Springer-Verlag, Berlin, 1976, p. 85.
[69] M.E. Jozefowicz, R. Laversanne, H.H.S. Javadi, A.J. Epstein, J.P. Pouget, X. Tang, A.G. MacDiarmid, Phys. Rev. B 39 (1989) 12958.

[70] D.A. Dos Santos, D.S. Galvao, B. Laks, M.C. dos Santos, Synth. Met. 51 (1992) 203.
[71] I. Hoogmartens, P. Adriaensens, R. Carleer, D. Vanderzande, H. Martens, J. Gelan, Synth. Met. 51 (1992) 219.
[72] N.F. Mott, E.A. Davis, Electronic Processes in Non-Crystalline Materials, Clarendon Press, Oxford, 1979.
[73] D. Duret, M. Beranger, M. Moussavi, Synth. Met. 27 (1988) B127.
[74] K. Mizoguchi, K. Kume, H. Shirakawa, Solid State Commun. 50 (1984) 213.
[75] F. Herlach (Ed.), Strong and Ultrastrong Magnetic Fields and their Applications, Springer-Verlag, Berlin, 1985.
[76] Yu.N. Molin, R.Z. Sagdeev, O.A. Anisimov, Khim. Fiz. (Russian) 4 (1983) 437.
[77] H.A. Kuska, M.I. Rogers, in: E.T. Kaiser, L. Kevan (Eds.), Radical Ions, Interscience Publisher, New York, 1968, p. 31.
[78] V.I. Krinichnyi, Russ. Chem. Rev. 65 (1996) 81, Uspekhi Khimii (Russian), 65 (1986) 84.
[79] V.I. Krinichnyi, Russ. Chem. Rev. 65 (1996) 521, Uspekhi Khimii (Russian), 65 (1986) 564.
[80] V.I. Krinichnyi, Russ. Solid State Phys. 39 (1997) 3.
[81] A.E. Pelekh, V.I. Krinichnyi, A.Yu. Brezgunov, L.I. Tkachenko, G.I. Kozub, Visokomol. Soedin. (Russian) 33 (1991) 1731.
[82] V.A. Livshits, Yu.A. Bobrov, Teor. Eksp. Khim. 22 (1986) 331.
[83] B.H. Robinson, L.R. Dalton, J. Chem. Phys. 72 (1980) 1312.
[84] J.D. Memory, Quantum Theory of Magnetic Resonance Parameters, McGraw-Hill, New York, 1968.
[85] L.D. Kispert, J. Joseph, G.G. Miller, R.H. Baughman, Mol. Cryst. Liq. Cryst. 118 (1985) 313.
[86] H.-K. Roth, H. Gruber, E. Fanghänel, T. vu Quang, Prog. Colloid Polym. Sci. 78 (1988) 75.
[87] H.-K. Roth, W. Brunner, G. Volkel, M. Schrödner, H. Gruber, Macromol. Chem., Macromol. Symp. 34 (1990) 293.
[88] R.L. Elsenbaumer, P. Delannoy, G. Muller, C.E. Forbes, N.C. Murthy, H. Eskhardt, R.H. Baughman, Synth. Met. 11 (1985) 251.
[89] Z. Wilamovski, B. Oczkiewicz, P. Kacman, J. Blinowski, Phys. Stat. Sol. B 134 (1986) 303.
[90] T. Sugano, G. Saito, M. Kinoshita, Phys. Rev. B 35 (1987) 6554.
[91] I.B. Goldberg, H.R. Crowe, P.R. Newman, A.J. Heeger, A.G. MacDiarmid, J. Chem. Phys. 70 (1979) 1132.
[92] P. Bernier, Mol. Cryst. Liq. Cryst. 77 (1982) 1089.
[93] R. Cosmo, E. Dormann, B. Gotschy, H. Naarmann, H. Winter, Synth. Met. 41 (1991) 369.
[94] D. Billand, F.X. Henry, P. Willmann, Synth. Met. 69 (1995) 9.
[95] V.I. Krinichnyi, O.Ya. Grinberg, I.B. Nazarova, L.I. Tkachenko, G.I. Kozub, M.L. Khidekel, Izvestia AN SSSR (Russian) 2 (1985) 467.
[96] L.M. Goldenberg, A.E. Pelekh, V.I. Krinichnyi, O.S. Roshchupkina, A.F. Zueva, L.N. Lyubonskaya, O.N. Efimov, Synth. Met. 36 (1990) 217.
[97] J.C.W. Chien, Polyacetylene: Chemistry, Physics and Material Science, Academic Press, Orlando, 1984.
[98] A.J. Heeger, in: T.E. Scotheim (Ed.), Handbook of Conducting Polymers, Vol. 2, Marcel Dekker, New York, 1986, p. 729.
[99] C. Riekel, H.W. Hässlin, K. Menke, S. Roth, J. Chem. Phys. 77 (1982) 4254.
[100] H.W. Hässlin, C. Riekel, K. Menke, S. Roth, Macromol. Chem. 185 (1984) 397.
[101] W. Markowitsch, F. Kuchar, K. Seeger, in: H. Kuzmany, M. Mehring, S. Roth (Eds.), Electronic Properties of Polymers and Related Compounds (Springer Series in Solid State Sciences, Vol. 63), Springer-Verlag, Berlin, 1985, p. 78.
[102] W. Markowitsch, G. Leising, Synth. Met. 51 (1992) 25.
[103] H. Thomann, L.R. Dalton, in: T.E. Scotheim (Ed.), Handbook of Conducting Polymers, Vol. 2, Marcel Dekker, New York, 1986, p. 1157.
[104] Y. Wada, J.R. Schrieffer, Phys. Rev. B 18 (1978) 3897.
[105] K. Maki, Phys. Rev. B 26 (1982) 2181.
[106] A. Terai, Y. Ono, Synth. Met. 57 (1993) 4672.
[107] S. Kivelson, Phys. Rev. Lett. 46 (1981) 1344.
[108] M. Nechtschein, F. Devreux, R.G. Green, T.C. Clarke, G.B. Street, Phys. Rev. Lett. 44 (1980) 356.
[109] T.C. Clarke, J.C. Scott, in: T.E. Scotheim (Ed.), Handbook of Conducting Polymers, Vol. 2, Marcel Dekker, New York, 1986, p. 1127.
[110] F. Masin, G. Gusman, R. Deltour, Solid State Commun. 40 (1981) 513.
[111] M. Ziliox, P. Spegt, C. Mathis, B. Francois, G. Weill, Solid State Commun. 51 (1984) 393.
[112] T.S. Zuravleva, Uspekhi Khimii (Russian) 56 (1987) 128.
[113] M. Nechtschein, in: T.A. Scotheim, R.L. Elsenbaumer, J.R. Reynolds (Eds.), Handbook of Conducting Polymers, Marcel Dekker, New York, 1997, p. 141.
[114] A. Grupp, P. Hofer, H. Kass, M. Mehring, R. Weizenhofer, G. Wegner, in: H. Kuzmany, M. Mehring, S. Roth (Eds.), Electronic Properties of Conducting Polymers (Springer Series in Solid State Sciences, Vol. 76), Springer-Verlag, Berlin, 1987, p. 156.
[115] A. Bartl, J. Frohner, R. Zuzok, S. Roth, Synth. Met. 51 (1992) 197.
[116] F. Rachdi, P. Bernier, in: H. Kuzmany, M. Mehring, S. Roth (Eds.), Electronic Properties of Conducting Polymers (Springer Series in Solid State Sciences, Vol. 76), Springer-Verlag, Berlin, 1987, p. 160.
[117] G. Leizing, H. Kahlert, O. Leitner, in: H. Kuzmany, M. Mehring, S. Roth (Eds.), Electronic Properties of Polymers and Related Compounds (Springer Series in Solid State Sciences, Vol. 63), Springer-Verlag, Berlin, 1985, p. 56.
[118] K. Mizoguchi, K. Kume, S. Masubuchi, H. Shirakawa, Solid State Commun. 59 (1986) 465.
[119] K. Mizoguchi, K. Kume, S. Masubuchi, H. Shirakawa, Synth. Met. 17 (1987) 405.
[120] K. Mizoguchi, S. Komukai, T. Tsukamoto, K. Kume, M. Suezaki, K. Akagi, H. Shirakawa, Synth. Met. 28 (1989) D393.
[121] Y. Tomkiewicz, T.D. Schultz, H.B. Broom, T.C. Clarke, G.B. Street, Phys. Rev. Lett. 43 (1979) 1532.
[122] N.S. Shiren, Y. Tomkiewicz, T.G. Kazyaka, A.R. Taranko, H. Thomann, L. Dalton, T.C. Clarke, Solid State Commun. 44 (1982) 1157.
[123] Y. Tomkiewicz, N.S. Shiren, T.D. Schultz, H. Thomann, L. Dalton, A. Zettl, G. Gruner, T.C. Clarke, Mol. Cryst. Liq. Cryst. 83 (1982) 1049.
[124] L.R. Dalton, H. Thomann, A. Morrobelsosa, C. Chiu, M.E. Galvin, G.E. Wnek, Y. Tomkiewicz, N.S. Shiren, B.H. Robinson, A.L. Kwiram, J. Appl. Phys. 54 (1983) 5583.
[125] J.C.W. Chien, G.E. Wnek, F.E. Karasz, J.M. Warakomski, L.C. Dickinson, A.J. Heeger, A.G. MacDiarmid, Macromolecules 15 (1982) 614.
[126] M. Nechtschein, F. Devreux, F. Genoud, M. Gugleielmi, K. Holczer, Phys. Rev. B 27 (1983) 61.
[127] J. Reichenbach, M. Kaiser, J. Anders, H. Burne, S. Roth, Synth. Met. 51 (1992) 245.
[128] K. Holczer, J.P. Boucher, F. Devreux, M. Nechtschein, Phys. Rev. B 23 (1981) 1051.
[129] V.I. Krinichnyi, A.E. Pelekh, Ya.S. Lebedev, L.I. Tkachenko, G.I. Kozub, A. Barrat, L.G. Brunel, G.B. Robert, Appl. Magn. Reson. 7 (1994) 459.
[130] E.A. Silinsh, M.V. Kurik, V. Chapek, Electronic Processes in Organic Molecular Crystals: The Phenomena of Localization and Polarization (Russian), Zinatne, Riga, 1988.
[131] Yu.S. Kivshar, B.A. Malomed, Rev. Mod. Phys. 61 (1989) 763.
[132] V.F. Traven', Electronic Structure and Properties of Organic Molecules (Russian), Khimija, Moscow, 1989.
[133] V.I. Krinichnyi, A.E. Pelekh, L.I. Tkachenko, G.I. Kozub, Synth. Met. 46 (1992) 13.
[134] V.I. Krinichnyi, A.E. Pelekh, A.Yu. Brezgunov, L.I. Tkachenko, G.I. Kozub, Mater. Sci. 17 (1991) 25.

[135] K. Mizoguchi, M. Nechtschein, J.P. Travers, C. Menardo, Phys. Rev. Lett. 63 (1989) 66.
[136] V.V. Mank, N.I. Lebovka, NMR Spectroscopy of Water in Heterogene Systems (Russian), Naukova Dumka, Kiev, 1988.
[137] G.M. Bartenev, S.Ya. Frenkel, Physics of Polymers (Russian), Khimija, Leningrad, 1990.
[138] V.I. Krinichnyi, A.E. Pelekh, L.I. Tkachenko, G.I. Kozub, Synth. Met. 46 (1992) 1.
[139] G. Tourillon, in: T.E. Scotheim (Ed.), Handbook of Conducting Polymers, Vol. 1, Marcel Dekker, New York, 1986, p. 293.
[140] M. Scharli, H. Kiess, G. Harbeke, W. Berlinger, K.W. Blazey, K.A. Muller, in: H. Kuzmany, M. Mehring, S. Roth (Eds.), Electronic Properties of Conducting Polymers (Springer Series in Solid State Sciences, Vol. 76), Springer-Verlag, Berlin, 1987, p. 277.
[141] G. Tourillon, D. Gouriez, F. Garnier, D. Vivien, J. Phys. Chem. 88 (1984) 1049.
[142] V.I. Krinichnyi, I.B. Nazarova, L.M. Goldenberg, Synth. Met. (to be published).
[143] R.L. Elsenbaumer, L.W. Shacklette, in: T.E. Scotheim (Ed.), Handbook of Conducting Polymers, Vol. 1, Marcel Dekker, New York, 1986, p. 213.
[144] C. Qing, L.K. Wang, Synth. Met. 49–50 (1992) 261.
[145] P. Pradere, A. Boudet, J. Mater. Sci. 22 (1987) 4240.
[146] P. Kovacic, M.B. Feldman, J.P. Kovacic, J.B. Lando, J. Appl. Polym. Sci. 12 (1968) 1735.
[147] L.M. Goldenberg, A.E. Pelekh, V.I. Krinichnyi, O.S. Roshchupkina, A.F. Zueva, L.N. Lyubonskaya, O.N. Efimov, Synth. Met. 41–43 (1991) 3071.
[148] P. Kuivalainen, H. Stubb, P. Raatikainen, C. Holmstrom, J. Phys. (Paris) 44 (1983) C3–757.
[149] G.B. Street, T.C. Clarke, R.H. Giess, V.Y. Lee, A. Nazzal, P. Pfluger, J.C. Scott, J. Phys. (Paris) 44 (1983) C3–C599.
[150] A.M. Wasserman, A.L. Kovarskii, Spin Labels and Probes in Physics and Chemistry of Polymers (Russian), Nauka, Moscow, 1986.
[151] H. Winter, G. Sachs, E. Dormann, R. Cosmo, H. Naarmann, Synth. Met. 36 (1990) 353.
[152] P. Audebert, G. Binan, M. Lapkowski, P. Limosin, in: H. Kuzmany, M. Mehring, S. Roth (Eds.), Electronic Properties of Conducting Polymers (Springer Series in Solid State Sciences, Vol. 76), Springer-Verlag, Berlin, 1987, p. 366.
[153] A.E. Pelekh, L.M. Goldenberg, V.I. Krinichnyi, Synth. Met. 44 (1991) 205.
[154] A.L. Buchachenko, Complexes of Radicals and Molecular Oxygen with Organic Molecules (Russian), Nauka, Moscow, 1984.
[155] V.I. Krinichnyi, Appl. Magn. Reson. 2 (1991) 29.
[156] A. Reddoch, S. Konishi, J. Chem. Phys. 70 (1979) 2121.
[157] F. Devreux, F. Genoud, M. Nechtschein, B. Villeret, in: H. Kuzmany, M. Mehring, S. Roth (Eds.), Electronic Properties of Conducting Polymers (Springer Series in Solid State Sciences, Vol. 76), Springer-Verlag, Berlin, 1987, p. 270.
[158] V.I. Krinichnyi, A.E. Pelekh, H.-K. Roth, K. Lüders, Appl. Magn. Reson. 4 (1993) 345.
[159] V.I. Krinichnyi, I.B. Nazarova, S.D. Chemerisov, H.-K. Roth, K. Lüders, Synth. Met. (to be published).
[160] V.I. Krinichnyi, E. Fanghänel, H.-K. Roth, K. Lüders, Appl. Magn. Reson. (to be published).
[161] F. Devreux, H. Lecavelier, Phys. Rev. Lett. 59 (1987) 2585.
[162] J.L. Brédas, in: T.E. Scotheim (Ed.), Handbook of Conducting Polymers, Vol. 2, Marcel Dekker, New York, 1986, p. 859.
[163] V.I. Krinichnyi, H.-K. Roth, G. Hinrichsen, I.B. Nazarova, S.D. Chemerisov, K. Lüders, Synth. Met. (to be published).
[164] S. Kivelson, Mol. Cryst. Liq. Cryst. 77 (1981) 65.
[165] A. Madhukar, W. Post, Phys. Rev. Lett. 39 (1977) 1424.
[166] E.A. Silinsh, Proc. XI Symp. on Mol. Crystals, Lugano, Switzerland, 1985, p. 277.
[167] G. Hempel, A.M. Richter, E. Fanghänel, H. Schneider, Acta Polymerica 41 (1990) 522.
[168] H.-K. Roth, H. Gruber, E. Fanghänel, A.M. Richter, W. Hörig, Synth. Met. 37 (1990) 151.
[169] H. Bleier, S. Roth, Y.Q. Shen, D. Schäfer-Siebert, Phys. Rev. B 38 (1988) 6031.
[170] H.-K. Roth, M. Schrödner, R.-I. Stohn, V.I. Krinichnyi, Synth. Met. 101 (1999) 832.
[171] V.I. Krinichnyi, H.-K. Roth, M. Schrödner, Synth. Met. (to be published).
[172] T.S. Cameron, R.C. Haddon, S.M. Mattar, S. Parsons, J. Passmore, A.P. Ramirez, J. Chem. Soc., Dalton Trans. (1992) 1563.
[173] V.I. Krinichnyi, R. Herrmann, E. Fanghänel, W. Mörke, K. Lüders, Appl. Magn. Reson. 12 (1997) 317.
[174] H. Bock, P. Rittmeyer, A. Krebs, K. Schultz, J. Voss, B. Kopke, Phosphorus Sulfur 19 (1984) 131.
[175] J.L. Brédas, C. Quattrocchi, J. Libert, A.G. MacDiarmid, J.M. Ginder, A.J. Epstein, Phys. Rev. B 44 (1991) 6002.
[176] A.A. Syed, M.K. Dinesan, Talanta 38 (1991) 815.
[177] D.C. Trivedi, in: H.S. Nalwa (Ed.), Handbook of Organic Conductive Molecules and Polymers, Vol. 2, Wiley, Chichester, 1997, p. 505.
[178] M. Laridjani, J.P. Pouget, A.G. MacDiarmid, A.J. Epstein, J. Phys. (France) 2 (1992) 1003.
[179] M.E. Jozefowicz, R. Laversanne, H.H.S. Javadi, A.J. Epstein, J.P. Pouget, X. Tang, A.G. MacDiarmid, Phys. Rev. B 39 (1989) 12958.
[180] F. Zuo, M. Angelopoulos, A.G. MacDiarmid, A.J. Epstein, Phys. Rev. B 36 (1987) 3475.
[181] A.J. Epstein, A.G. MacDiarmid, Synth. Met. 41 (1991) 601.
[182] Z.H. Wang, C. Li, E.M. Scherr, A.G. MacDiarmid, A.J. Epstein, Phys. Rev. Lett. 66 (1991) 1745.
[183] Z.H. Wang, E.M. Scherr, A.G. MacDiarmid, A.J. Epstein, Phys. Rev. B 45 (1992) 4190.
[184] Z.H. Wang, H.H.S. Javadi, A. Ray, A.G. MacDiarmid, A.J. Epstein, Phys. Rev. B 42 (1990) 5411.
[185] Z.H. Wang, A. Ray, A.G. MacDiarmid, A.J. Epstein, Phys. Rev. B 43 (1991) 4373.
[186] P. Grosse, Free Electrons in Solids (Russian), Mir, Moscow, 1982.
[187] J. Joo, E.J. Oh, G. Min, A.G. MacDiarmid, A.J. Epstein, Synth. Met. 69 (1995) 251.
[188] S. Kivelson, A.J. Heeger, Synth. Met. 22 (1988) 371.
[189] K. Lee, A.J. Heeger, Y. Cao, Synth. Met. 72 (1995) 25.
[190] C. Menardo, F. Genoud, M. Nechtschein, J.P. Travers, P. Hani, in: H. Kuzmany, M. Mehring, S. Roth (Eds.), Electronic Properties of Conducting Polymers (Springer Series in Solid State Sciences, Vol. 76), Springer-Verlag, Berlin, 1987, p. 244.
[191] M. Lapkowski, E.M. Genies, J. Electroanal. Chem. 279 (1990) 157.
[192] A.G. MacDiarmid, A.J. Epstein, in: W.R. Salaneck, D.T. Clark, E.J. Samuelson (Eds.), Science and Application of Conducting Polymers, Adam Hilger, Bristol, 1991, p. 95.
[193] J.L. Brédas, R.R. Chance, R. Silbey, Phys. Rev. B 26 (1982) 5843.
[194] N.S. Sariciftci, A.J. Heeger, Y. Cao, Phys. Rev. B 49 (1994) 5988.
[195] N.S. Sariciftci, A.C. Kolbert, Y. Cao, A.J. Heeger, A. Pines, Synth. Met. 69 (1995) 243.
[196] K. Mizoguchi, M. Nechtschein, J.P. Travers, Synth. Met. 41 (1991) 113.
[197] K. Mizoguchi, K. Kume, Synth. Met. 69 (1995) 241.
[198] D.S. Galvao, D.A. don Santos, B. Laks, C.P. de Melo, M.J. Caldas, Phys. Rev. Lett. 63 (1989) 786.
[199] L.W. Shacklette, R.H. Baughman, Mol. Cryst. Liq. Cryst. 189 (1990) 193.
[200] F. Lux, G. Hinrichsen, V.I. Krinichnyi, I.B. Nazarova, S.D. Chemerisov, M.-M. Pohl, Synth. Met. 53 (1993) 347.
[201] H.-K. Roth, V.I. Krinichnyi, Macromol. Chem., Macromol. Symp. 72 (1993) 143.

[202] B.Z. Lubentsov, O.N. Timofeeva, S.V. Saratovskikh, V.I. Krinichnyi, A.E. Pelekh, V.I. Dmitrenko, M.L. Khidekel, Synth. Met. 47 (1992) 187.
[203] V.I. Krinichnyi, S.D. Chemerisov, Ya.S. Lebedev, Synth. Met. 84 (1997) 819.
[204] V.I. Krinichnyi, S.D. Chemerisov, Ya.S. Lebedev, Phys. Rev. B 55 (1997) 16233.
[205] S.M. Long, K.R. Cromack, A.J. Epstein, Y. Sun, A.G. MacDiarmid, Synth. Met. 55 (1993) 648.
[206] J.G. Masters, J.M. Ginder, A.G. MacDiarmid, A.J. Epstein, J. Chem. Phys. 96 (1992) 4768.
[207] V.I. Krinichnyi, O.Ya. Grinberg, A.A. Dubinski, V.A. Livshits, Yu.A. Bobrov, Ya.S. Lebedev, Biofizika (Russian) 32 (1987) 534.
[208] F. Zuo, M. Angelopoulos, A.G. MacDiarmid, A.J. Epstein, Phys. Rev. B 39 (1989) 3570.
[209] L. Zuppiroli, S. Paschen, M.N. Bussac, Synth. Met. 69 (1995) 621.
[210] Y. Cao, S. Li, Z. Xue, D. Guo, Synth. Met. 16 (1986) 305.
[211] Y.W. Park, C. Park, Y.S. Lee, C.O. Yoon, H. Shirakawa, Y. Suezaki, K. Akagi, Solid State Commun. 65 (1988) 147.
[212] A.B. Kaiser, Phys. Rev. B 40 (1989) 2806.
[213] Y. Nogami, H. Kaneko, T. Ishiguro, A. Takahashi, J. Tsukamoto, N. Hosoito, Solid State Commun. 76 (1990) 583.
[214] J. Tsukamoto, A. Takahashi, Synth. Met. 41 (1991) 7.
[215] M.C. Itow, T. Kawahara, N. Kachi, H. Sakamoto, K. Mizoguchi, K. Kume, Y. Sahara, S. Masubuchi, S. Kazama, Synth. Met. 84 (1997) 749.
[216] E.P. Nakhmedov, V.N. Prigodin, A.N. Samukhin, Sov. Phys. Solid State 31 (1989) 368, Fiz. Tverd. Tela, 31 (1989) 31.
[217] L. Pietronero, Synth. Met. 8 (1983) 225.
[218] K. Aasmundtveit, F. Genoud, E. Houz, M. Nechtschein, Synth. Met. 69 (1995) 193.
[219] T.N. Khazanovich, Visokomol. Soedin. (Russian) 5 (1963) 112.
[220] T. Schimmel, W. Reiss, J. Gimeiner, G. Denninger, M. Schwoerer, H. Naarmann, N. Theophilou, Solid State Commun. 65 (1988) 1311.
[221] H.H.S. Javadi, A. Chakraborty, C. Li, N. Theophilou, D.B. Swanson, A.G. MacDiarmid, A.J. Epstein, Phys. Rev. B 43 (1991) 2183.